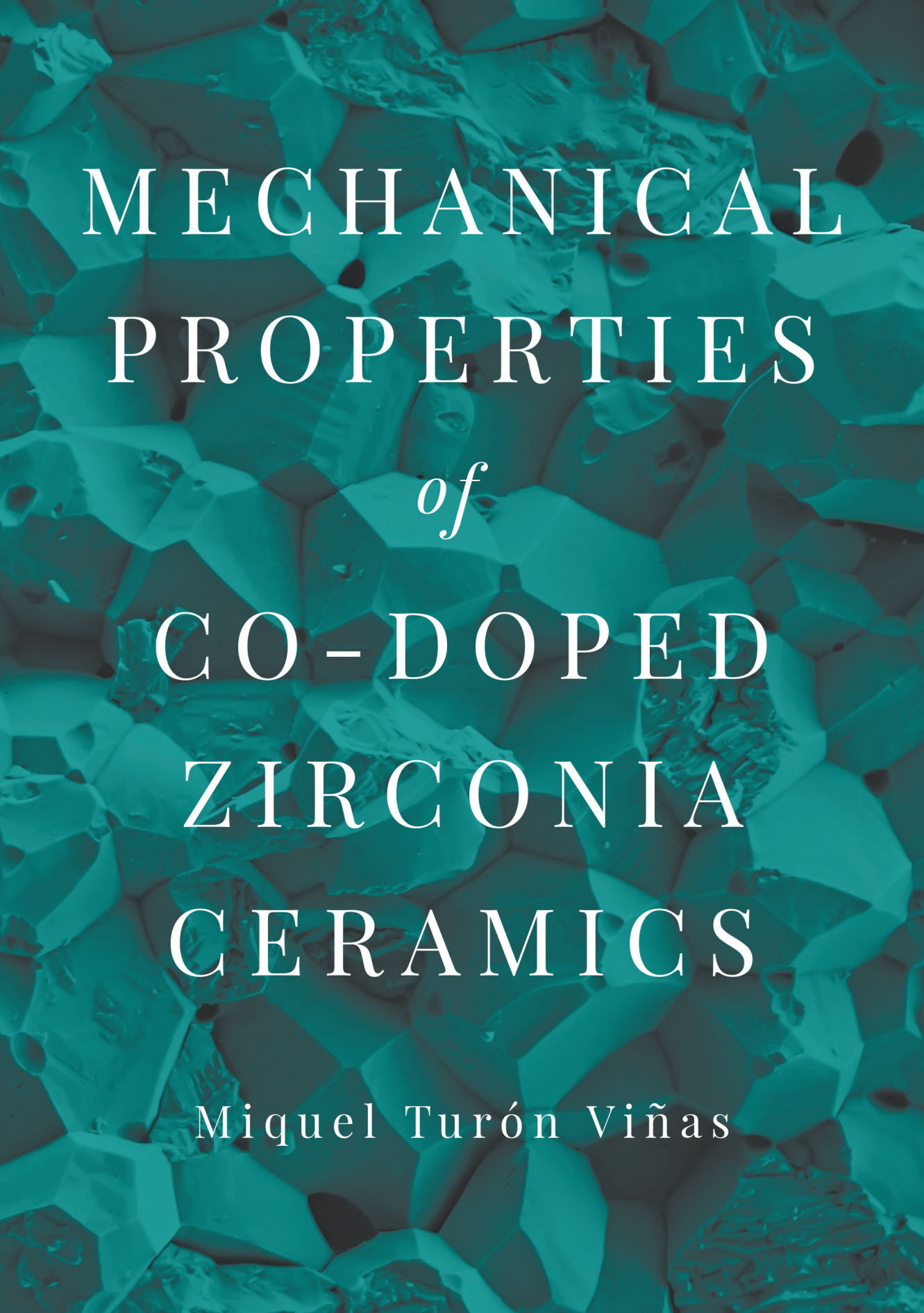

MECHANICAL PROPERTIES *of* CO-DOPED ZIRCONIA CERAMICS

Miquel Turón Viñas

UNIVERSITAT POLITÈCNICA DE CATALUNYA BARCELONATECH

Mechanical properties of co-doped zirconia ceramics

Miquel Turón Viñas

UNIVERSITAT POLITÈCNICA DE CATALUNYA
BARCELONATECH
Departament de Ciència dels Materials
i Enginyeria Metal·lúrgica

Centre d'Integritat Estructural
i Fiabilitat dels Materials

MECHANICAL PROPERTIES OF CO-DOPED ZIRCONIA CERAMICS

Miquel Turón Viñas

Marc J. Anglada Gomila, supervisor

Thesis as a compendium of publications

Barcelona, November 2017

A dissertation submitted in partial fulfilment of the requirements for the degree of Doctor of Philosophy by

Miquel Turón Viñas (M. Turon-Vinas)

In Doctoral Program in Materials Science and Engineering
Department of Materials Science and Metallurgical Engineering
Universitat Politècnica de Catalunya (UPC)

Printed in Barcelona, Spain, on 100% recycled paper
(unless this is a PDF)

Cover: SEM image of intergranular fracture surface of 12Ce-TZP, taken by T. Trifonov.

"Science is like sex: sometimes something useful comes out,
but that is not the reason we are doing it."

—Richard Feynman (attrib.)

ABSTRACT

Tetragonal polycrystalline zirconia, commonly stabilised with 3 mol% yttria (3Y-TZP), became one of the most interesting ceramics for biomedical applications due to its biocompatibility and high mechanical properties. Among them, its high fracture toughness should be highlighted, which is due to the stress-induced tetragonal-to-monoclinic ($t \rightarrow m$) phase transformation near a crack tip. However, the tetragonal grains can also spontaneously transform to monoclinic phase in a humid environment, phenomenon known as low-temperature degradation (LTD), which is an important issue for applications in which water is present.

Several methods have been proposed to increase the LTD resistance in zirconia, which range from improving the fabrication process in terms of grain size, density or residual stresses, to doping zirconia with other oxides, like magnesia or ceria.

Particularly, ceria-stabilised zirconia (Ce-TZP) possesses higher LTD resistance and fracture toughness than 3Y-TZP, but lower fracture strength and hardness, partly because of its larger grain size. The proposed approach consists in improving the mechanical properties controlling the grain growth by the addition of solutes.

Thus, on the one hand, this work focuses on obtaining and characterising compositions that balance a high resistance to LTD with mechanical properties.

Regarding the latter, fracture toughness is a key parameter to characterise advanced ceramics. Sometimes, the brittle behaviour of ceramics is an important hindrance for measuring fracture toughness. Elastic fracture mechanics is based on the assumption that materials are homogenous, continuous, isotropic, and cracks are idealised with zero crack-tip radius. Inducing a crack sharp enough and with a controlled shape and length in ceramics has been a critical issue during decades.

Hence, the other main objective of this work is to develop a methodology to measure the fracture toughness of ceramics more accurately and easy to reproduce. The method proposed consists in the fabrication of small notches by ultra-short pulsed laser ablation.

This dissertation is presented as a compendium of published articles. The first chapter consist in an introductory state-of-the-art of zirconia materials, the different approaches to produce better compositions and the problems determining some of its mechanical properties. Chapter 2 consist in the objectives and coverage of the thesis. A summary of the most important findings can be found in Chapter 3, and Chapter 4 includes the final conclusions and future perspectives derived from this work. The articles are included at the end of this dissertation, as well with an additional supplementary non-published-yet work.

This thesis is submitted for the degree of Doctor of Philosophy at the Universitat Politècnica de Catalunya. The research described in this work was carried out by the author during the period from December 2012 to October 2017 under the supervision of Prof. M. Anglada in the Department of Materials Science and Metallurgical Engineering at the Universitat Politècnica de Catalunya, and during 3 research stays during 2015, 2016 and 2017 (406 days in total) in MTM Department at KU Leuven under the supervision of Prof. J. Vleugels. The work described in this dissertation is original, unless otherwise detailed references are provided.

Keywords: ceramics, zirconia, dental materials, mechanical properties, fracture toughness

ACKNOWLEDGEMENTS

This is one of the most important, if not the most important section of this thesis. It is well-known that this section will be the most read, so it is one of the hardest to write and typically the last one. So there is a lot of pressure on writing this, and everyone who knows me knows that I gave my best on trying to postpone it.

First of all, I would like to thank my supervisor, Marc Anglada, for all his support and knowledge given during these long five years that contributed to my professional and personal growth, and for being always available to discuss about the research and many other topics (such as politics or my fashion decisions). I am (was) his last doctoral student, so I hope to have lived up to the occasion.

I am also grateful to the Spanish "Ministerio de Economía y Competitividad" for the financial support and for teaching me that the less you have, the less you need. One should keep in mind that all the information and views set out in this dissertation are those of the author and do not necessarily reflect the official opinion of the Spanish Ministry. And probably they do not, as we seem to disagree in many other things.

Also to the JECS Trust (and especially Véronique for dealing with all the paperwork and my constant questions) and "La Caixa" Foundation, which kindly allowed me visit Leuven for the third time.

I would also like to give my gratitude to all the CIEFMA group, particularly to Luis, Emilio, Joan Josep and Fernando for all their constant help. Also, Trifon and Montse from the former CRnE (Multiscale from now on) for their capability and predisposition.

I would not have finished my thesis without the priceless help of Irene. Without her I would still be lost in the intricate bureaucratic nooks and crannies like Asterix in The Twelve Tasks. Neither without María Ángeles, for trying every day to fix the world and for keeping my plants alive.

I also want to express my gratitude to Javier Peña, who taught me that there is something called materials science and gave me the interest to start on this strange path I find myself in.

I cannot thank enough those that have made this tedious and sustained pain of doing a PhD one of the best moments of my life: Berni, both Danielas, Erica, Erik, Giuseppe, Ina, Jing, Jose, Latifa, Mireia, Newsha, Quentin, Roberta, Romain, Yassine; and also to Andreas, Anna, Clàudia, Joanna and Yago, among others. Without them I would probably have finish the thesis much earlier. Also to Mar, for everything she has to deal with every day.

My sincere gratitude to Jef for allowing me to work repeatedly with them in Leuven and to Fei for all her patience to teach me. I would also like to extend my gratitude to all the MTM staff, especially to Paul and the people from the Secretariaat for organising those amazing events and barbecues.

And, of course, all the great friends I made there: Aljaž, Andrea, Annabel, Bensu, Bey, Gaurav, Goku, Iñigo, Karel, Kim, María, Miguel (and Pimienta), Matteo, Nachi, Pierre, Tomas, and everyone else I met in my already second home. I will for sure come back, probably when the weather is a bit better (as a migratory bird).

I will always be thankful and in debt with my brother from another mother, Ramón, Sandra and their not-so-little-anymore Leia, for keeping me open-minded and sceptical about my results, proceedings and life choices, and for celebrating my small victories as their own.

I also want to include all the amazing people I met during these long years and with whom I shared great experiences. Without them I would not be the person I am today. So it is all your fault.

Of course, to all my family (including Atlas) that supported me and tried to understand what I was doing with my life. I still do not know, please stop asking. I am especially grateful to my parents for their daily concerns about the thesis and their constant reminder that "I had better finish it soon".

And finally, I would like to thank to anyone taking their time to read this thesis, even who is reading only this section wondering if they are included. Now you are.

PREFACE

Materials are the perfect scapegoat: they meekly suffer our anger and clumsiness. If the screen of our phone cracks because it fell from our pockets while biking too fast, or if we ham-fistedly throw the just-washed dish on the floor. We always blame materials.

Unlike the common thinking of considering materials as "inert, static things", materials also react to environment, as we do. Like human psyche, most materials require of a certain specific environment to keep being stable; losing their integrity if they remain in a situation they do not like. Some materials even change their colour when heated [1] or exposed to UV light [2], just like British in Benidorm.

The subject of this thesis, zirconia, is a bit of a drama queen: it is deeply affected by humidity, grain size, small differences in dopant content, impurities, density, slight variations on temperature, oxygen supply during sintering, stress rate, a sloppy polishing… One should really take care of every parameter when testing this histrionic material.

In front of adverse situations, materials can get tensed, in the form of internal residual stresses, and if the stresses are too high they may crack, like when the deadline to finish an everlasting thesis is approaching. It is probably not a coincidence that the term resilience, the capacity of overcoming an adversity, is applied both in human psychology and materials science. In some cases, some materials develop an increasing resistance against cracks, like our immune system trying to fight a cold.

Despite the unfounded nostalgic saying of "things are not made like before", technological advances and scientific research are succeeding in producing better materials, understanding their fundamentals and optimising their properties for each application. However, things are still breaking.

[1] Day, J. H. Thermochromism. *Chem. Rev.* **63,** 65–80 (1963).
[2] Hirshberg, Y. Photochromie dans la serie de la bianthrone. *C. R. Acad. Sci.* **231,** 903 (1950).

Unlike us (or at least, some people), materials are not smart (even if some of them are just called like that). Therefore, we should be the ones using the not-so-smart materials smartly.

In most cases, especially in the case of brittle ceramics, the fault does not lay in the material itself. Very often there is a lack of good mechanical design due to an insufficient understanding of the material, and an improper fabrication, machining, handling or use. Materials are not inherently bad, only sometimes misused.

Thus, this dissertation is only a small attempt to contribute to the better understanding of certain aspects of particular compositions of a specific material used in delimited conditions of defined applications.

—Miquel Turón Viñas

LIST OF PUBLICATIONS

This dissertation is based on the publications listed below: [§]

Article I

Turon-Vinas, M. & Anglada, M. Fracture toughness of zirconia from a shallow notch produced by ultra-short pulsed laser ablation. *J. Eur. Ceram. Soc.* **34**, 3865–3870 (2014). **IF**: 2.947. **Q1:** 1/26 in "Materials science, ceramics".

Article II

Turon-Vinas, M. & Anglada, M. Assessment in Si_3N_4 of a new method for determining the fracture toughness from a surface notch micro-machined by ultra-short pulsed laser ablation. *J. Eur. Ceram. Soc.* **35**, 1737–1741 (2015). **IF**: 2.933. **Q1**: 1/27 in "Materials science, ceramics".

Article III

Turon-Vinas, M., Morillas, J., Moreno, P. & Anglada, M. Evaluation of damage in front of starting notches induced by ultra-short pulsed laser ablation for the determination of fracture toughness in zirconia. *J. Eur. Ceram. Soc.* **37**, 5127–5131 (2017). **IF**: 3.454. **Q1**: 1/26 in "Materials science, ceramics". *(JCR data from 2016)*

Article IV

Turon-Vinas, M., Roa, J. J., Marro, F. G. & Anglada, M. Mechanical properties of $12Ce–ZrO_2/3Y–ZrO_2$ composites. *Ceram. Int.* **41**, 14988–14997 (2015). **IF**: 2.758. **Q1**: 3/27 in "Materials science, ceramics".

[§] **IF:** Impact factor on the moment of publication; **Q:** Quartile

Additional work on co-doping of zirconia done in collaboration with MTM Department in KU Leuven (Belgium) is included:

Appended manuscript

Turon-Vinas, M., Zhang, F., Vleugels, J. & Anglada, M. Effect of calcia co-doping on ceria-stabilized zirconia. *Submitted to J. Eur. Ceram. Soc.* (2017).

Non-included related articles

Roa, J.J., Turon-Vinas, M., Tovar, D., Ledesma, J. & Anglada, M. Chemical and nanoindentation study of diffusion during sintering of 12Ce-ZrO_2/3Y-ZrO_2 powder layers. *Accepted in Ceram. Int.* doi: 10.1016/j.ceramint.2017.10.226 (2017).

Melk, L., Turon-Vinas, M., Roa, J. J., Antti, M.-L. & Anglada, M. The influence of unshielded small cracks in the fracture toughness of yttria and of ceria stabilised zirconia. *J. Eur. Ceram. Soc.* **36,** 147–153 (2016).

Melk, L., Mouzon, J., Turon-Vinas, M., Akhtar, F., Antti, M.-L. & Anglada, M. Surface microstructural changes of spark plasma sintered zirconia after grinding and annealing. *Ceram. Int.* **42,** 15610–15617 (2016).

Roa, J. J., Turon-Vinas, M. & Anglada, M. Surface grain size and texture after annealing ground zirconia. *J. Eur. Ceram. Soc.* **36,** 1519–1525 (2016).

Other contributions

Poster and oral presentations

Turon-Vinas, M. & Anglada, M. Effect of small additions of calcia on the grain size and mechanical properties of ceria-stabilized tetragonal zirconia. *15th European Inter-Regional Conference on Ceramics (CIEC15).* Oral presentation (Lyon, France, 5th -7th September 2016).

Roa, J. J., Aboulfadl, H., Barrirero, J., Turon-Vinas, M., Mücklich, F. & Anglada, M. Analysis and 3D microstructural characterization for the Ce, Y and Zr elements through the grain boundaries of 12Ce-ZrO_2/3Y-ZrO_2 composites as a

function of the sintering temperature. *15th European Inter-Regional Conference on Ceramics (CIEC15)*. Poster (Lyon, France, 5th -7th September 2016).

Turon-Vinas, M. & Anglada, M. Fabricación de entallas mediante ablación láser de pulso ultracorto para la determinación de la tenacidad de fractura de circona (Notch fabrication by ultrashort pulsed laser ablation for fracture toughness determination of zirconia). *XIV Congreso Nacional de Materiales (CNM14)*. Oral presentation (Gijón, Spain, 8th -10th June 2016).

Turon-Vinas, M., Morillas, J., Moreno, P. & Anglada M. Análisis de entallas realizadas por ablación láser mediante tomografía FIB (Analysis of notches produced by laser ablation by means of FIB tomography). *XXXIII Encuentro del Grupo Español de Fractura (GEF33)*. Oral presentation (San Sebastián, Spain, 9th -11th March 2016).

Turon-Vinas, M. & Anglada, M. Determinación de la tenacidad de fractura a partir de entallas producidas por láser de femtosegundo en circona nanométrica (Fracture toughness determination from notches produced by femtosecond laser of nanometric zirconia). *XXXI Encuentro del Grupo Español de Fractura (GEF31)*. Oral presentation (San Lorenzo del Escorial, Spain, 2nd-4th April 2014).

Turon-Vinas, M., Melk, L. & Anglada, M. Determinación de la tenacidad de fractura de zirconia dopada con itria (3Y-TZP) y de materiales nanocompuestos de 3Y-TZP reforzados con nanotubos de carbono (Fracture toughness determination of yttria-doped zirconia (3Y-TZP) and 3Y-TZP nanocomposites reinforced with carbon nanotubes) *LIII Sociedad Española de Cerámica y Vidrio / XII Congreso del Técnico Cerámico (SECV-ATC)*. Poster (L'Alcora, Spain, 23rd-25th October 2013).

Thesis co-supervision

Ludwig, M. Producción y caracterización mecánica y microestructural de circona estabilizada con ceria (Production and mechanical and microstructural characterization of zircona stabilized with ceria). Master thesis (2015).

Morillas, J. Microfisuración de entallas en cerámicas mediante mecanizado por ablación con pulsos láser ultracortos (Notch microcracking on ceramics by ultrashort pulsed laser ablation). Master thesis (2015).

Joly, A. Desarrollo y caracterización de circona dopada con itria y ceria (Development and characterization of zircona doped with yttria and ceria). Master thesis (2015).

Lallemand, S. Desarrollo y caracterización de un material compuesto (Ce,Y)-TZP/Al_2O_3 (Development and characterization of (Ce,Y)-TZP/Al_2O_3 composite material). Master thesis (2014).

TABLE OF CONTENTS

Abstract i

Acknowledgements iii

Preface v

List of publications vii

Table of contents xi

List of figures and tables xiii

Chapter 1 Introduction 1

1.1 Zirconia ceramics 3

1.1.1 History of zirconia 3

1.1.2 Applications 5

1.1.3 Classification 7

1.2 Stabilisation 8

1.2.1 Effect of dopants 8

1.2.2 Tetragonal-to-monoclinic transformation 16

1.2.3 Low-temperature degradation (LTD) 23

1.3 Improving LTD resistance 29

1.3.1 Ceria-stabilised zirconia 32

1.3.2 Grain boundary segregation 33

1.4 Improving mechanical properties 35

1.4.1 Grain size refinement 36

1.4.2 Composites 37

1.5 Fracture toughness 39

1.5.1 Vickers indentation 40

1.5.2 Precracked bending specimens 42

1.5.3 R-curve 46

1.5.4 Toughening mechanisms 48
1.5.5 Relation between fracture toughness and strength 49
Chapter 2 Aims and scope 53
2.1 Fracture toughness determination 55
2.1.1 Fabrication of small notches 55
2.1.2 Analysis of the damage 56
2.1.3 Assessment of the methodology 56
2.2 Novel co-doped zirconia materials 57
2.2.1 Yttria-ceria 58
2.2.2 Ceria-calcia 58
Chapter 3 Summary of results 61
3.1 Fracture toughness determination 63
3.2 Novel co-doped zirconia materials 65
Chapter 4 Conclusions and perspectives 67
4.1 Ultra-short pulsed laser ablation 69
4.2 Grain growth inhibition 69
References 71
Article I Fracture toughness of zirconia from a shallow notch produced by ultra-short pulsed laser ablation 91
Article II Assessment in Si_3N_4 of a new method for determining the fracture toughness from a surface notch micro-machined by ultra-short pulsed laser ablation 99
Article III Evaluation of damage in front of starting notches induced by ultra-short pulsed laser ablation for the determination of fracture toughness in zirconia 107
Article IV Mechanical properties of $12Ce–ZrO_2/3Y–ZrO_2$ composites 115
Appended manuscript Effect of calcia co-doping on ceria-stabilized zirconia 127
Glossary of acronyms 145

LIST OF FIGURES AND TABLES

Figure 1.1 Pure zirconia polymorphs: (a) cubic, (b) tetragonal and (c) monoclinic. Red spheres represent Zr and blue goes for O [3]. **3**

Figure 1.2 Oxygen vacancies formation into the ZrO_2 lattice through the addition of Y_2O_3 [43]. **8**

Figure 1.3 Schematic illustration of tetravalent doping of zirconia: decrease of the tetragonality in the case of oversized dopants (left) and increase in the case of undersized dopants (right). Numbers indicate atom positions in *b* direction [51]. **10**

Figure 1.4 Zirconia-yttria phase diagram evolution. (a) Original diagram by Duwez in 1951 [54], (b) a revision proposed by Scott in 1975 [55], (c) a recent diagram, and (d) the metastable diagram [29]. **12**

Figure 1.5 Zirconia-ceria phase diagram (redrawn by [29] from [56]). **13**

Figure 1.6 Zirconia-magnesia phase diagram. The shaded area corresponds to the most commonly used compositions, and the arrows indicate the favoured annealing temperatures (adapted by [3] from [62]). **14**

Figure 1.7 Zirconia-calcia phase diagram (adapted from [64]). **15**

Figure 1.8 Steps of the tetragonal (*t*) to monoclinic (*m*) phase transformation. (a) Single metastable *t* phase. (b) First *m* martensite plate nucleation, which is followed by (c) a second plate, with an opposite shear strain direction than the first *m* variant. (d) This process is repeated successively to accommodate the shear strain [3]. **16**

Figure 1.9 Schematic illustration of a martensitic plate (monoclinic) formed in a parent phase (tetragonal) through a habit plane [29]. **17**

Figure 1.10 (a) Schematic view of a surface relief produced by a pair of martensite variants [73] and (b) AFM image (3D-view) of a surface uplift produced by the $t \rightarrow m$ transformation [74]. **18**

Figure 1.11 Schematic view of transformation zones and toughness increments (ΔK_c) development with different crack extensions (from [79] after [80]). **19**

Figure 1.12 Critical tetragonal grain size as function of Y2O3 content (from [25] after [84]). **20**

Figure 1.13 Hysteresis loops for (A) ferromagnetic, (B) ferroelectric, and (C) ferroelastic materials. The shaded area in (C) is the energy absorbed in reorientation of domains during fracture [90]. **21**

Figure 1.14 Representation of all six possible orientations of *c*-axis in a polydomain basic cell. The arrows indicate the directions of *c*-axes [96]. **22**

Figure 1.15 First steps of LTD in Y-TZP: (a) Diffusion of water species via oxygen vacancies and (b) the resulting variation of lattice parameters [29]. **24**

Figure 1.16 Process of microcracking and monoclinic phase propagation process: (a) in a grain boundary inside the material and (b) in the surface [106]. **25**

Figure 1.17 Time-temperature-transformation curve of a 2.8 mol% yttria-stabilised zirconia [124]. **26**

Figure 1.18 Kinetics of LTD of zirconia stabilised with 10 mol% of ceria (10Ce-TZP), with 3 mol% of yttria (3Y-TZP), magnesium partially stabilised zirconia (Mg-PSZ), alumina-toughened zirconia (A80Z3Y) and zirconia-toughened alumina (A10Z0Y) measured at 134 °C on the bottom X-axis and expected at 37 °C on the top. The shadowed areas give uncertainty ranges when they can be evaluated [29]. **27**

Figure 1.19 Defect distributions in the grain boundary interfaces and the space-charge layers of YSZ [133]. **28**

Figure 1.20 Phase transformation dependence on yttria content for TZPs with grain size of ~0.4 μm aged in air at 300 °C (from [25] after [83]). **30**

Figure 1.21 Grain size dependence (from [25] after [83]). **31**

Figure 1.22 HAADF-STEM images and STEM-EDS elemental maps and distribution of 3Y-TZPs doped with 0.3 mol% Al_2O_3 and 0.4 mol% Sc_2O_3, Nd_2O_3 and La_2O_3. The spheres represent qualitatively the size of the dopant cations, Al^{3+}, Sc^{3+}, Nd^{3+} and La^{3+}, respect to the Zr^{4+} host cation [118]. **34**

Figure 1.23 Relationship of yttria and ceria composition and a) fracture toughness and b) bending strength [147]. **35**

Figure 1.24 Surface monoclinic phase content as a function of hydrothermal testing time at 134 °C for 2Y-TZP with different amounts of alumina [116]. **38**

Figure 1.25 Fraction of monoclinic phase measured after 40 h of hydrothermal ageing as a function of the 3Y-TZP volume content in the ZTA composite. The grey area represents the percolation threshold [210]. **39**

Figure 1.26 Imprint and cracks formed by a Vickers indentation: Palmqvist-type crack on left and median crack on right (adapted from [212,213]). **40**

Figure 1.27 Relation between the shape of the crack and the determined K_{Ic}: solid curve corresponds to radial median cracks, and dashed line to Palmqvist cracks [215]. **41**

Figure 1.28 Schematic geometry of V-notch obtaining by a saw cut and thinning its tip with a razor blade [228]. **44**

Figure 1.29 Dependence of measured fracture toughness (K_{Ic}) on notch-root radius (ρ) (from [215] after [225]). **44**

Figure 1.30 a) Schematic view of a crack with length a in front of a notch with radius R, b) and its influence on stress intensity factor [230]. **45**

Figure 1.31 Representation of the stress intensity factor variation with crack extension a) flat and b) rising crack-resistance curve (R-curve) [215]. **46**

Figure 1.32 Instability for fracture for a rising R-curve [215]. **47**

Figure 1.33 Schematics of flat and rising R-curves. A material with a flat R-curve has a single value of toughness, while for materials with rising R-curves there is no single value of toughness [241]. **47**

Figure 1.34 R-curves for various ceramics, obtained from long cracks. [3] **48**

Figure 1.35 Schematic illustration of different examples of intrinsic toughening occurring in front of the crack tip and extrinsic mechanisms that act primarily behind the tip [245]. **49**

Figure 1.36 Failure behaviour of materials with R-curve and an initial a) short and b) long crack [215]. **50**

Figure 1.37 Strength-toughness relation for various PSZ and TZP ceramics. [249] **51**

Table 1.1 Mechanical properties of different ceramics for biomedical applications [21]. **6**

Table 1.2 Effective ionic radii for 8-fold coordination of different metallic oxides [50]. **9**

CHAPTER 1
INTRODUCTION

This chapter is divided in five sections:

The first part, Zirconia, consist in a brief history of zirconia ceramics and their applications, and the first studies that successfully lead to the stabilised zirconia materials. All the different types of zirconia-based ceramics and the discoveries and problematics are written in chronological order as they arose.

The second part, Stabilisation, address the causes and effects of the stabilisation of the tetragonal phase of zirconia, focusing on how to obtain the metastable phase and the, good and bad, consequences.

The third and fourth sections, Improving LTD resistance and Improving mechanical properties, respectively, focus on the theoretical background to obtain novel zirconia materials that enhance the advantages and reduce the disadvantages of transformable zirconia-based ceramics.

Finally, the fifth part, Fracture toughness, is an introduction of fracture mechanics and the problematics of measuring the crack-growth resistance of ceramic materials, emphasizing how to correctly measure it in the case of transformable ceramics such as zirconia.

1.1 Zirconia ceramics

1.1.1 History of zirconia

Zirconium dioxide (ZrO_2), known as zirconia, is a crystalline ceramic material identified as such in 1789 by the German chemist Martin Heinrich Klaproth. The word zirconium comes from the mineral zircon, which derives from the Persian *zargun* (زرگون) "gold-colored" [1]. It is found in nature mainly in baddeleyite in its monoclinic form. During centuries, it was only used blended with rare earth oxides as a pigment for ceramics due to the impossibility of producing solid and dense bricks after firing.

During the early 20's, it attracted interest because of its excellent refractory properties due to its high melting point (~2715 ºC). However, some failures observed on its use as an enamel opacifier led to some investigations about its high temperature crystal structures [2].

At room temperature, the stable structure of pure zirconia is monoclinic (*m*), which transforms to tetragonal (*t*) phase upon heating (~1170–2370 ºC) and to cubic (*c*) structure (fluorite) at higher temperatures (2370–2680 ºC), as depicted in Figure 1.1 [3].

The transformation from tetragonal to monoclinic ($t \rightarrow m$) is athermal and diffusionless, i.e. martensitic and reversible, and it involves a volume expansion of ~4%. Nowadays it is known that this expansion creates high internal stresses, which

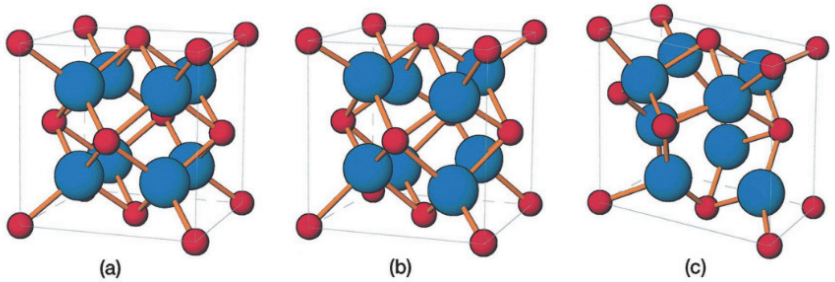

Figure 1.1 Pure zirconia polymorphs: (a) cubic, (b) tetragonal and (c) monoclinic. Red spheres represent Zr and blue goes for O [3].

induce cracking and may result in a failure of the component upon cooling from sinterization, and for that reason the applications of zirconia as structural ceramic were very limited.

During decades, the interest was focused in obtaining those high temperature structures at lower temperatures. However, the first experiments by rapid quenching did not offer consistent results [4].

The tetragonal structure of zirconia was first reported in 1929 by Ruff et al. [5]. They also observed that the addition of different oxides (MgO [5], SrO, BaO, Sc_2O_3, Y_2O_3, La_2O_3, CeO_2, FeO, Al_2O_3, CaO [6], ThO_2 [7] or BeO [8]) changed the transformation temperature and could stabilise the cubic form at lower temperatures.

Thus, it was finally possible to stabilise at room temperature the cubic phase of zirconia by the addition of large amounts (16 to 30 mol%) of either calcia or magnesia [9]. These materials are known as fully-stabilised zirconia (FSZ).

Clark and Reynolds, in 1937, were able to produce metastable tetragonal zirconia at room temperature for the first time by annealing amorphous zirconia obtained from salts [2], but the first results were not consistent and reproducible as the nature of the transformation was not fully understood.

The martensitic nature of the $t \rightarrow m$ transformation was first suggested in 1963 [10]. In 1965, Garvie [11] observed that there is a critical crystallite size above which the metastable tetragonal phase cannot exist at room temperature, and therefore the control of powder processing was of great importance.

Garvie and Nicholson [12] then observed that improved mechanical properties were obtained in a cubic stabilised material containing nanometric monoclinic precipitates, known as partially-stabilised zirconia (PSZ).

In 1975, Garvie et al. [13] discovered that a fine dispersion of nanometric tetragonal particles in a cubic matrix of zirconia stabilised with calcia enhanced enormously the strength of the material due to the stress-induced transformation of the metastable tetragonal phase to monoclinic.

It was stated that the increase of strength was produced mainly by the "absorption of energy" during the martensitic $t \rightarrow m$ transformation. This phase transformation is accompanied by a ~4% increase in volume around the crack tip which closes the crack and increases its propagation resistance, increasing the

fracture toughness, therefore the mechanism is referred to as transformation toughening [3].

Finally, Rieth et al. [14] and Gupta et al. [15] were the first ones succeeding on the fabrication of PSZ containing only tetragonal phase, which were later known as tetragonal zirconia polycrystals (TZP), by stabilising with yttria.

Since then, zirconia-based ceramics found application as a structural material due to their excellent mechanical properties and chemical stability.

1.1.2 Applications

These properties make zirconia ceramics suitable for applications in aggressive environments involving high refractory, corrosion and thermal shock resistant parts like extrusion dyes, valves and port liners for engines and in foundry, thermal barrier coatings (TBCs), wear resistant components like blades and bearings and high temperature ionic conductive applications like solid electrolytes in fuel cells and in oxygen sensors. Also, its biocompatibility and good mechanical properties makes zirconia interesting as a biomaterial [16,17].

In 1988, Christel et al. [18] introduced the first use of zirconia to manufacture ball heads for total hip replacements (THR). Even though at the early stages several stabilising oxides (like CaO or MgO) were used, in the 90's, zirconia-yttria ceramics became the most interesting alternative to alumina in orthopedics because of its higher strength and fracture toughness, which allows smaller femoral heads (see Table 1.1). More recently, zirconia has found application in prosthetic dentistry for dental implants, crowns, bridges and abutments, due to its good mechanical properties, aesthetics, and also easy color modification [17,19].

However, even though biomedical grade 3% mol yttria-tetragonal polycrystalline zirconia (so-called 3Y-TZP) exhibits the best mechanical properties of oxide ceramics due to phase transformation toughening, its application in femoral heads has been limited due to the discovery of the spontaneous transformation of the metastable tetragonal phase to its monoclinic form in aqueous atmospheres, which deteriorates the surface mechanical properties of 3Y-TZP. This phenomenon, known as aging, hydrothermal degradation or low-temperature degradation (LTD), was first observed in 1981 by Kobayashi et al. [20].

Table 1.1 Mechanical properties of different ceramics for biomedical applications [21].

Material	Toughness (MPa $m^{1/2}$)	Strength (MPa)	Vickers hardness
Alumina	4.2	400–600	1800–2000
Zirconia	5.4	1000	1200–1300
A10Z0Y	5.8	700–900	1800
Hydroxyapatite	0.9	50–60	500
Tricalcium phosphate	1.3	50–60	900
Mg-PSZ	8.0	600	1000
12Ce-TZP	7.8	700	1000–1100
Micro-nano-alumina-zirconia	6.0	600	1800
Nano-nano-Ce-TZP-alumina	8.4	900	1300

This sudden transformation to monoclinic produces internal stresses due to the higher volume of the monoclinic phase that may lead to microcracking, reducing drastically the mechanical properties of the ceramic (LTD will be discussed in more detail in section 1.2.3).

In 1997, the Food and Drugs Administration (FDA) sent a warning of the possible aging effects in zirconia prostheses after sterilisation [22] and, due to a posterior sudden increase in the percentage of in vivo failure of 400 Prozyr® (Saint-GoBain, France) femoral heads in 2001–2002 [23], the use of zirconia ceramics for prostheses stopped abruptly in Europe and opened a controversial debate [24].

This phenomenon has been extensively studied [25–30] but not yet fully understood. It is known that it takes place in presence of water vapour or aqueous solutions, it is time-dependent and proceeds most rapidly at temperatures of 200-300 ºC, but it can occur also at lower temperatures [25,31].

Y-TZP is not currently used in orthopaedic applications in Europe. In spite of that, surprisingly, the use of zirconia in the recent years for dental restorations is becoming increasingly popular [19]. Partly, this is due to the development of novel zirconia grades with increased resistance to LTD. Also, in some dentistry restorations, zirconia is not in direct contact with the environment since it is coated by porcelain, and the consequences of a lack of reliability is less dramatic than in hip or knee replacements.

Although there is no clear clinic evidence of serious problems of dental zirconia related to LTD, the number of clinical studies is still small, and the majority

are not controlled clinical trials and have limited 3- to 5-year follow-up [32–37]. Therefore, the long-term performance of dental zirconia is still unknown, and it is very likely that degradation is still an issue in those applications where degradation of surface mechanical properties are of paramount importance, like in the interface between the ceramic core and the veneering.

The use of full-contour Y-TZP restorations without the aesthetic veneering porcelain is increasing in the last years, because it avoids chipping of the veneering porcelain, which is the most commonly reported issue for dental zirconia restorations [38,39]. However, that exposes the Y-TZP to the oral cavity, which represents a hostile environment: aqueous saliva, pH and temperature changes, and cyclic loading during mastication threaten the stability of the restoration [40]. It has also been reported that corrosive environments (such as acidic and alkaline environments) can also trigger spontaneous phase transformation and affect mechanical properties [41].

Hence, in the last years, most effort has been put to make TZP ceramics more resistant to LTD. This will be discussed in section 1.3.

1.1.3 Classification

Broadly, zirconia-based ceramics can be classified in three major groups according to the final microstructure achieved:

Fully stabilised zirconia (FSZ), also known as cubic-stabilised zirconia (CSZ), is obtained with large concentration of stabilisers. It has a single-phase microstructure formed by large cubic grains. It is mostly used for high-temperature applications (heat exchangers, thermal barrier coatings, solid electrolytes, fuel cells or oxygen sensors), but recently they also found application in dentistry due to their high translucency. Moreover, single crystals of cubic zirconia are used as a synthetic substitute of diamonds.

Partially stabilised zirconia (PSZ) consists of nanosized tetragonal or monoclinic precipitates embedded in a cubic matrix, and it is generally obtained with the addition of magnesia or calcia.

Tetragonal zirconia polycrystals (TZP) are generally considered as fully tetragonal, but may contain also a secondary cubic phase depending on the amount of stabiliser. These ceramics (as well as PSZ with tetragonal precipitates) possess high fracture toughness due to the stress-induced $t \rightarrow m$ transformation around the crack during its propagation.

This thesis will be mainly focused on TZP-based ceramic materials.

1.2 Stabilisation

1.2.1 Effect of dopants

As stated previously, the method to stabilise high-temperature phases of zirconia at low temperature is by doping with certain aliovalent ions.

The Zr atom is too small to maintain the 8-fold fluorite structure at low temperatures due to the oxygen overcrowding around it, which generates internal strain that is partially relieved by changing the atom ordering to a 7-fold monoclinic structure (as the cation-anion radius ratio is below 0.732 [42]). The addition of dopants with typically higher cation radius and lower valence, substitute Zr^{4+} and introduce oxygen vacancies in order to maintain charge neutrality, as illustrated in Figure 1.2.

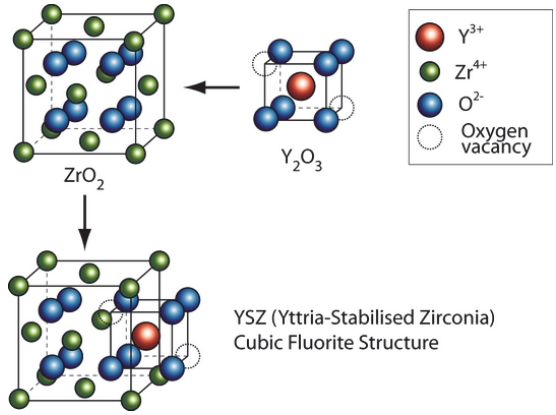

Figure 1.2 Oxygen vacancies formation into the ZrO_2 lattice through the addition of Y_2O_3 [43].

For example, in the case of doping with Y_2O_3 one vacancy is formed for every two yttrium ions. Using Kröger-Vink notation [44]:

$$Y_2O_3(ZrO_2) \rightarrow 2Y'_{Zr} + 3O_O^x + V_O^{\bullet\bullet} \quad 1.1$$

where, Y'_{Zr} represents the Y^{3+} ions on cationic sites, substituting Zr^{4+} ions and, therefore, with a relative charge of -1. O_O^x stands for oxygen ions on anionic sites and with neutral charge and $V_O^{\bullet\bullet}$ means the double positively charged oxygen vacancies introduced in the lattice for charge compensation.

Thus, the stabilization is only a consequence of the oxygen overcrowding relief and the consequent lattice relaxation around the oxygen vacancies associated to Zr atom introduced by these dopants for charge compensation rather than for the aliovalent dopant itself, as it occurs with oversized (respect to the Zr^{4+}) trivalent dopants such as Y^{3+} or Gd^{3+} [45–47].

The presence of these vacancies reduces the average cation coordination number to a value between 7 and 8 depending on the dopant concentration, making the local atomic environments in the stabilised material different from the corresponding stoichiometric high-temperature phases (tetragonal and cubic) [47,48].

These oxygen vacancies show a preference to be closer to the smaller cation. Therefore, for oversized cations, the vacancies will be closer to Zr ions, while in the case of undersized they will be bonded to the dopant cations [46,49]. The effective ionic radii of different cations can be seen in Table 1.2.

Table 1.2 Effective ionic radii for 8-fold coordination of different metallic oxides [50]. * 6-fold coordination

Cation	Ionic radius (Å)	Cation	Ionic radius (Å)
Ge^{4+}	0.53*	Mg^{2+}	0.89
Al^{3+}	0.535*	In^{3+}	0.92
Cr^{3+}	0.615	Ce^{4+}	0.97
Ga^{3+}	0.62*	Yb^{3+}	0.985
Ti^{4+}	0.74	Y^{3+}	1.019
Nb^{5+}	0.74	Gd^{3+}	1.053
Fe^{3+}	0.78	Nd^{3+}	1.109
Hf^{4+}	0.83	Ca^{2+}	1.12
Zr^{4+}	0.84	Ce^{3+}	1.143
Sc^{3+}	0.87	La^{3+}	1.160

However, the tetragonal phase of zirconia, can also be stabilised either by smaller cations and/or with higher valences. As the stabilising mechanism is explained by the oxygen vacancies associated to Zr ions, the stabilization effect of undersized trivalent (or divalent) dopants (such as Fe^{3+}, Ga^{3+} and Al^{3+}) and tetravalent cations that do not introduce vacancies (such as Ge^{4+} or Ce^{4+}), cannot be explained by the described model [46,51].

Undersized trivalent dopants, such as Fe^{3+} and Cr^{3+}, compete with Zr cation for the oxygen vacancies (as the anionic vacancies tend to be close to the smaller cation [49]) and highly distort the network, and therefore their ability to relieve the oxygen crowding around Zr is diminished and, consequently, their stabilization effect. Their stabilising effect can be explained by the large distortion of the lattice they create, but that also decreases their solubility [46].

In the case of dopants with similar radius than Zr^{4+}, oxygen vacancies have no particular preference, thus being less prone to be tied up by the cations, increasing their mobility and making these dopants suitable for ion conductivity applications such as solid oxygen fuel cells (SOFC) [49].

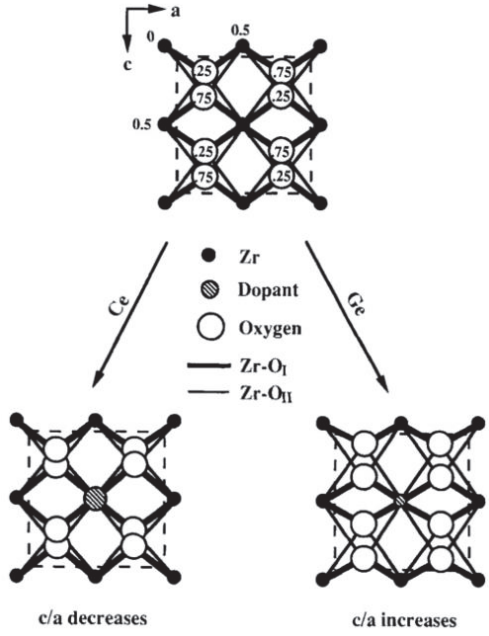

Figure 1.3 Schematic illustration of tetravalent doping of zirconia: decrease of the tetragonality in the case of oversized dopants (left) and increase in the case of undersized dopants (right). Numbers indicate atom positions in *b* direction [51].

For oversized tetravalent dopants, such as Ce^{4+}, the large difference in the distance between dopant-O and Zr-O produces a large distortion that dilates the cation network and reduces the tetragonality (see Figure 1.3), which increases the stability of the tetragonal phase because of the decrease in strain energy [51]. In the case of undersized tetravalent dopants, such as Ge^{4+}, the network is not distorted and therefore the tetragonality increases. However, they provide a stronger cation-O bond and create a solute cation ordering that reduces the internal strain energy of the Zr cation sublattice [51].

Therefore, the stabilisation of the tetragonal (or cubic) structure is obtained by the relaxation of the internal strain of the lattice, which can be achieved by two different mechanisms:

a) by introducing oxygen vacancies associated to Zr ions (the case of trivalent oversized dopants, such as Y^{3+}), or

b) by stabilising the cation network (which relieves internal strain), either distorting the network (like undersized trivalent dopants), dilating the network (in the case of oversized tetravalent dopants, like Ce^{4+}) or creating a strong cation-O bond (in the case of undersized tetravalent dopants).

For divalent dopants, the mechanism is expected to be similar than that for trivalent cations, that is, by oxygen vacancies generation and consequent release of lattice stresses.

A deep study of the stabilisation effect of aliovalent dopants on zirconia can be found on [46,51] and [52]. It has also been observed that the unit-cell parameters and volume increase not only with an increase of cation radius but also with the dopant charge [53].

Yttria

The most common dopant to stabilise the tetragonal phase in zirconia is yttria, generally with a 3% molar content (known as 3Y-TZP).

The zirconia-yttria phase diagram has been refined many times since it was introduced first in 1951 by Duwez et al. [54]; some of them showed in Figure 1.4. The reason is that for reaching equilibrium, transformations need long times because of the slow cation diffusion in zirconia below 1500 ^{o}C: it is estimated that at this sintering temperature, commonly used, several weeks are needed to achieve compositional homogeneity of a 3 μm grain size material [29].

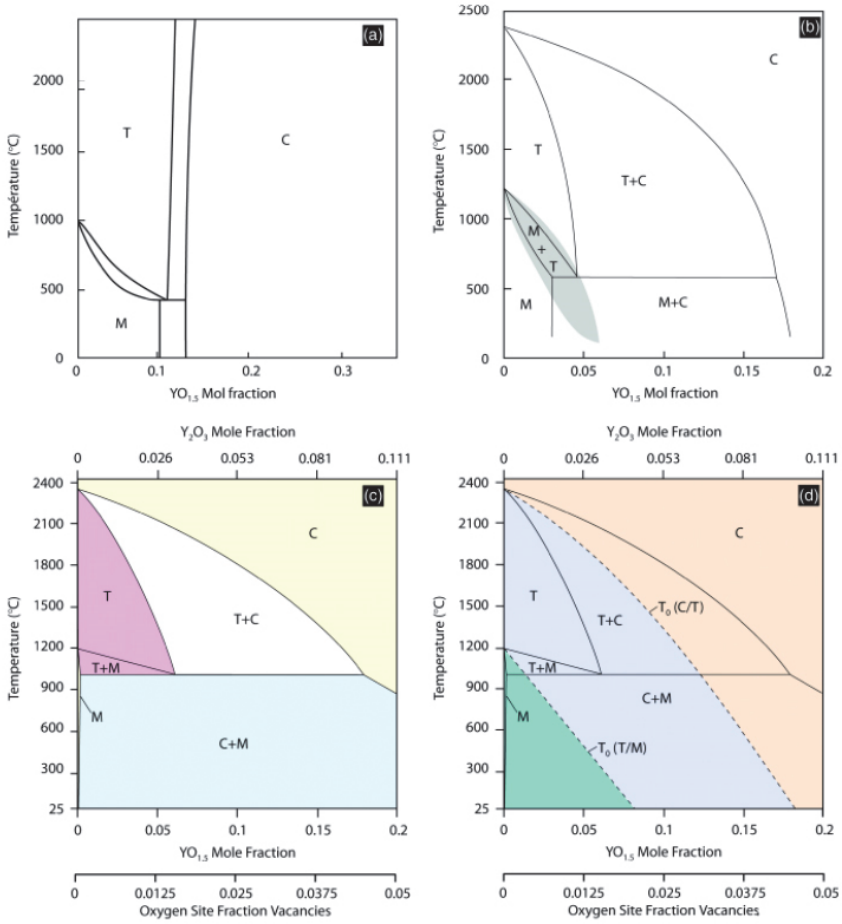

Figure 1.4 Zirconia-yttria phase diagram evolution. (a) Original diagram by Duwez in 1951 [54], (b) a revision proposed by Scott in 1975 [55], (c) a recent diagram, and (d) the metastable diagram [29].

Also, the martensitic transformation has further complicated the location of phase boundaries, and that produced obvious disagreements, as showed by Yashima et al. [56]. Most recent studies combine experimental and computational data [57–61], but there are still some uncertainties, especially in the tetragonal boundary, due to the exceptionally slow diffusion of yttria [29].

As the phase diagrams show the phases present in thermodynamic equilibrium and the tetragonal phase is not thermodynamically stable at room temperature, it is of importance to represent a metastable phase diagram showing the t→m transformation temperature ($T_0^{t\rightarrow m}$, also known as martensitic start

temperature, M_s), below which tetragonal phase is metastable after a non-equilibrium cooling, as seen in dotted lines in Figure 1.4d. The importance of this temperature on the mechanical properties and aging behaviour will be addressed in the next section 1.2.2.

Compositions with 2.5–3 mol% Y_2O_3 are the most typically used for commercial TZP ceramics, generally fabricated from coprecipitated powders. At sintering temperature (typically 1400–1500 ºC), this range composition is either in the tetragonal field, close to the cubic one, or in the *t+c* field. Thus, these compositions usually contain around 60–100% of tetragonal phase of submicrometric equiaxed grain size, being cubic the remaining with larger grains [3].

Ceria

Ceria is also a common dopant for zirconia stabilisation. The main difference with the ZrO_2-Y_2O_3 phase diagram is the wider tetragonal field, as seen in Figure 1.5, which allows stabilization of the tetragonal phase over a wide range of compositions, around 10–16 mol%, being the most common 12 mol% CeO_2 (known as 12Ce-TZP).

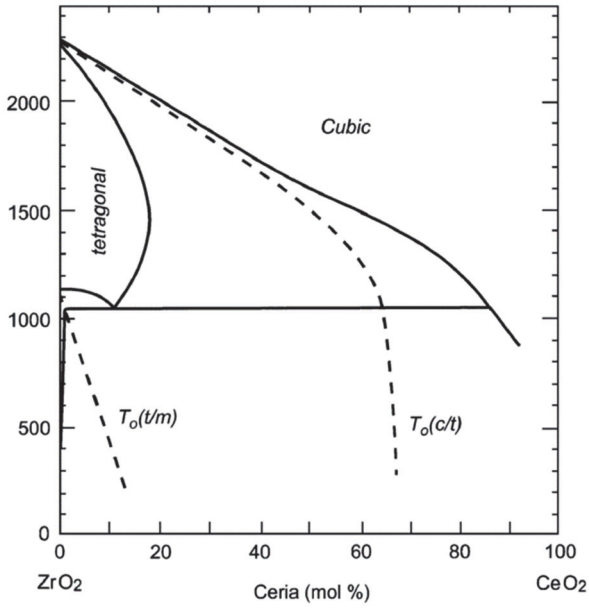

Figure 1.5 Zirconia-ceria phase diagram (redrawn by [29] from [56]).

As-sintered microstructures are similar to those obtained with yttria but with larger tetragonal grain size (1.5–3 μm), which is partly due to the need of higher sintering temperatures and/or longer times for full densification.

As seen previously in this section, Ce^{4+} cations stabilise by dilating the network and not by inducing oxygen vacancies, and this will have an important impact on the low-temperature degradation behaviour. This will be addressed in more detail in section 1.3.1.

Magnesia

Magnesia is typically used in the range 8–10 mol% to produce partially-stabilised zirconia (Mg-PSZ), consisting in a cubic matrix with embedded tetragonal precipitates.

These compositions typically require complex high sintering temperatures (in the cubic single-phase boundary) and complex heat treatments to develop the tetragonal precipitates, with the consequence of coarse microstructure, with grains of 30–60 μm.

Compositions below 8 mol% are not commonly used due their need of higher solid-solution temperatures (see Figure 1.6), and the precipitates formation

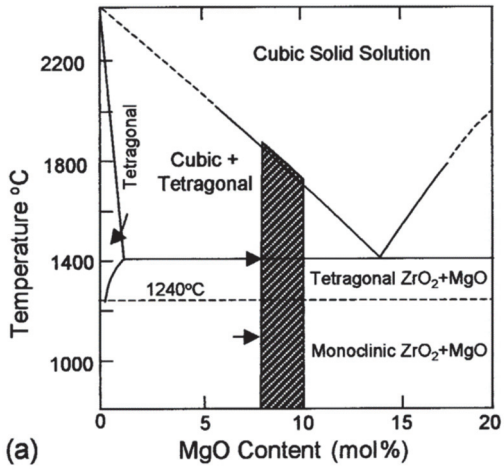

Figure 1.6 Zirconia-magnesia phase diagram. The shaded area corresponds to the most commonly used compositions, and the arrows indicate the favoured annealing temperatures (adapted by [3] from [62]).

needs a high control of temperature, while with amounts higher than 10 mol% the tetragonal particles are not transformable enough to take advantage of the transformation toughening [3]. Transformation toughening will be discussed in detail in the next section 1.2.2.

Calcia

Along with magnesia, calcia was one of the first stabilisers used in zirconia. The first experimental phase diagram was developed in 1929 by Ruff, where they discovered the intermediate $CaZrO_3$ compound [6]. These compounds have a high melting point, which makes them suitable for high refractory applications [9]. The phase diagram for the CaO-poor region can be seen in Figure 1.7.

Further recent investigations discovered other two intermediate compounds at high temperature with >18 mol% CaO contents: $CaZr_4O_9$ ($\square_1$) with monoclinic structure and an hexagonal-ordered phase $Ca_6Zr_{19}O_{44}$ ($\square_2$), and their stability has been discussed [63–69].

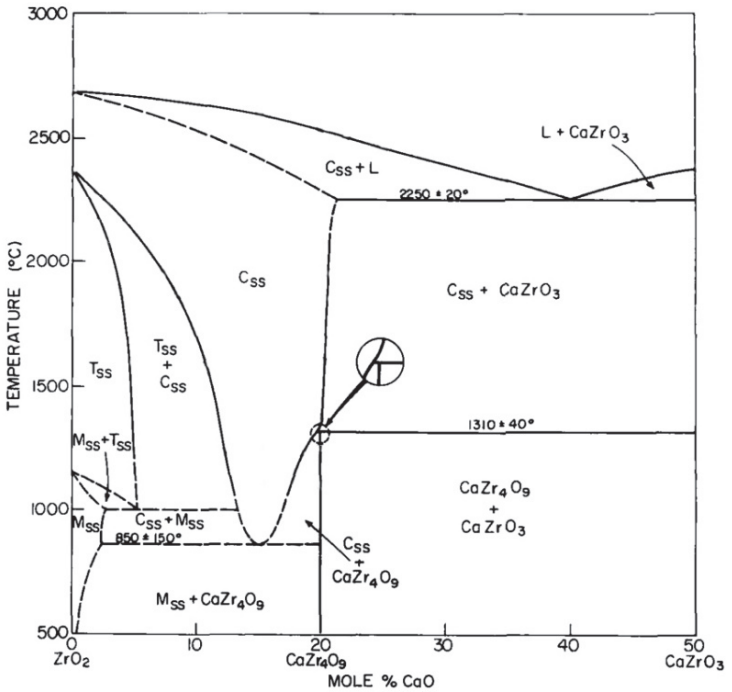

Figure 1.7 Zirconia-calcia phase diagram (adapted from [64]).

Although calcia is more commonly used for producing PSZ, it can also be used as a stabiliser for TZP ceramics [70]. The fabrication of Ca-PSZ also involves high temperatures and heat treatments similar to Mg-PSZ.

1.2.2 Tetragonal-to-monoclinic transformation

The high fracture toughness of zirconia ceramics is mainly achieved thanks to phase transformation toughening, discovered in 1975 by Garvie et al. [13] (more details on toughening mechanisms are given in section 1.5.4). Subbarao et al. published in 1974 an extensive review about the state-of-the-art of zirconia transformation that led to the discovery of transformation toughened ceramics [4].

The transformation of the metastable tetragonal to monoclinic phase involves a volume expansion of ~4%, which produces internal stresses and may induce microcracking. The resulting compressive stresses around the transformed area and the energy spent for the transformation and the microcracking can enhance the fracture toughness of the material when occurs at the crack tip. This transformation is diffusionless, i.e. martensitic, reversible, and can be triggered by both external and internal stresses.

The martensitic nature of the tetragonal-to-monoclinic ($t \rightarrow m$) transformation was suggested in 1963 by Wolten [10], and, about the same time, Bailey [71] reported for the first time the appearance of twins in the resulting monoclinic phase.

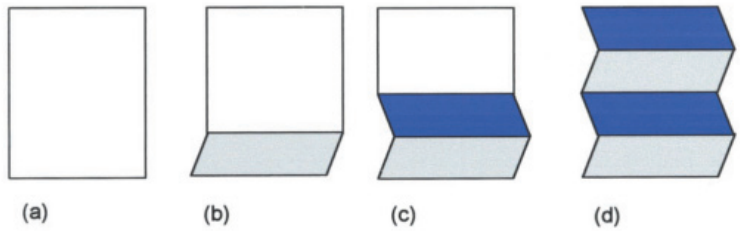

Figure 1.8 Steps of the tetragonal (*t*) to monoclinic (*m*) phase transformation. (a) Single metastable *t* phase. (b) First *m* martensite plate nucleation, which is followed by (c) a second plate, with an opposite shear strain direction than the first *m* variant. (d) This process is repeated successively to accommodate the shear strain [3].

The transformation follows the sequence illustrated in Figure 1.8.The first step of the transformation is the nucleation and growth of a martensite plate of monoclinic phase through a habit plane (see Figure 1.9), which involves a positive volumetric and shear strains that generates opposing stresses in the untransformed surrounding material. Those opposite stresses may induce the formation of another martensite plate (nucleated at the stress concentration regions, which use to be at the end of the previous variant) with a habit plane close to that of the original martensite plate and with an opposite shear strain direction. Thus, the transformation is autocatalytic and those pairs of martensite plates will result in a positive volumetric strain and zero shear strain. This is known as the formation of self-accommodating martensite variants [72].

As the volumetric strain cannot be accommodated, this will result in internal stresses which may induce new nucleation points of martensite plates, microcracking or an effective dilatation of the material.

When this transformation occurs at a free surface it produces a pyramidal relief in the material, as it can be appreciated in Figure 1.10.

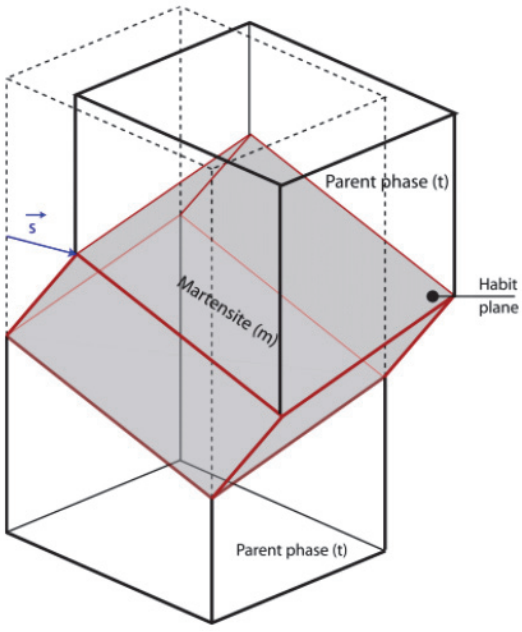

Figure 1.9 Schematic illustration of a martensitic plate (monoclinic) formed in a parent phase (tetragonal) through a habit plane [29].

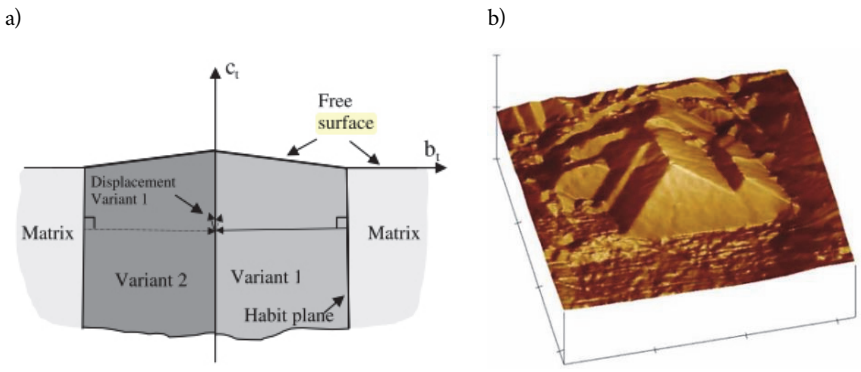

Figure 1.10 (a) Schematic view of a surface relief produced by a pair of martensite variants [73] and (b) AFM image (3D-view) of a surface uplift produced by the *t→m* transformation [74].

Considering a spherical tetragonal particle embedded within a matrix and a spontaneous and uniform transformation along the whole particle, Lange [75] described the change of total free energy ($\Delta G_{t\rightarrow m}$) due to the tetragonal to monoclinic transformation by:

$$\Delta G_{t\rightarrow m} = \Delta G_C + \Delta U_{SE} + \Delta U_S \quad 1.2$$

where ΔG_C (< 0 at temperatures below the transformation temperature $T_0^{t\rightarrow m}$) is the change in chemical free energy between the tetragonal and monoclinic phases, dependent on temperature and composition; ΔU_{SE} (> 0) is the change in strain energy associated with the transformed monoclinic particles and surrounding tetragonal phase, and it is dependent on the surrounding matrix, the size and shape of the particle and the presence of stresses; and ΔU_S (> 0) is the change in energy associated with the surface of the particle, corresponding to the creation of new interfaces.

Being the condition for the *t→m* transformation to occur that:

$$\Delta G_{t\rightarrow m} \leq 0 \quad 1.3$$

Therefore, when:

$$|\Delta G_C| \geq \Delta U_{SE} + \Delta U_S \quad 1.4$$

The addition of stabilisers decreases the driving force of the *t→m* transformation by a decrease of $|\Delta G_C|$ and an increase of ΔU_{SE}, and hence its transformation temperature $T_0^{t\rightarrow m}$ also decreases (see Figure 1.4d and Figure 1.5).

The presence of external or internal tensile stresses will reduce ΔU_{SE} and therefore increase the driving force of the transformation, destabilising the tetragonal phase [28,76].

Transformation toughening

Thus, *t→m* transformation can be stress-induced, which means that it can be triggered at high stress concentration regions, like in front of the tip of a crack.

The tensile stresses in front of a crack can induce the *t→m* transformation in the vicinity of the crack tip. The volume expansion associated to the transformation will induce in the surrounding elastic material a reaction compressive stress on the transformed region. Thus, this compressive stress will tend to hinder the crack propagation, increasing the fracture toughness (K_{Ic}) as the crack advances, as depicted in Figure 1.11 [3,77,78].

A deep review about transformation toughening of zirconia ceramics can be found in Hannink et al. [3].

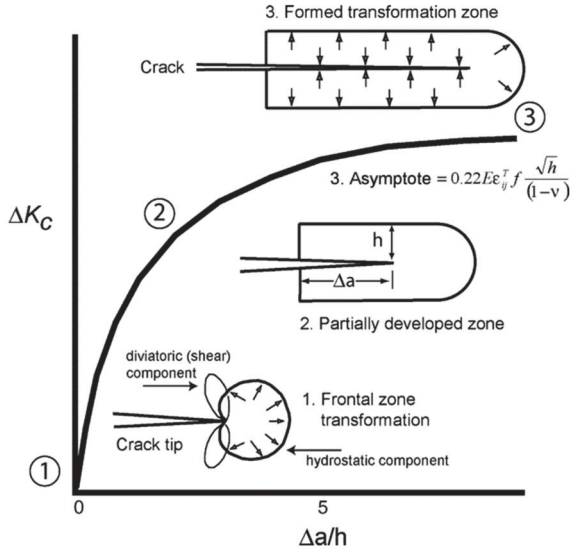

Figure 1.11 Schematic view of transformation zones and toughness increments (ΔK_c) development with different crack extensions (from [79] after [80]).

Transformation temperature

As seen in section 1.2.1, the metastability of the tetragonal phase is proportional to the undercooling below the martensitic $t \rightarrow m$ transformation temperature ($T_0^{t \rightarrow m}$ or M_s). If T_0 is too low, the tetragonal and not the monoclinic phase will be "stable", being the transformation toughening ineffective. On the other hand, if it is too high, the thermodynamic driving force for the transformation will be also high and the tetragonal phase will spontaneously transform to monoclinic upon cooling [29]. Typically, a T_0 of about ~400 ºC offers a highly transformable metastable tetragonal phase at room temperature.

As can be seen on the metastable phase diagram (see for example Figure 1.4d and Figure 1.5 as dashed lines), the addition of stabilisers will lower T_0 of a given composition, resulting in a tetragonal phase with high stability and low tetragonality. The transformation temperature T_0 also decreases with a decreasing grain size [81].

Critical grain size

Therefore, there is a critical grain size above which $t \rightarrow m$ transformation can occur [25,82–85]. This was first theorised by Garvie in 1965 [11], observing a critical crystallite size below which tetragonal phase was metastable at room temperature. Controlling the crystallite size on powder fabrication led to the production of fine-grained metastable tetragonal phase.

Below this critical tetragonal grain size, no transformation is thermodynamically or kinetically possible, and this explains the lower fracture

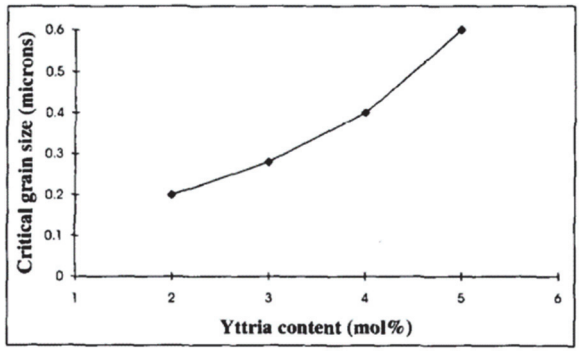

Figure 1.12 Critical tetragonal grain size as function of Y2O3 content (from [25] after [84]).

Below this critical tetragonal grain size, no transformation is thermodynamically or kinetically possible, and this explains the lower fracture toughness of nanosized zirconia ceramics [86,87]. However, if the grain size is too big, spontaneous transformation can occur after sintering during cooling, being the grains unable to retain the tetragonal crystal structure at room temperature.

As higher stabiliser contents decrease the transformation driving force and consequently the transformation temperature, the critical grain size for transformation increases, as can be seen in Figure 1.12 for the case of Y_2O_3 as stabiliser [84].

Cubic-to-tetragonal transformation

As the stress-induced transformation in zirconia is achieved by the metastability of the tetragonal phase, it is expected to decrease with increasing temperature and disappear above ~900 °C in Y-TZP (see Figure 1.4), as there is no driving force for the *t*→*m* transformation [88–90]. However, high strength and toughness at temperatures up to 1500 °C have been observed in Y-PSZ, much higher than those of Y-CSZ (in cubic form), even though no monoclinic was found on the fracture surfaces [83,89,91,92].

Michel et al. [89] and later Virkar and Matsumoto [90] proposed the phenomenon of ferroelasticity to explain the high toughness found in tetragonal zirconia at high temperatures; however it is still not completely understood. The reorientation of ferroelastic domains by externally applied stress was first observed in Ce-TZP [90] and later in Y-TZP [93], and present a hysteresis loop, analogous to ferroelectric and ferromagnetic materials, as seen in Figure 1.13. The area enclosed

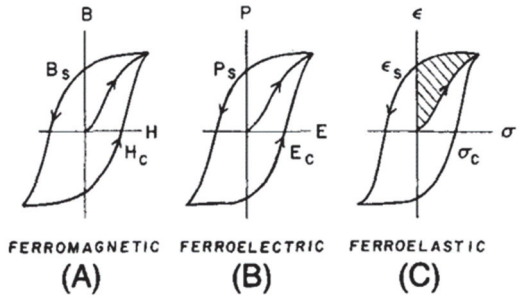

Figure 1.13 Hysteresis loops for (A) ferromagnetic, (B) ferroelectric, and (C) ferroelastic materials. The shaded area in (C) is the energy absorbed in reorientation of domains during fracture [90].

by the loop corresponds to the mechanical energy dissipated in reorientation of domains when a tension higher than a coercive stress (σ_c) is applied [90].

This ferroelastic toughening is possible in tetragonal grains (*t'*) produced by an invariant displacive reaction from cubic phase, typically by rapid cooling from the stability range of cubic zirconia (≥ 2100 °C). These tetragonal-prime grains contain a higher yttrium content and have lower tetragonality than regular tetragonal phase obtained in (semi-) equilibrium by diffusive processes [94,95].

Since the tetragonal crystal structure is a distorted fluorite type (*a*=*c*), when this non-stoichiometric cubic-to-tetragonal transformation occur, as two variants with their *c*-axes lying on the same plane are possible on three different orthogonal directions, there are six different equiprobable and crystallographically equivalent orientations possible of the *c*-axis in the new-formed tetragonal grain, as seen in Figure 1.14, forming a polydomain structure [96]. Each of these variants has the same energy and can re-orient when a stress above σ_c is applied, transforming the *c*-axis into an *a*-axis and vice versa, rotating 90° [29,89,90].

Thus, these domains can switch to a different orientation by the application of external stresses or in the presence of a propagating crack, and it is believed to contribute to toughening, even though these tetragonal-prime grains do not show any tetragonal-to-monoclinic transformation [29,90]. Unlike in transformation toughening, this toughening effect is related to the change from one equilibrium state, or variant, to another equilibrium state.

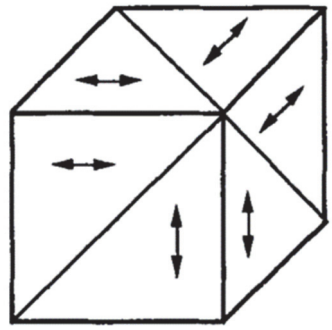

Figure 1.14 Representation of all six possible orientations of *c*-axis in a polydomain basic cell. The arrows indicate the directions of *c*-axes [96].

1.2.3 Low-temperature degradation (LTD)

As stated before, even though the *t→m* transformation can produce a toughening effect when it occurs in front of the tip of an advancing crack (stress-induced transformation, as seen in previous section 1.2.2), it can also occur spontaneously in aqueous environments (water-assisted transformation), known as ageing or low-temperature degradation (LTD), which is the main issue concerning zirconia ceramics as structural material and in biomedical applications.

The degradation of the surface in contact with water is a complex process that leads to surface roughening, micro- and macro-cracking, grain pull-out and the consequent loss of mechanical properties.

It was first observed in 1981 by Kobayashi et al. [20] and it is well-documented in the literature [24,26,27,31,97–102]. It is known that is produced by the diffusion of water-derived species in the material, however the details of the mechanism are not yet fully understood.

The experimental observations on LTD were summarised in 1988 by Yoshimura [31] as follows:

- The degradation is time-dependent and proceeds most rapidly at temperatures of 200–300 ºC.
- The degradation is caused by microcracking produced by the *t→m* transformation.
- The transformation proceeds from the surface to the bulk of the material.
- Water or water vapour enhances the transformation [103].
- The transformation can be retarded by decreasing the grain size or increasing the stabiliser content.

There are diverging theories for explaining the water-assisted degradation [104]. The most accepted present explanation is that the transformation occurs due to the reduction of vacancies associated with the penetration of water radicals (OH^-) inside the zirconia lattice, where oxygen from OH^- is placed on vacancy sites and hydrogen is located on an adjacent interstitial site, producing a lattice contraction that leads to the formation of tensile stresses in the surrounding network, as can be

depicted in Figure 1.15. This, added to the increase of oxygen overcrowding destabilise the *t* phase [97–99,105].

Due to the oxygen vacancies introduced by a trivalent cation such as Y^{3+} (see Equation 1.1), the diffusion of water radicals is easier in Y-TZP than in zirconia with other tetravalent dopants (like Ce-TZP), which explains the poorer LTD resistance of Y-TZP ceramics [105].

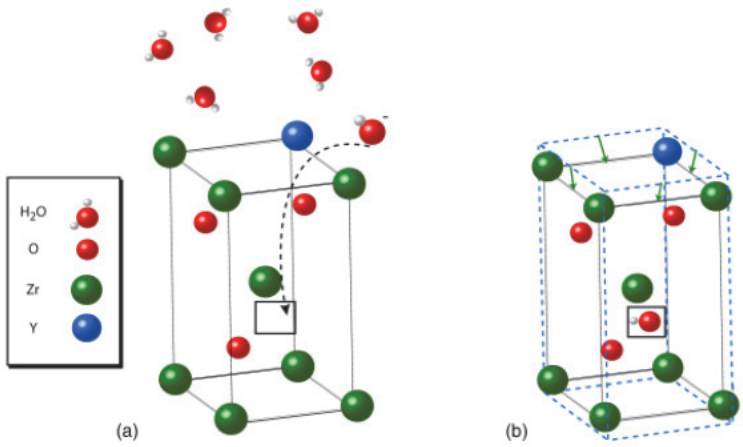

Figure 1.15 First steps of LTD in Y-TZP: (a) Diffusion of water species via oxygen vacancies and (b) the resulting variation of lattice parameters [29].

During LTD, the *t*→*m* transformation starts in the near-surface and it grows progressively deeper inside the bulk material, creating a transformed and microcracked surface layer of a few or even hundreds of microns. Mainly, these microcracks are located in the grain boundary to accommodate the shear stress produced by the first martensite plate, following the mechanism described in Figure 1.16 [106].

Experimental observations indicate that the kinetics of LTD can be fitted to the standard Mehl-Avrami-Johnson (MAJ) equations for a nucleation and growth process (see Figure 1.18) [107]:

$$f = 1 - exp(-(bt)^n) \qquad 1.5$$

where f is the transformation fraction, t is the time, b is the kinematic parameter that describes the rate of nucleation and growth and is dependent on the

temperature, and n is the Avrami exponent, a constant related to the geometry of the transformation [26].

It appears that the rate at which the transformation progresses below the surface is initially linear with time and dependent on temperature [25,108–110].

The transformation kinetics are often plotted in a time-temperature transformation curves (TTT), as shown in Figure 1.17. As it can be observed, even though the hydrothermal degradation is accelerated at temperatures around 200–300 ºC, it can also occur at room and body temperature (37 ºC) in humid environments with much longer times [110], where the kinetics (b) follow an Arrhenius dependence:

$$b = b_0 \exp\left(-\frac{Q}{RT}\right) \qquad 1.6$$

where b_0 is a constant, Q is an apparent activation energy, R is the universal gas constant, and T is the absolute temperature. The apparent activation energy for the degradation of different zirconia ceramics ranges from ~70–108 kJ/mol [17,26,111–118], values similar to the activation energy for oxygen vacancy diffusion extrapolated from higher temperatures (88–100 kJ/mol) [112,119–123].

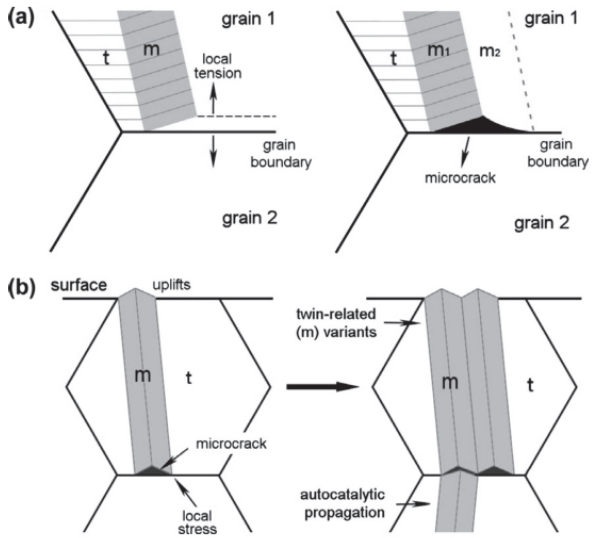

Figure 1.16 Process of microcracking and monoclinic phase propagation process: (a) in a grain boundary inside the material and (b) in the surface [106].

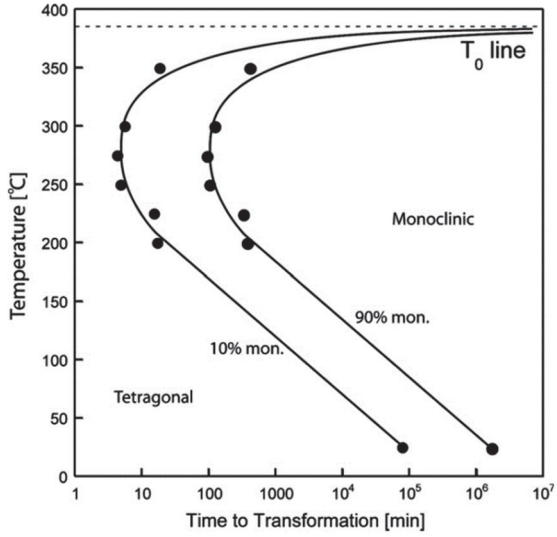

Figure 1.17 Time-temperature-transformation curve of a 2.8 mol% yttria-stabilised zirconia [124].

This behaviour cannot be explained by diffusion alone, but for the driving force associated to the difference between the temperature which the zirconia is exposed and the transformation temperature $T_0^{t\rightarrow m}$. Thus, although the diffusional flux of water species may increase with yttria concentration (and other divalent or trivalent dopants) because of the higher content of vacancies, the transformation temperature decreases and therefore the tendency to transform [29].

The ageing resistance of zirconia-based materials is typically simulated in an autoclave under water vapour at 134 ºC with an associated pressure of ~2 bar, as this was the most common standard sterilisation procedure [125,126]. It is commonly accepted that 1h in autoclave in those conditions is equivalent to 3–4 years exposure in vivo [127], although that is only a rough estimation [110,117]. A comparison of the different techniques for the determination of hydrothermal degradation sensitivity in zirconia can be found in [128].

There is a high variability in the zirconia sensitivity to LTD, which seems to be associated to the influence of the microstructure and processing conditions, besides the type of stabilising dopant. Composition, homogeneity, density and pore distribution, the presence of cubic phase, residual stresses induced during fabrication, grain size, surface finish and sintering conditions, all of them have a strong effect on LTD [24,29,100,129,130].

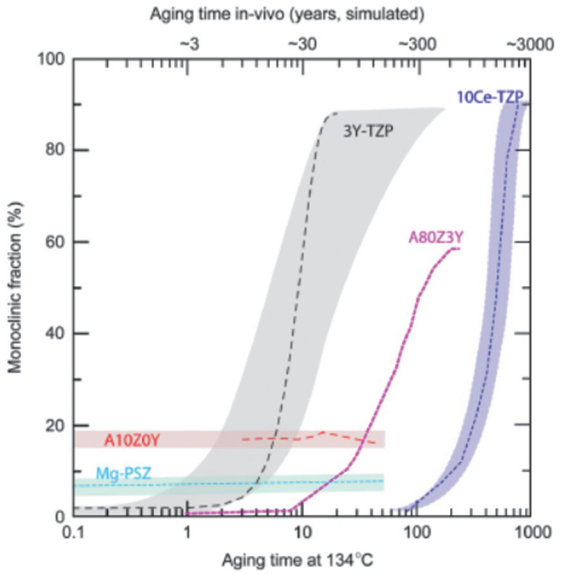

Figure 1.18 Kinetics of LTD of zirconia stabilised with 10 mol% of ceria (10Ce-TZP), with 3 mol% of yttria (3Y-TZP), magnesium partially stabilised zirconia (Mg-PSZ), alumina-toughened zirconia (A80Z3Y) and zirconia-toughened alumina (A10Z0Y) measured at 134 °C on the bottom X-axis and expected at 37 °C on the top. The shadowed areas give uncertainty ranges when they can be evaluated [29].

As seen in the phase diagrams (see Figure 1.4d and Figure 1.5), 3Y-TZP and 10Ce-TZP have a similar T_0, implying a similar driving force for the $t \rightarrow m$ transformation temperature. However, they exhibit different LTD kinetics, as seen in Figure 1.18. This can be explained by the different stabilising mechanisms (see section 1.2.1).

As stated before, trivalent ions such as yttrium stabilise the tetragonal phase by creating oxygen vacancies (see Equation 1.1). These oxygen vacancies act as a pathway for the water radicals to diffuse in the lattice, generating stresses that destabilise the tetragonal phase, triggering the spontaneous $t \rightarrow m$ transformation [97–99]. This has been observed as oxygen vacancies annihilation during hydrothermal ageing [104]. Thus, LTD is more susceptible in materials that are stabilised by generation of oxygen vacancies: as can be seen in Figure 1.18, the ageing resistance of 10Ce-TZP is much higher than 3Y-TZP. Even though, Ce-TZP still presents certain slow ageing, that can be explained by the partial presence of Ce^{3+} ions (by reduction from Ce^{4+}) and their associated oxygen vacancies [29].

Therefore, there are a critical minimum and maximum oxygen vacancy concentrations for the range of stability of cubic, tetragonal and monoclinic phases [131], to such a degree that not only tetragonal phase is susceptible to hydrothermal degradation, as it has been observed that cubic phase is also able to spontaneously transform to monoclinic after exposure times of several years in autoclave [132].

Space-charge layer

Due to their disordered nature, the grain boundaries may carry an electric potential through the presence of excess ions of one sign, which is compensated by an adjacent space-charge layer with a potential of the opposite sign [133], as depicted in Figure 1.19.

In zirconia and in most ionic crystals, the potential on the grain boundaries is determined by the charge of the aliovalent dopant and impurities. This potential will affect the segregation of solutes to the grain boundary, causing a lattice-defect (such as vacancies) concentration or depletion in the space-charge layers, which will change the grain boundary electrical resistivity [99,133–136].

This accumulation or decrease of vacancies in the grain boundaries also dictates the LTD resistance of the material. In general, most acceptor-doped

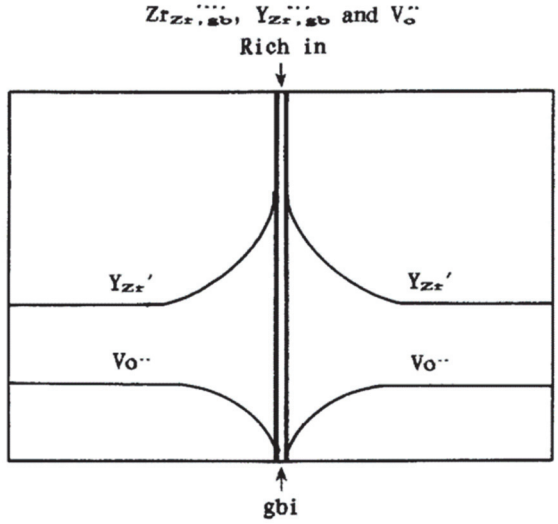

Figure 1.19 Defect distributions in the grain boundary interfaces and the space-charge layers of YSZ [133].

zirconias consist in a positively charged grain boundary and a negative space charge layer due to the enrichment of oxygen vacancies in the grain boundaries and their depletion in the adjacent space-charge layers [104,133,136–138]. The reduction of vacancies in the space-charge layer makes the grain boundary more vulnerable to be destabilised by water radicals [98], which explains the intergranular cracks produced by hydrothermal ageing and the different ageing response by different stabilisers.

Therefore, as degradation can be explained by oxygen vacancies annihilation, increasing the vacancy concentration in the space-charge layer is a method to improve LTD resistance. This can be influenced by the amount of dopant (as more vacancies will be present in the space-charge layer), the grain size (the concentration increases with decreasing grain size [138]) and the segregation of impurities or solutes [134,139]. This will be discussed in more detail in next section 1.3.

1.3 Improving LTD resistance

Besides a better control of the fabrication process, different methods have been proposed to reduce and/or avoid LTD in TZP-based materials [24,29,100,130].

Even following ISO standards [140], a strong variability of LTD resistance in vivo has been found [24]. A revision of the standard ISO 13356 was made in 2008 [140], however, a better understanding of LTD process is needed to achieve reliability in terms of LTD for long-term biomedical parts [24].

In general terms, the method to improve the ageing resistance of zirconia ceramics consists on increasing the stability of the tetragonal phase. This can be achieved in different ways:

Stabiliser type

The different stabilising mechanisms related to different dopants (see section 1.2.1) also affect the aging response. The lack of vacancies of tetravalent dopants such as CeO_2 makes them highly resistant to LTD. Using CeO_2, for example, instead of Y_2O_3 contributes to drastically change the degradation kinetics and drastically increase the aging resistance (see Figure 1.18) [141]. This will be addressed in more detail in the next section 1.3.1.

Moreover, using more than one stabiliser can also offer balanced properties. For instance, co-doping zirconia with both yttria and ceria may increase the stabilisation of the tetragonal phase and therefore the ageing resistance, but also affect the grain size and mechanical properties [142–151]. This topic will be discussed in sections 1.3.1 and 1.4.1.

Also, small amounts of certain oxides can segregate to the grain boundaries, modifying the vacancy distribution in the space-charge layer and therefore affecting the ageing resistance [118,152,153]. Grain boundary segregation will be treated in section 1.3.2.

Stabiliser content

An increase of dopant content reduces the tetragonality and increases the stability of the tetragonal phase, being less transformable and susceptible to ageing [83,103,154], as it can be seen in Figure 1.20. Therefore, higher dopant contents decrease the transformation temperature ($T_0^{t\rightarrow m}$ or M_s) and increase the critical particle size for phase transformation, below which no transformation can occur.

As expected from the phase diagrams (see section 1.2.1) more cubic phase is formed with increasing amount of dopant [155,156], which is considered resistant to hydrothermal degradation (although it has been observed that cubic phase is also susceptible to degradation after very long exposure times [132]). However, an increase of cubic phase content leads to a decrease of fracture toughness and strength, as

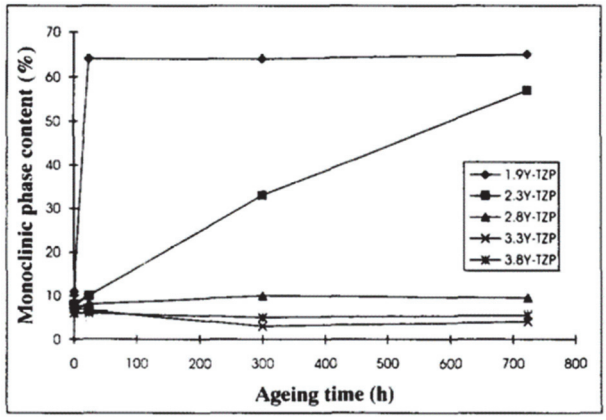

Figure 1.20 Phase transformation dependence on yttria content for TZPs with grain size of ~0.4 μm aged in air at 300 °C (from [25] after [83]).

transformation toughening only occurs on metastable tetragonal phase. Also, the formation of cubic phase, richer in stabiliser, can impoverish the surrounding tetragonal grains, making them more susceptible to LTD [129].

Grain size

As stated before (see section 1.2.2), there is a critical grain size below which transformation does not occur [25,82–85], whose size increases with higher dopant content (see Figure 1.12). Also, a higher dopant content increases both the grain size and the volume fraction of the cubic phase, with tetragonal grains retaining approximately the same size [84]. However, as a decrease in grain size also decreases the driving force for the $t \rightarrow m$ transformation, it also leads to a decrease in fracture toughness. [157,158].

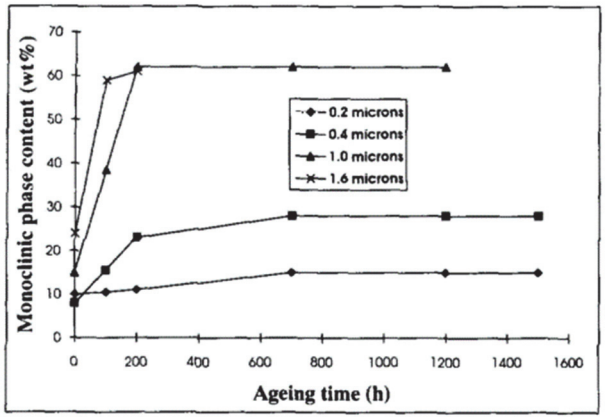

Figure 1.21 Grain size dependence (from [25] after [83]).

Stress

As seen in Equation 1.2, the change in strain energy is partly dependent on the presence of internal or external stresses. Therefore, tensile stresses will increase the driving force of the transformation, while compressive stresses will hinder the transformation [28,76,100,105,159]. Thus, surface treatments that generate compressive stresses, such as sandblasting, grinding or rough polishing, increase the ageing resistance [100,160–163] although making the surface not suitable for wear applications. Fine polishing, however, can also lead to tensile stresses that act as nucleation points for LTD [100].

Processing

A good control of all the processing steps is not only necessary to achieve finer enough powders to retain the tetragonal phase, but also to obtain a good ageing resistance, as the stability of the tetragonal phase depends, among other things, on the density [82]. For example, impurities, defects and inhomogeneities in phase distribution (which may lead to local depletion of stabiliser content) act as nucleation points for the transformation; and open porosity and cracks increase the surface in contact with water species, acting as a pathway to access the bulk of the material [164,165].

1.3.1 Ceria-stabilised zirconia

According to the phase diagram (see Figure 1.5), tetragonal zirconia stabilised with 10 mol% ceria (10Ce-TZP) has almost the same T_0 (*t/m*) temperature (~400 ºC) than 3Y-TZP (Figure 1.4d), implying that the driving force for *t→m* transformation is almost the same [29]. However, as showed in Figure 1.18, 10Ce-TZP is far more resistant to LTD, which indicates that even if 3Y-TZP and 10Ce-TZP have the same driving force for *t→m* transformation, they can exhibit very different LTD kinetics.

The effect of ceria into the zirconia network is explained in section 1.2.1. Instead of creating oxygen vacancies, like yttria, the higher size of Ce^{4+} creates a dilation of the lattice, decreasing oxygen overcrowding around zirconium atoms and improving the stability of tetragonal phase [51].

Due to the tetravalent nature of Ce^{4+}, vacancies are not created for charge compensation when stabilising with ceria. As the mechanism of LTD is related to oxygen vacancy annihilation by the penetration of OH^- ions, this could explain the higher resistance of Ce-TZP to LTD. However, even without vacancies, LTD still occurs at much slower kinetics, so the effect is not fully understood. One possible explanation is that the native thermal oxygen vacancies present at sintering temperature are still retained at lower temperature. Another possibility is that there is a small amount of Ce^{3+} ions producing vacancies [29].

Ce^{4+} ions are able to reduce to Ce^{3+} in reduced partial oxygen pressure conditions and sintered in different atmospheres due to an oxygen deficiency. This change of oxidation state is typically accompanied by a change of colour [166–174].

Besides the higher ageing resistance, ceria-stabilised zirconia also generally offers higher fracture toughness, but lower strength, mainly because of its higher grain size [175–177].

Dense Ce-TZP ceramics containing about 7 to 16 mol% CeO_2 and with different grain sizes were fabricated and evaluated in terms of hardness, strength and fracture toughness by Tsukuma and Shimada in 1985 [175]. They found a high fracture toughness, but also low hardness and fracture strength, which was associated to the relatively large micrometre grain size and high transformability under stress of the metastable tetragonal phase. Even though nowadays it is possible to produce ceria-stabilised zirconia materials with finer grain size due to a better control and process of the powders, they are typically substantially larger than 3Y-TZP.

Several studies have been addressed to achieve a combination of Y-TZP and Ce-TZP properties by doping with both ceria and yttria. The partial substitution of ceria by yttria in ceria-doped zirconia resulted in a reduced grain size with respect to a Ce-TZP and in a more stabilised tetragonal structure, which decreased fracture toughness but increased hardness and LTD resistance [142–144,146,147,149].

Another strategy was proposed by Zhao et al. [178], who studied a functionally-graded material (FGM), which composition varies from a fully Ce-TZP to Y-TZP, together with their LTD resistance and mechanical properties. As LTD starts from the surface, a graded distribution of Ce-TZP from the surface can avoid LTD, while keeping the mechanical properties of the bulk. In that sense, Marro et al. [179] coated 3Y-TZP samples pressing cerium oxide powder or depositing a very thin layer of cerium and modifying the surface by allowing diffusion of cerium to depth less than 1 μm by high temperature heat treatment. Camposilvan et al. [180] also modified the surface of 3Y-TZP impregnating pre-sintered samples in a solution containing cerium, improving LTD resistance without losing mechanical properties.

1.3.2 Grain boundary segregation

As stated above, it has been reported that small amounts of certain oxides may segregate to the grain boundaries, affecting their electric potential and varying the vacancy distribution in the space-charge layer [134,139], which will affect the ageing response of the material.

For instance, it has been reported that small amounts of homogeneously distributed alumina (less than 0.5 wt%) in yttria-stabilised zirconia will increase the conductivity of the grain boundary due to an oxygen vacancy enrichment in the space-charge layer, resulting also in a better LTD resistance [21,116,134,135,152,181]. Recent studies suggest that the ageing resistance can be enhanced even more by the addition of small amounts of both alumina and lanthania [153,182] or alumina and germania [183] in 3Y-TZP.

The segregation of different elements on yttria-stabilised zirconia and their influence in the ageing resistance has been studied recently [153]. It has been concluded that the segregation on the grain boundaries is related to the cation valence and radius of the solute. Larger oversized cations (such as La^{3+} or Nd^{3+}) as well as smaller undersized trivalent cation dopants (like Al^{3+}), respect to the Zr^{4+}, (see Table 1.2 for the effective radii of some solutes) exhibit a strong segregation, as can be seen in Figure 1.22. On the contrary, cations with similar size to Zr^{4+} (such as Sc^{3+}) do not show any segregation or enhancement of LTD resistance. It has also been observed that hydrothermal stability increases with increasing cation size [118,153].

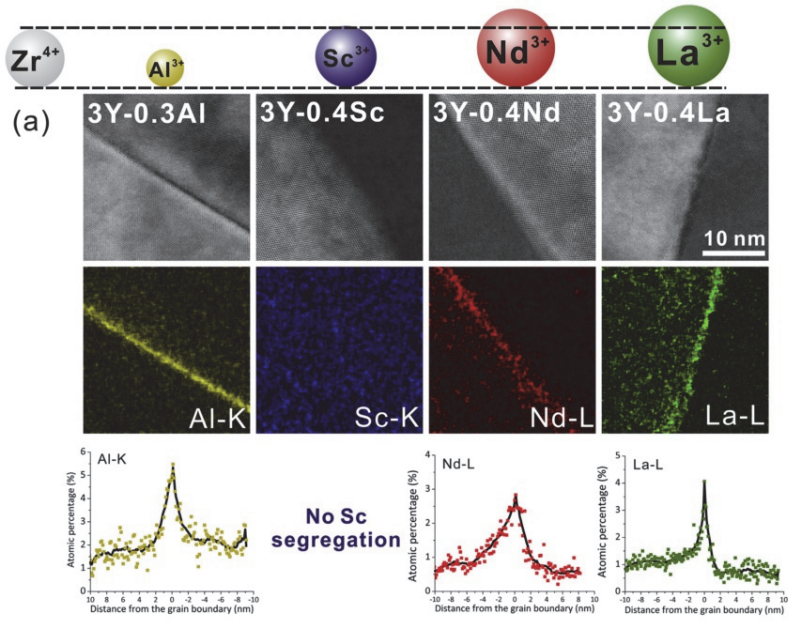

Figure 1.22 HAADF-STEM images and STEM-EDS elemental maps and distribution of 3Y-TZPs doped with 0.3 mol% Al_2O_3 and 0.4 mol% Sc_2O_3, Nd_2O_3 and La_2O_3. The spheres represent qualitatively the size of the dopant cations, Al^{3+}, Sc^{3+}, Nd^{3+} and La^{3+}, respect to the Zr^{4+} host cation [118].

1.4 Improving mechanical properties

As seen previously, ceria-stabilised zirconia ceramics are characterised by a high hydrothermal stability and fracture toughness, but lower strength and hardness than Y-TZP, partly due to its larger grain size [146,175–177].

According to the studies of Tsukuma and Shimada [175], 10-12 mol% of ceria is the optimal concentration in terms of fracture strength. The presence of other stabilisers, like yttria, also affects the optimum concentration (see Figure 1.23), as well as the grain size, density, and transformability [142–151].

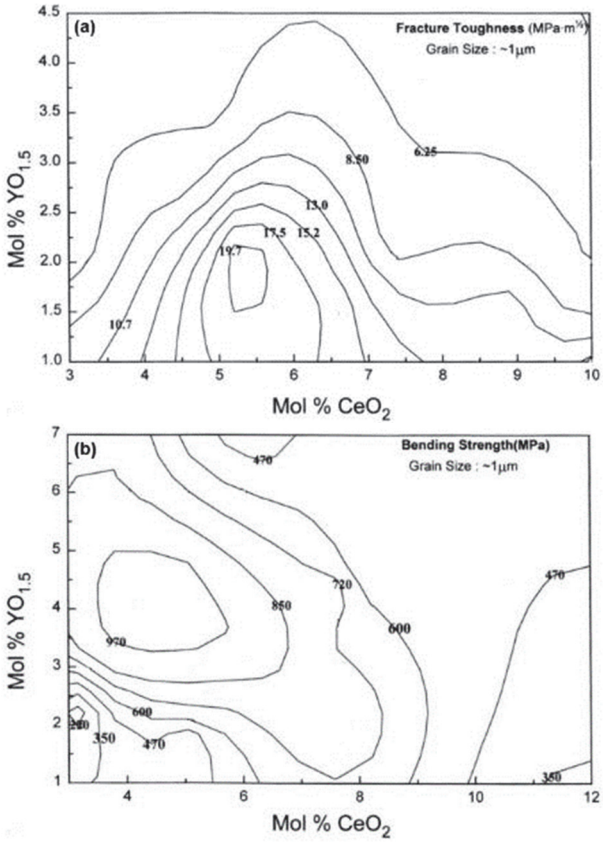

Figure 1.23 Relationship of yttria and ceria composition and a) fracture toughness and b) bending strength [147].

The larger grain size of ceria-stabilised zirconia compared with 3Y-TZP is in part explained by the need of higher sintering temperatures and/or longer times for full densification. The grain growth of Ce-TZP at low temperatures is slow due to the slow diffusion kinetics of $Ce^{3+/4+}$ (compared to Y^{3+}), requiring higher sintering temperatures, producing a larger and broader grain size distribution due to the absence of an effective grain-growth retarding mechanism as it occurs in 3Y-TZP [146].

As the mechanical properties strongly depend on the grain size, it is expected that limiting the grain growth during sintering will have an impact on the strength, hardness and transformability of Ce-TZP. In principle, this can be achieved by the addition of specific solutes which might segregate to the grain boundaries during sintering, reducing their mobility by a solute drag mechanism [146,184,185].

1.4.1 Grain size refinement

One of the first studies dealing with the influence of different oxides on the grain size of 3Y-TZP was carried out by Sato et al. [142]. They co-doped 3Y-TZP with 0-12 mol% of either CaO, MgO, CeO_2 or TiO_2 revealing that alloying with TiO_2 accelerated the grain growth and suppressed densification, but alloying with less than 6 mol% of CeO_2 caused no significant changes in grain size. CaO was the most effective oxide in reducing the tetragonal grain size, and cubic zirconia phase was already detected with only 2 mol% CaO addition [142]. In 12Ce-TZP, CaO was also found to reduce grain growth and increase fracture strength and stability of the tetragonal phase [177,186].

In acceptor-doped zirconia (i.e. stabilised with dopants with a lower valence than Zr^{4+}), oxygen vacancy diffusion is much faster than cation diffusion, so that grain boundary mobility is controlled by cation solutes [186]. Therefore, the resistance to grain boundary mobility is related to the segregation of these ions at the grain boundaries. It increases with a higher solute concentration and a larger valence and radius difference between the solute and the host cation [186–188] (see Table 1.2 for the effective radii of some oxides).

Since most stabilised zirconia are characterised by positively charged grain boundaries [104,133,136–138], only cations with a negative effective charge are attracted to the lattice discontinuities as a space charge. Therefore, only divalent and trivalent cations (such as Y^{3+} and Ca^{2+}) segregate to the grain boundary, but tetravalent and

pentavalent cations (like Ce^{4+} and Nb^{5+}) do not, and therefore they have no effect in reducing grain growth [177,186,189].

Furthermore, beside the effective charge of the dopants controlling grain boundary mobility, it is secondly controlled by the lattice diffusivity of the dopants. Thus, the slower diffusivity of larger cations makes them more effective on dragging grain boundary mobility [186].

1.4.2 Composites

As a different strategy, second-phase hard particles, typically alumina, are often used to obtain better LTD resistance and mechanical properties [190–192].

In particular, nano-composites (with grain sizes below a few hundred nanometers) consisting of zirconia and alumina, aluminates (including spinels), titanates or niobates offer a good combination of high strength, toughness and ageing resistance [193–201].

The morphology of the second-phase particles has a strong effect on mechanical properties of the composite. While rounded-shaped particles retain grain growth, increasing fracture strength, elongated particles increase fracture toughness through bridging or crack-deflection mechanisms [202].

Besides second-phase particles reinforcement, ceramic composites with a layered structure are another way to improve the mechanical properties, increasing fracture toughness and showing a non-catastrophic failure behaviour [203]. Particularly, alumina/zirconia layered structure has been deeply studied [204–206].

Since the Prozyr® incident [23], manufacturers have tried different alternatives to monolithic zirconia. Zirconia/alumina particle composites have become the most successful materials for prostheses, being commercialised by several companies.

Based on the majority phase, these composites can be divided in two main groups. When the main phase is zirconia, the composites are called alumina-toughened zirconia (ATZ) and when the main phase is alumina, they are known as zirconia-toughened alumina (ZTA). In both cases, the secondary phase is in the form of particles.

Alumina-toughened zirconia (ATZ)

Small amounts of alumina on TZP modifies the grain boundaries, suppress grain growth, enhance LTD resistance and increase the hardness, strength and fracture toughness of TZP materials [111,112,192,207–209].

Due to the very limited solubility of alumina (below 0.5 wt%), only a small amount can be dissolved in the zirconia grains, which increases LTD resistance, as seen in section 1.3.2. Higher amounts will form secondary Al_2O_3 phase grains in the triple points of zirconia grains, which will produce a pinning effect on the grain boundaries, resulting in a reduced grain size. However, since the thermal expansion coefficient of zirconia is higher than that of alumina, the alumina particles are subjected to compression and produce a net hydrostatic tensile stress into the zirconia matrix, enhancing the $t \rightarrow m$ transformation. This slightly decreases LTD resistance but it is still higher than that of 3Y-TZP without alumina, as seen in Figure 1.24 [29,116].

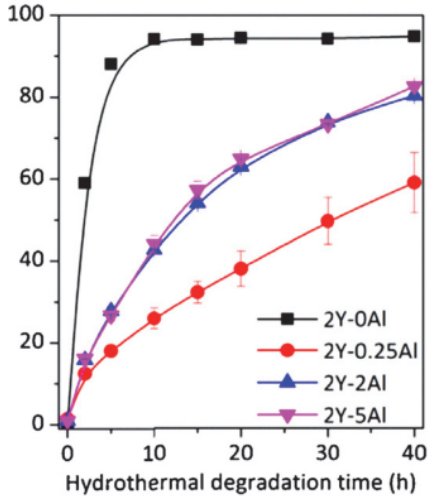

Figure 1.24 Surface monoclinic phase content as a function of hydrothermal testing time at 134 °C for 2Y-TZP with different amounts of alumina [116].

Zirconia-toughened alumina (ZTA)

These composites consist in dispersed tetragonal zirconia particles embedded inside an alumina matrix. Even though these particles are also subjected to tensile stresses due to the thermal expansion mismatch like in ATZ composites,

the higher stiffness of alumina matrix increases the value of the strain energy of the particles (ΔU_{SE} in Equation 1.2, see section 1.2.3), which depends on the elastic modulus of the surrounding matrix, and thus stabilising the tetragonal phase and hindering the transformation [29,207].

Moreover, if the zirconia particles do not form a continuous phase (below the percolation threshold, estimated to be ~16 vol.% [210], as seen in Figure 1.25), there is not a pathway for the water species to diffuse into the bulk of the material, so the degradation will be limited into the surface.

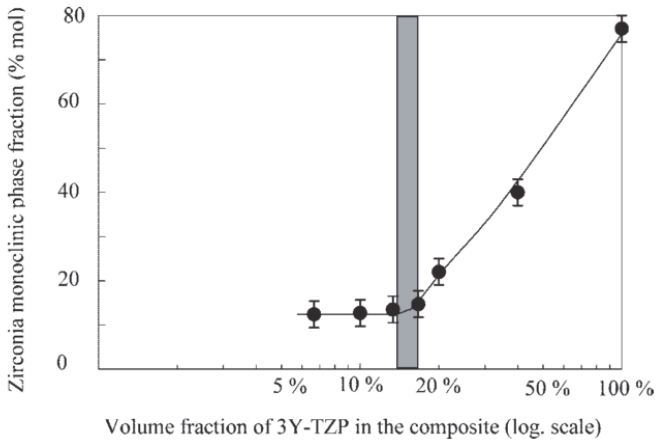

Figure 1.25 Fraction of monoclinic phase measured after 40 h of hydrothermal ageing as a function of the 3Y-TZP volume content in the ZTA composite. The grey area represents the percolation threshold [210].

1.5 Fracture toughness

In most cases, ceramic materials fail by unstable propagation of natural flaws, such as pores, cracks, inclusions, machining defects, etc.

According to linear elastic fracture mechanics (LEFM), the stress field close to a crack tip can be described by only one parameter: the stress intensity factor, K [211]. Fracture starts when K reaches a critical value, which is the fracture toughness.

In mode I, that is, when the stress is applied perpendicularly to the crack plane, K is written as K_I and the fracture toughness as K_{Ic}. In general, K_I can be written as:

$$K_I = Y\sigma\sqrt{a} \tag{1.7}$$

where σ the applied stress, a is the crack length and Y is a factor that depends on the crack length and geometry of the sample.

In general, measuring the fracture toughness of a material consist in the following steps:

· generate a crack with a known length in a specimen with a specific shape,

· test the specimen to failure to obtain the load at failure,

· calculate K_{Ic} from Equation 1.7 by incorporating the stress at failure, σ_f:

$$K_{Ic} = Y\sigma_f\sqrt{a} \tag{1.8}$$

The generation of an initial sharp crack with a simple geometry is an important problem in ceramics. Several methods have been proposed, which are described below.

1.5.1 Vickers indentation

One of the most commonly used methods for determining the fracture toughness of a material is the Vickers indentation fracture toughness test (VIF), due to its ease of use.

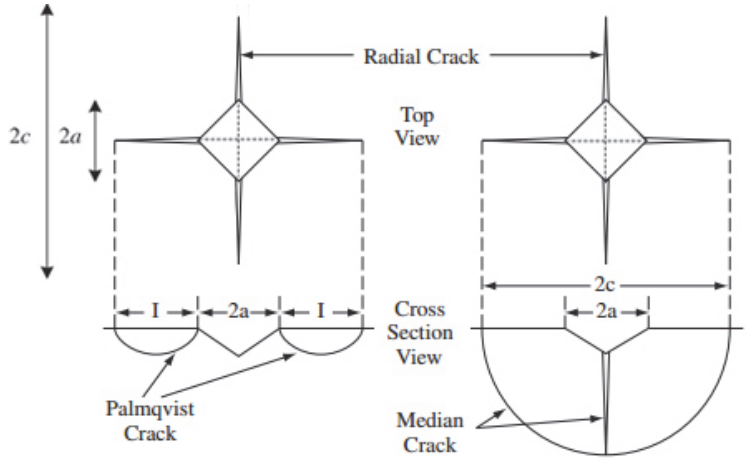

Figure 1.26 Imprint and cracks formed by a Vickers indentation: Palmqvist-type crack on left and median crack on right (adapted from [212,213]).

It consists in the penetration of a Vickers indenter on a polished surface and the measurement of the dimensions of the imprint and the lengths of the indentation cracks (see Figure 1.26).

Brittle materials show several Vickers crack systems. The most used in brittle materials are median surface semielliptical cracks which often are taken as semi-circular. For high fracture toughness materials they tend to be Palmqvist-type cracks, when 0.25 < (c/a-1) < 2.5, according to Niihara et al. [214] (see Figure 1.27).

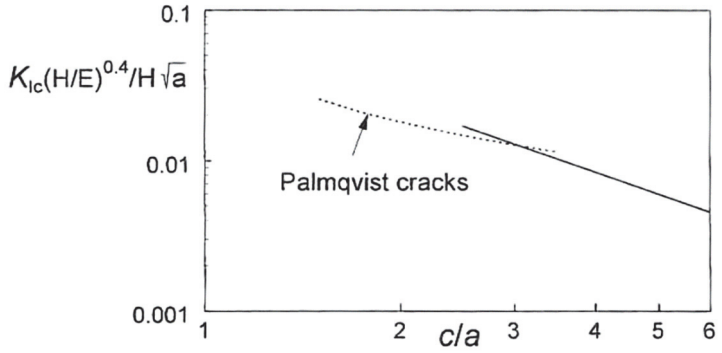

Figure 1.27 Relation between the shape of the crack and the determined K_{Ic}: solid curve corresponds to radial median cracks, and dashed line to Palmqvist cracks [215].

There are many equations proposed for measuring fracture toughness from indentations. One of the most used was proposed by Anstis et al. [216] for median radial cracks:

$$K_{ind} = 0{,}032H\sqrt{a}\left(\frac{E}{H}\right)^{1/2}\left(\frac{c}{a}\right)^{-3/2} \quad 1.9$$

where K_{ind} is the residual stress intensity factor measured in MPa$\sqrt{}$m, H the hardness, E the elastic modulus, a is the half of the imprint, c the distance between the center of the indentation and the crack tip (as seen in Figure 1.26).

For Palmqvist cracks Niihara [214] proposed another equation:

$$K_{ind} = 0{,}018H\sqrt{a}\left(\frac{E}{H}\right)^{0.4}\left(\frac{c}{a}-1\right)^{-1/2} \quad 1.10$$

Even though the value of K_{ind} has been typically related to the fracture toughness of the material (K_{Ic}), the VIF technique in general is not a reliable method to measure fracture toughness for brittle materials. In particular, in high transformable materials such as high toughness zirconia, the cracks might be severely affected by the $t \rightarrow m$ transformation around the imprint and not only by the transformation generated by the crack itself during its extension.

Moreover, in highly transformable ceramics, the cracks are extremely short and the c/a ratio often does not even obey the conditions for the validity of indentation equations. Consequently, there are serious discrepancies between indentation fracture toughness and robust fracture mechanics standardised tests [217]. Many authors recommend not to use the indentation test for the determination of K_{Ic} (see, for example, Quinn and Bradt [217]).

1.5.2 Precracked bending specimens

There are several methods for measuring the actual fracture toughness of ceramic materials from flexure tests. Some of them are standardised [218] using beam test specimens with a sharp crack. These methods are often referred as surface crack in flexure (SCF), chevron-notched beam (CVN), single-edge-precracked beam (SEPB), and single-edge-notched beam (SENB). The main difference is the shape of the crack and how it is produced [215,218].

Surface crack in flexure (SCF)

The initial crack is produced by a Knoop indenter, and then the surface is polished until the imprint and residual stress field are removed. The sample is tested in four-point bending configuration [219,220].

One of the main advantages of the SCF test is that it can offer reliable results, and the fracture toughness is measured from precracks with a size similar to the natural defects. However, the identification of the fracture origin and the accurate measurement of its size can be difficult [221][219,221]. Moreover, for K_{Ic} determination it is often assumed that the crack shape is semi-circular or semielliptical, which is not always true, especially in high-toughness materials. Also, the residual stresses are not completely known, which may have an influence on the obtained values [221].

Chevron-notched beam (CN)

The fracture toughness is calculated from the maximum force applied in either three- or four-point bending after a stable extension of the crack propagated from a chevron notch.

The main advantage of this method is that no sharp precrack has to be introduced, as the crack is produced during loading [222]. However, the "V" shape groove, called chevron, is difficult to machine with cutting discs, and the obtained values are very sensitive to load rate and deviations in the crack plane during its propagation [221,222].

Single-edge precracked beam (SEPB)

A straight precrack is produced propagating cracks from one or more Vickers indentations by, typically, bridge-flexure technique, and tested in three- or four-point bending [218,223].

With this method, the tip of the precrack is significantly sharp, but its propagation is difficult to control and its final size on the fracture surface is difficult to identify and measure. Also, K_{Ic} values can be influenced by the residual stresses produced by the indentations [221,223].

Single-edge notched beam (SENB)

A beam with a sawed through notch is tested in usually four-point bending, and it is assumed that either the notch tip is sharp enough or that fracture originates from a small defect in front of the notch. Its use is extended as it is cheap and easy to produce, although the values obtained can be influenced by the notch width [224,225].

Single-edge V-notched beam (SEVNB)

In order to make K_{Ic} testing more user-friendly, there have been attempts to use sharp notches instead of precracks as the starting defect on bending test specimens, such as the single-edge v-notched beam method (SEVNB), which is a variation of the SENB method proposed by Nishida et al. [226] and successfully applied by Kübler [227,228].

This method is based on machining a notch with a saw cut and thinning its tip by honing with a razor blade impregnated with diamond slurry, obtaining the notch configuration depicted in Figure 1.28.

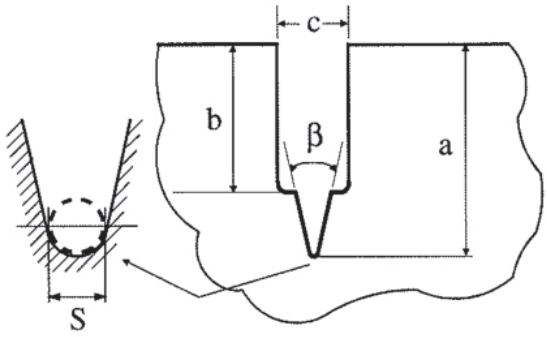

Figure 1.28 Schematic geometry of V-notch obtaining by a saw cut and thinning its tip with a razor blade [228].

By following this procedure, notch radii of several dozen microns can be obtained. However, elastic fracture mechanic is developed under the assumption that the crack tip radius is equal to zero, so that in order to measure the fracture toughness the crack tip radius should be as small as possible. Above a critical notch-root radius (ρ_c) the values of K_{Ic} are overestimated (see Figure 1.29).

This critical notch radius is proportional to the size of the fracture-initiating defect, which use to be in the range of 1-3 times the grain size [225].

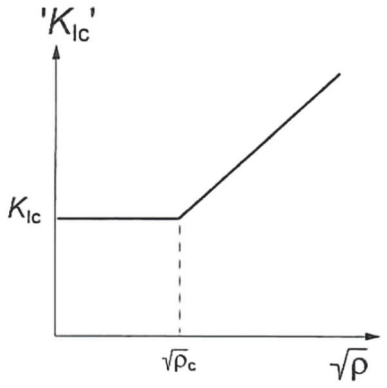

Figure 1.29 Dependence of measured fracture toughness (K_{Ic}) on notch-root radius (ρ) (from [215] after [225]).

Fett [229] analysed the stress intensity factor of a crack in front of a circular notch tip, as depicted in Figure 1.30, and concluded that if the length of the crack, *a*, in front of the notch is much higher than the radius of the notch tip, *R*, the stress intensity factor is the same as that of a crack with a length equal to the sum of the length of the notch and the crack in front of it (a_0+*a*). If not, the stress intensity factor in front of the crack will be affected by the notch tip radius and that approximation will not be true so that the K_{Ic} value will be overestimated.

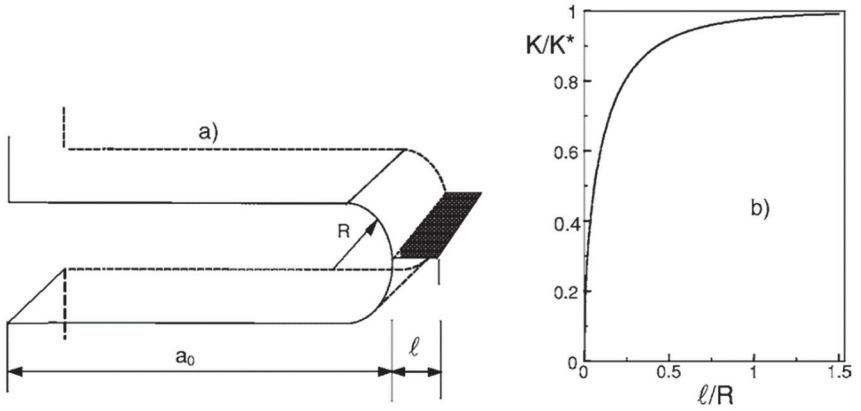

Figure 1.30 a) Schematic view of a crack with length *a* in front of a notch with radius *R*, b) and its influence on stress intensity factor [230].

In the case of coarse grain ceramics, the damage in front of the notch may comply with that condition. However, in the case of finer grain size ceramics, this condition is more difficult to fulfil, if not impossible, as the radius of the notch will be always limited by the mechanical tool.

Because of that, there is a need for a method which can produce a very sharp notch in ceramics with very fine microstructures in a controlled manner.

Ultra-short pulsed laser ablation (UPLA)

One possible method to introduce a sharp crack in ceramics is by laser ablation, which is a technique sometimes used in polymers [231–233]. Although the damage left in brittle ceramics may be expected to be much relevant than in polymers, there has been previous work using laser ablation on zirconia mainly focused on surface micromachining for dental applications [234–237].

The physics behind laser ablation has been extensively studied, proving that there is a minimization of thermal effects during ablation using ultra-short pulsed lasers, with pulses in the range of the femtosecond (fs) [238–240].

With this technique, it is in principle possible to produce small notches with radius under the micron and with different sizes.

1.5.3 R-curve

In the case of ideally brittle materials, fracture toughness is independent of crack extension, Δa, so that K_{Ic}=constant and independent of crack length. Many ceramics with toughening mechanisms, however, show a different behaviour, with an increasing crack growth resistance with an increase of crack extension. Such is the case of many zirconia ceramics, in which transformation toughening occurs (see section 1.2.2).

In these cases, the resistance to crack propagation is not described by a single value of K_{Ic} but by a crack-resistance curve, known as R-curve, as shown in Figure 1.31.

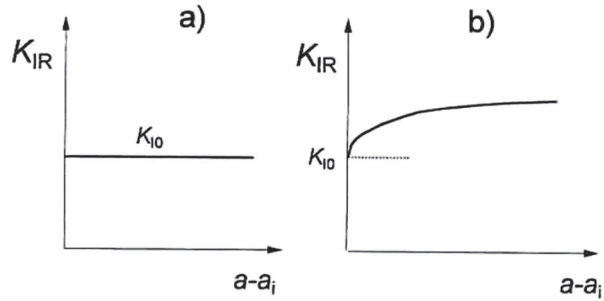

Figure 1.31 Representation of the stress intensity factor variation with crack extension a) flat and b) rising crack-resistance curve (R-curve) [215].

Unstable fracture occurs when the stress intensity factor increases faster than the materials resistance to fracture. That is, when the corresponding K_{Iappl}-curve is tangent to the K_{IR}-curve, as seen in Figure 1.32. Therefore, in mode I, fracture will occur when both conditions are fulfilled: [215]

$$K_{Iappl} = K_{IR} \tag{1.11}$$

and:

$$\frac{\partial K_{Iappl}}{\partial a} = \frac{dK_{IR}}{da} \tag{1.12}$$

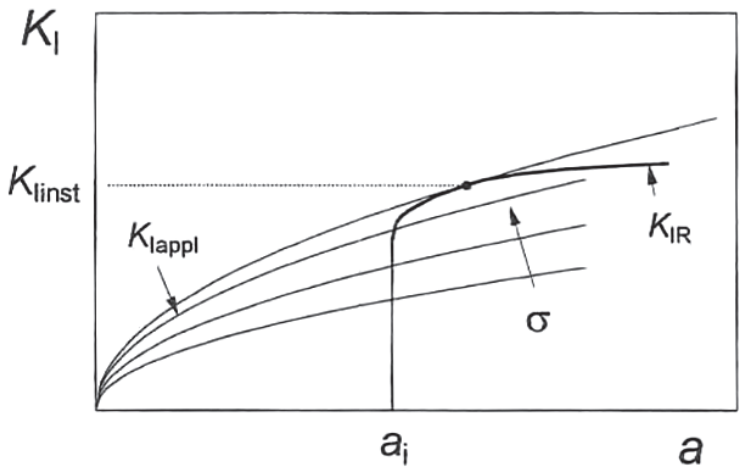

Figure 1.32 Instability for fracture for a rising R-curve [215].

A material with a flat R-curve has a single value of toughness, while for materials with rising R-curves there is no single value of toughness (see Figure 1.33), as this tangency point, K_{Iinst}, depends on the shape of the K_{IR}-curve, the initial crack size, a_i, and the type of loading [215,241].

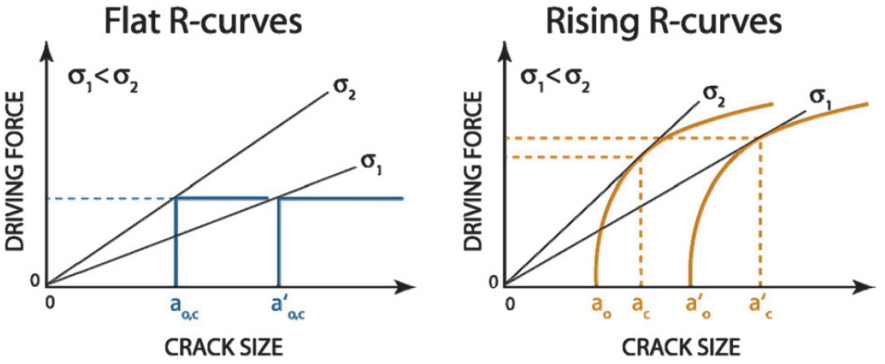

Figure 1.33 Schematics of flat and rising R-curves. A material with a flat R-curve has a single value of toughness, while for materials with rising R-curves there is no single value of toughness [241].

Zirconia materials offer a wide range of different R-curve behaviour depending on the dopant and grain size, as seen in Figure 1.34.

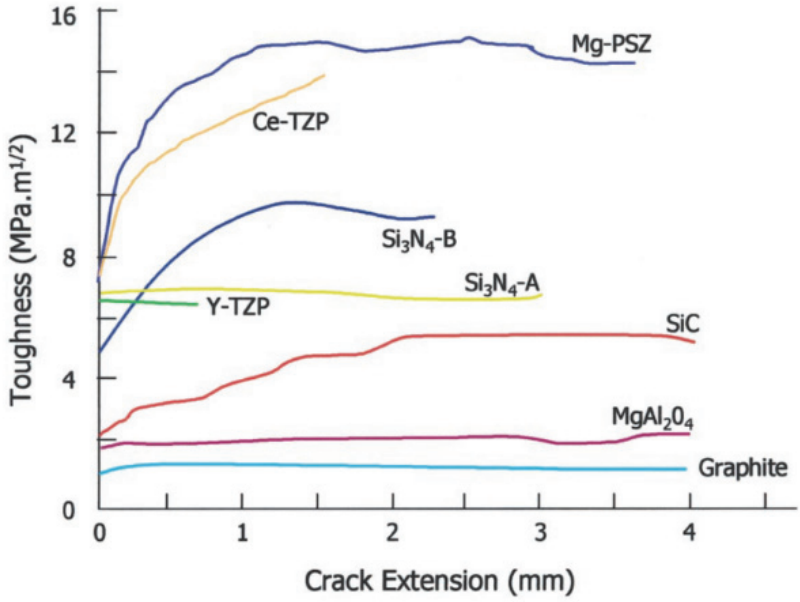

Figure 1.34 R-curves for various ceramics, obtained from long cracks. [3]

It is often assumed that the R-curve is unique and invariable for each material. However, it depends on different parameters like grain size, initial crack size and shape, and loading conditions [215,230,242–244].

1.5.4 Toughening mechanisms

Broadly, there are two general types of toughening: intrinsic damage processes that occur in front of the crack tip and extrinsic shielding that acts behind the crack tip [245]. Examples of these processes can be seen in Figure 1.35.

Intrinsic toughening: this type of process increases both crack-initiation and crack-growth resistance by relaxing the stresses ahead of the crack by enlarging the plastic zone in front of the crack tip. In ceramics, as plasticity is very limited, it can be produced mainly by phase transformation (in the case of zirconia $t \rightarrow m$ transformation, see section 1.2.2), crack deflection and branching or microvoid coalescence, among others.

Extrinsic toughening: shielding mechanisms are only effective in increasing crack propagation resistance and they have no effect on crack initiation. These processes act behind the crack tip to hinder its further opening by lowering the local stresses in the crack tip. Examples are crack bridging (by fibers or second phase particles), frictional interlocking of grains during intergranular fracture or crack wedging, among others.

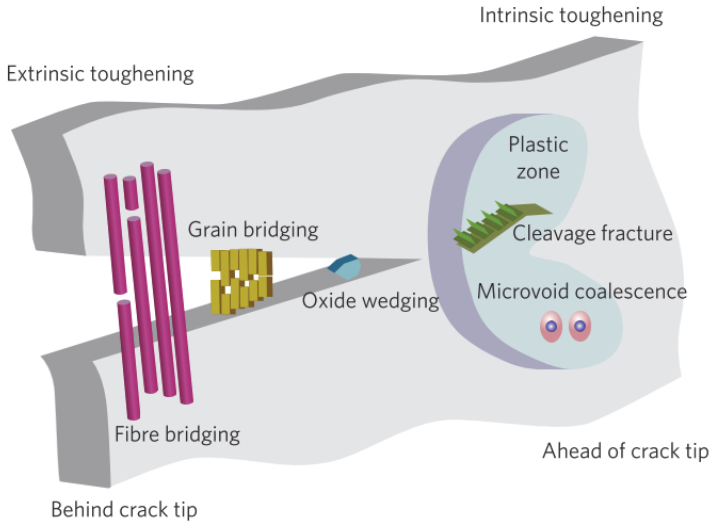

Figure 1.35 Schematic illustration of different examples of intrinsic toughening occurring in front of the crack tip and extrinsic mechanisms that act primarily behind the tip [245].

1.5.5 Relation between fracture toughness and strength

In general, R-curve behaviour is usually measured from specimens containing macrocracks (a detailed explanation of different methods can be found in [215] and [246]). Therefore, the obtained K_{Iinst} values of the tangency points for unstable crack propagation are reached after stable crack extension (see Figure 1.36).

As strength is governed by small natural defects, which are often in the range of the grain size, in principle, one should expect that a material with a strong R-curve giving high fracture toughness should also show a high fracture strength.

However, materials with strong R-curves can show discrepancies between measured fracture toughness and strength, being usually mutually exclusive [245,247]. Some Ce-TZP materials, for instance, are known for having a strong R-curve and high fracture toughness but low strength compared to 3Y-TZP [175,176,248]. This can be explained, in part, due to the small initial crack does not make use of the full R-curve, as the transformation zone size at maximum strength is dependent on the initial flaw size and therefore the K_{Iinst} values obtained for small a_i are always smaller than for larger a_i values, schematised in Figure 1.36 [249].

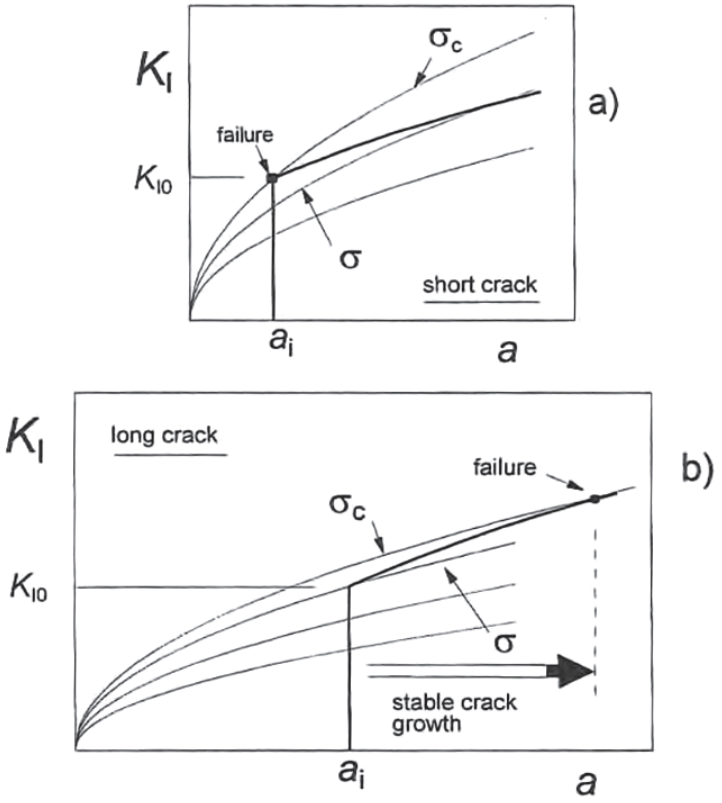

Figure 1.36 Failure behaviour of materials with R-curve and an initial a) short and b) long crack [215].

In very transformable zirconia ceramics, the strength can be limited by the critical stress to induce $t \rightarrow m$ phase transformation. It has been shown that for transformable materials with high toughness (above ~8 MPa$\sqrt{}$m, see Figure 1.37), the loss of strength is attributed to a stress-induced $t \rightarrow m$ phase transformation in the

surface that occurs at a lower stress than the fracture stress from pre-existing flaws, leading to cracks generation. Thus, fracture does not take place from the natural defects initially present, but from defects generated by the nucleation of the transformation [3,249].

In the case of materials with lower fracture toughness (below ~8 MPa√m), the strength is limited by flaw size, following the well-known Griffith flaw-size/strength relationship [250]:

$$\sigma_f = \frac{K_{Ic}}{Y\sqrt{a}} \tag{1.13}$$

where σ_f is the fracture strength, a is the critical flaw radius and Y a crack shape parameter.

However, that makes them more susceptible to flaw generation during processing and less tolerant to damage, which will reduce strength drastically [79,249].

Therefore, it is often generalised that zirconia ceramics with K_{Ic} below ~8 MPa√m are flaw-size sensitive, while above this value the strength is controlled by stress-activated transformation [3]. The peak observed in Figure 1.37 show the transition from flaw-size control to transformation-limited strength [249].

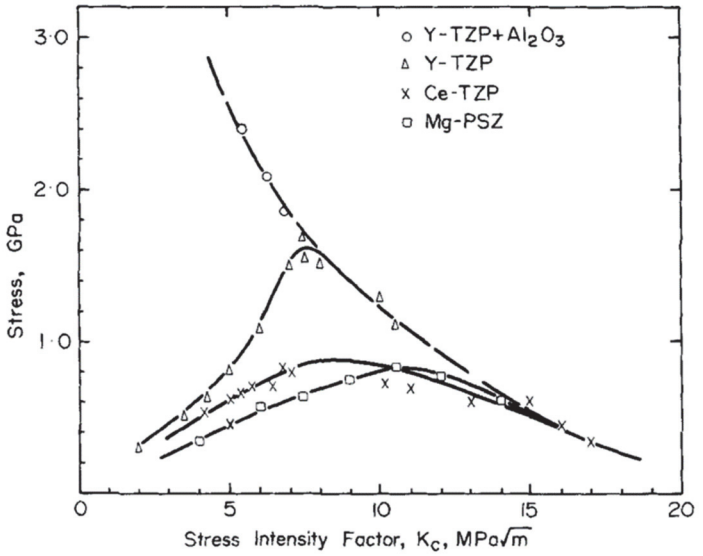

Figure 1.37 Strength-toughness relation for various PSZ and TZP ceramics. [249]

CHAPTER 2
AIMS AND SCOPE

As it has been shown in the previous chapter, machining a sharp notch on the surface of ceramics for fracture toughness testing has been a critical issue during many years. It often requires high-qualified technicians and certain artistry, and even then, the success rate is rather low, and the results are not accurate in some cases or the equations used are not applicable, especially in the case of nanograin-sized ceramics.

Therefore, one first objective of this thesis is to develop and assess a novel method to determine accurately fracture toughness of ceramics with small grain size. This should be achieved through an easy-to-carry-out technique to introduce small notches with a sharp radius.

On the other hand, it has also been seen that one of the main issues of 3Y-TZP is its low resistance to LTD, which casts doubt on the long-term reliability of biomedical implants and dental prostheses.

Thus, the second main objective of the thesis is to develop new zirconia-based materials combining both high LTD resistance and good mechanical properties.

2.1 Fracture toughness determination

As stated in the introduction, indentation techniques are not a reliable method for fracture toughness determination. Other methods involve notches and long cracks, which are typically difficult to propagate in a stable manner and to identify in the fracture surfaces. Moreover, in the case of materials with R-curves, measured values from long cracks have no correspondence with the strength of the material, which fractures from small natural defects.

Therefore, a, easy to reproduce method to determine the fracture toughness of materials with small grain size and with cracks similar to natural defects is developed an assessed in this thesis.

2.1.1 Fabrication of small notches

Ablation by means of ultra-short pulsed laser, with pulses in the range of the femtosecond (fs) is proposed to produce small notches with a very sharp tip radius.

Most of the studies on laser ablation of zirconia have been focused on surface ablation and microstructuring. In this sense, it has been reported that micromachining the surface of 3Y-TZP by a pulsed picosecond laser does not affect the strength [236].

Microgrooves on the surface of Y-TZP crowns have been induced by ultrafast laser to aid dental bonding [235] and dental crowns have been manufactured by laser microstructuring of hot-isostatically pressed zirconia [234]. Also, high quality microstructures (grooves and pores) on the surface of cylindrical zirconia dental implants have been created by means of laser ablation [237]. The main interest in these works was focused on the description and analysis of the modified surfaces to evaluate their potential to improve implant performance

It has been stated that there is a minimization of any thermal effect during ablation using pulses in the range of the femtosecond (fs) [238–240]. In this case, the

material is removed by direct vaporization and the heat affected zone is expected to be extremely small as compared to other techniques, provided the deposition of laser energy on the surface of the material occurs in a timescale which is much shorter than the typical time for energy transfer between electrons and lattice [251,252].

Therefore, this technique seems appealing for producing small notches with radius under the micron and with sizes in the range of dozen microns. This should make the technique suitable for materials with submicrometric grain size, and also to help to determine the initiation fracture toughness of materials with small natural defects. This is addressed in Article I.

2.1.2 Analysis of the damage

Even though it has been reported that using pulses in the range of the femtosecond limits the thermal effects [238–240], the pulses to produce sharp notches are focused in a very narrow area, and therefore certain possible damage cannot be neglected. The existence of damage and its possible influence on the determined fracture toughness should be considered. This is addressed in Article I.

Also, the quality of the notches and the influence of different laser parameters on their shape, length and damage in front of its tip is studied in Article III.

2.1.3 Assessment of the methodology

This technique should be suitable for a wide range of advanced ceramics, especially adequate for submicrometre grains-sized materials and with R-curves. Therefore, besides 3Y-TZP it can be also applied to other ceramic materials.

This thesis is focused on zirconia ceramics. However, in order to validate this new methodology, zirconia is not the best ceramic because of the strong effect of many variables on its fracture toughness, such as grain size, environment, stabiliser content, stress rate and R-curve behaviour. A more sound validation of the method is possible by using a ceramic for which K_{Ic} is very well known and is less sensitive to these variables.

Therefore, here it has been used a well-documented commercial silicon nitride (Si_3N_4) with a grain size of a few microns, which in the past was the object of a 'Reference Material Testing Program' (RMTP) of the European Structural Integrity Society (ESIS) Technical Committee 6 for measuring K_{Ic} and other mechanical properties [253,254].

The objective is twofold:

On the one hand, obtained values using the new technique to induce notches can be compared to the values reported in literature for the exact same material. As its grain size is above the micrometre, the influence of the notch-tip radius should be smaller than for 3Y-TZP with submicrometric grain sizes. Therefore, results are expected to be very similar to the reported ones. Also, R-curve of this material appears to be moderately flat, and the influence of initial crack length is then diminished.

On the other hand, the reproducibility of the notches on different types of material, a nitride in this case, is also assessed. The geometry of the notch and the effect of the laser is analysed and compared to previous results in 3Y-TZP. This topic is addressed in Article II.

2.2 Novel co-doped zirconia materials

The second main objective of this thesis consist in the development of novel zirconia ceramics with high resistance to LTD maintaining the good mechanical properties of 3Y-TZP.

As seen in the introduction, there are several ways to improve LTD resistance of 3Y-TZP. One of the approaches is developing composites materials with other oxide or non-oxide phases. However, the objective of this work consists on developing only-zirconia compositions with high performance which could also be used as enhanced matrices for composites.

Using ceria instead of yttria to stabilise the tetragonal phase increases enormously the ageing resistance, but the mechanical properties are rather different. Doping with 12 mol% ceria results in a substantially higher transformability and

fracture toughness compared to 3Y-TZP, but the strength and hardness are lower, which partly can be associated to its larger grain size.

Therefore, the studies are focused on two interrelated approaches. On one side, as one of the goals is to obtain a material with the good mechanical properties of 3Y-TZP and the good LTD resistance of 12Ce-TZP, it seems worthwhile to investigate if combining both materials one could obtain the best properties of each component.

On the other hand, as there is a strong dependence of mechanical properties on grain size, it is expected that controlling the grain growth of Ce-TZP during sintering may increase its strength and hardness.

2.2.1 Yttria-ceria

As discussed in section 1.3.1 in the introduction, using ceria instead of yttria to stabilise the tetragonal phase results in an improved LTD resistance. Therefore, it is expected that the ageing behaviour of 3Y-TZP will improve when mixing 12Ce-TZP with 3Y-TZP, although also with an increase of grain size and concomitant decline of mechanical properties.

Producing several compositions, covering the full range from 100% 3Y-TZP to 100% 12Ce-TZP should be useful to determine the optimum composition where a balance between the good mechanical properties of 3Y-TZP and high LTD resistance of 12Ce-TZP is maintained.

This study is performed in Article IV.

2.2.2 Ceria-calcia

As detailed in section 1.4.1 in the introduction, grain size refinement is one approach to improve the mechanical properties of ceria-stabilised zirconia. In principle, this can be achieved by the addition of specific solutes, which might reduce the grain boundary mobility during sintering [146,184,185].

Due to its low valence and large ionic size (ionic radius of Ca^{2+} and Zr^{4+} are 112 and 84 pm respectively), it is expected calcia to be one of the strongest grain-growth inhibitors, reducing the transformability of ceria-stabilised zirconia and increasing the hardness and strength.

Calcia has only been reported to be effective on reducing the grain growth of 3Y-TZP in one study in 1986 [142], and 12Ce-TZP, in 1990 [186] and 1994 [177]. Surprisingly, even if there are several recent articles about the segregation effect of different elements on 3Y-TZP and its effect on LTD resistance, there is a lack of studies about segregation effects on Ce-TZP and its effect on the mechanical properties. New findings on segregation of elements on the grain boundaries might shed some light on the problem of reducing the grain size of Ce-TZP to increase its mechanical properties.

This topic is discussed in detail in Appended manuscript.

CHAPTER 3
SUMMARY OF THE RESULTS

This thesis has been focused in two main objectives: on the one hand, a strategy to develop novel zirconia materials with better LTD resistance and good mechanical properties, and on the other hand a method to determine accurately the small-crack fracture toughness of these materials, typically with submicrometric grain sizes and R-curve behaviour. In this chapter, the major findings are outlined.

3.1 Fracture toughness determination

The methodology is first developed in Article I for a commercial 3Y-TZP widely used for biomedical applications.

The method proposed is a variation of the SEVNB test (see section 1.5.2). Considering the average grain size of this 3Y-TZP (~330 nm), it was estimated that a notch-tip radius below 1 μm is needed to correctly determine K_{Ic}. These sharp notches are impossible to achieve by the common method of thinning the notch-tip with a razor blade [226]. In this case, the K_{Ic} values are expected to be overestimated, as a clear relation of K_{Ic} with notch root radius has been observed [225,227,255].

Using ultra-short pulsed laser ablation (UPLA), with pulses in the femtosecond (fs) range, it is possible to obtain notches with a tip radius below a micron and a length between 20 and 40 μm. This process creates a damage in the direction of the notch and in front of its tip.

The damaged area consists in a directional narrow band (~2–4 μm) in front of the notch tip with a length of ~15 μm with a high density of microcracks, and its integrity was analysed. Also, no phase transformation was detected in that region. A deeper study of this damage is carried out in Article III.

The physical explanation of this microcracked region cannot be related to photo-thermal effects and it seems likely related to thermomechanical waves induced by the laser ablation process since they are localised in the direction of the notch [256,257] without producing any detectable $t \rightarrow m$ transformation.

It is concluded that the conditions for fracture toughness determination are fulfilled, since not only the tip radius of the notch is very sharp (of less than 1 μm) but also there is a non-transformed microcracked region in front of the notch so that, in principle, the total crack length can be taken as an unshielded edge straight crack with a length equal to that of the notch + microcracked band [229]. After testing the samples, the notch and microcracked area are clearly revealed on fracture surfaces, so that their lengths are measured easily.

As the microcracked density is very high and almost all microcracks are interconnected (see Article III), it is then expected that when the load is increased to

fracture during flexure test, the microcracked region will coalesce and form with the notch one sole crack that under higher loads will become unstable inducing failure [258].

The relatively small values obtained in 3Y-TZP by this method (compared to values reported in the literature) can be explained because the condition for unstable fracture for small unshielded cracks makes very unlikely the exploitation of the toughening from the modest and sharp R-curve present in 3Y-TZP with 330 nm grain size [259] (see section 1.5.5 in Chapter 1). The condition of fracture in case of the presence of R-curve behaviour is reached before the crack can grow in a stable manner.

The influence of different laser parameters is studied in Article III for 3Y-TZP. As expected, the notch depth increases with the total of radiation energy per unit of length. However, the length of the band of microcracks in front of the ablated notches depends on the laser pulse energy but not on the total energy absorbed during ablation of the notch.

As the same configuration of notch and microcracks and small notch tip radius is observed in all cases, it is not expected to have a relevant influence on the determined fracture toughness values. It seems, then, that the method is rather tolerant to different laser parameters, and therefore easier to apply on different setups.

The applicability of this technique to other materials is studied in Article II. Using a silicon nitride with a well-documented mechanical properties and larger grain size than 3Y-TZP, it is possible to assess the methodology, as obtained values are in agreement with literature [228,253,254]. Also, it is observed that the same geometry of notch + microcracks is obtained with materials different from zirconia, a nitride in this case.

This technique has been also applied to Ce-TZP-based materials developed in Article IV and Appended manuscript. Even if Ce-TZP has a higher Vickers indentation fracture toughness and a stronger R-curve behaviour than 3Y-TZP, the obtained values of K_{Ic} are rather similar but lower than those reported by other methods with long cracks [248]. That confirms that stable fracture does not take place when testing small cracks in load control and therefore the full potential toughening of the R-curve is not exploited.

In summary, this method may be of great interest in nanograin size ceramics in which the microstructure is too fine for using the technique based on a machined

notch sharpened via honing. It is also of interest to determine the initiation fracture toughness from small cracks similar to natural defects, so that the K_{Ic} measured is closer to the fracture toughness that determines the strength.

3.2 Novel co-doped zirconia materials

The study realised in Article IV combining both yttria and ceria resulted in compositions with smaller grain sizes, less transformability and ageing resistance than 12Ce-TZP. It is possible to produce intermediate compositions combining the properties of 3Y-TZP and 12Ce-TZP according to the particular needs of every application.

Small amounts of ceria do not seem to have a strong impact in the microstructure and properties of 3Y-TZP. Thus, a composition containing 15 wt% of 12Ce-TZP and 85 wt% of 3Y-TZP also shows important amounts of monoclinic phase after autoclaving at 134 ºC for 72 h.

However, the opposite case, a composition with 85 wt% 12Ce-TZP and 15 wt% 3Y-TZP presents a high hydrothermal stability, with barely no traces of monoclinic phase after the same treatment. It also possesses higher transformability and resistance to contact loading than 3Y-TZP, and a smaller grain size than 12Ce-TZP.

The segregation of different elements of this particular composition has been studied in more detail in a related work [260], not included in this thesis.

On the other hand, the addition of small amounts of calcia (1 to 3 mol%) to 10 and 12 mol% ceria-stabilised zirconia reduces strongly the grain size, increasing hardness and fracture strength and maintaining the high resistance to LTD; as seen in Appended manuscript.

The amount of cubic phase also increases with increasing calcia content, which produces inhomogeneity in the dopant distribution. Cubic grains are highly enriched in Ce and Ca solutes, while overall stabiliser content in the tetragonal neighbouring grains is lowered. This reduces the stabilisation of the tetragonal grains, making them more transformable, which translates in a higher fracture toughness. At the same time, hardness is increased due to the presence of a higher

fraction of cubic phase. This effect is more significant in the composition with 3 mol% calcia and 10 mol% ceria. This particular composition possesses mechanical properties comparable to 3Y-TZP while maintaining the high ageing stability of Ce-TZP. Higher strengths are achievable with only 1 mol% calcia addition, at the expense of lowering slightly the fracture toughness and transformability.

CHAPTER 4
CONCLUSIONS AND PERSPECTIVES

This last chapter includes the general conclusions of the thesis, together with the scientific impact and possible future implications.

4.1 Ultra-short pulsed laser ablation

Ultra-short pulsed laser ablation is a straightforward process to fabricate sharp notches for an accurate determination of fracture toughness that may be of great interest especially in submicrometre-sized ceramics and composites.

This is particularly interesting to determine fracture toughness from small unshielded cracks in materials with R-curve behaviour. Unless the R-curve presents high steepness at the beginning of crack extension, the fracture toughness measured is the initiation fracture toughness.

The method developed can be also applied to sharpen the blunt tip of much longer notches introduced by classic mechanical methods like, for example, through a diamond saw [261,262], or to produce directly long notches [263].

Due to the reliability and precision of the technique, the scatter and uncertainties from measurements are highly reduced, in comparison with other techniques like SCF, where the small crack is difficult to identify and measure, or SEVNB with blunt notches, where measurements depend on notch-tip radius.

The processing times of this technique are proportional to notch depths, but much faster compared to other methods.

4.2 Grain growth inhibition

Through an understanding of the segregation behaviour of the cations in solution in zirconia ceramics, it is possible to control and tailor the microstructure of ceria-stabilised zirconia, obtaining materials with a good combination of mechanical properties and high hydrothermal resistance.

Cation segregation at the grain boundaries and grain growth inhibition due to a solute drag mechanism depends on cation valence and radius, being the larger divalent cation dopant the most successful on reducing the grain boundary mobility.

Thus, small amounts of calcia inhibits strongly the grain growth of ceria-stabilised zirconia, reducing at the same time the transformability and increasing the

hardness and the fracture strength. The content of cubic phase also increases, leading to a phase partition that diminishes the stabiliser of the tetragonal phase, being more transformable. However, the hardness is maintained due to the increase of cubic phase. Besides the consequent good combination of high fracture toughness, hardness and strength, these compositions possess high ageing resistance.

Therefore, phase partition seems an interesting approach to obtain an only-zirconia "composite" material, consisting in a harder phase (cubic phase) and a very transformable and tough one (impoverished tetragonal grains). Future work on this topic should be focused on the precise optimization of the composition to control the extend of this phase partition, which could enhance the mechanical properties, along with the optimization of the mixing and sintering conditions. Future studies could also aim to apply these co-doped ceramics in composites as matrices with reinforcements of hard particles such as alumina.

The use of ceria as a dopant is especially delicate due to its different oxidation states, so future work could be focused on their influence on the microstructure and mechanical properties. As it has been seen in section 1.3.2 in Chapter 1, segregation of solutes in the grain boundaries is due to their attraction to the electric potential of the space-charge layer. As this potential is produced mostly by the accumulation or depletion of oxygen vacancies, and as ceria does not stabilise by the generation of vacancies (when processed in oxygen-rich atmospheres it should be present as Ce^{4+}), ceria-stabilised zirconia, theoretically, should not possess a space-charge layer. However, it is believed that a certain amount of Ce^{3+} is always present even when sintering in air, which would form oxygen vacancies and segregate to the grain boundaries (in some cases, Ce has been found slightly segregated at the grain boundaries [260,264], as also shown in Appended manuscript. It is expected that the segregation tendency of Ce^{3+} to be higher than Ce^{4+} because of its larger ionic size (see Table 1.2 in section 1.2.1 in the introduction) and different valence than Zr^{4+}, so that it is often assumed that the segregated Ce ions at the grain boundaries are in the Ce^{3+} form. Therefore, it seems that the amount of Ce^{3+}, which depends on the sintering conditions, could influence the segregation of other solutes on the grain boundaries.

There is also a lack of understanding about the influence of the different ratios of Ce^{4+}/Ce^{3+} on the microstructure, mechanical properties, LTD resistance and aesthetical appearance. The improvement of precision and resolution of equipment such as XPS might clarify this topic, helping on the better control of the manufacture of Ce-TZPs.

REFERENCES

[1] Harper, D. Zircon. *Online Etymology Dictionary* Available at: http://www.etymonline.com/index.php?term=zircon. (Accessed: 22nd January 2013)

[2] Clark, G. L. & Reynolds, D. H. Chemistry of zirconium dioxide, X-ray diffraction studies. *Ind. Eng. Chem.* **29,** 711–715 (1937).

[3] Hannink, R. H. J., Kelly, P. M. & Muddle, B. C. Transformation Toughening in Zirconia-Containing Ceramics. *J. Am. Ceram. Soc.* **83,** 461–487 (2000).

[4] Subbarao, E. C., Maiti, H. S. & Srivastava, K. K. Martensitic Transformation in Zirconia. *Phys. status solidi* **21,** 9–40 (1974).

[5] Ruff, O. & Ebert, F. Beiträge zur Keramik hochfeuerfester Stoffe l. Die Formen des Zirkondioxyds. *Zeitschrift für Anorg. und Allg. Chemie* **180,** 19–41 (1929).

[6] Ruff, O., Ebert, F. & Stephan, E. Beiträge zur Keramik hochfeuerfester Stoffe II. Das System ZrO2-CaO. *Zeitschrift für Anorg. und Allg. Chemie* **180,** 215–224 (1929).

[7] Ruff, O., Ebert, F. & Woitinek, H. Beiträge zur Keramik hochfeuerfester Stoffe III. Das System ZrO2-ThO2. *Zeitschrift für Anorg. und Allg. Chemie* **180,** 252–256 (1929).

[8] Ruff, O., Ebert, F. & Stephan, E. Beiträge zur Keramik hochfeuerfester Stoffe IV. Das System ZrO2-BeO. *Zeitschrift für Anorg. und Allg. Chemie* **185,** 221–224 (1929).

[9] Duwez, P., Odell, F. & Brown, Frank H., J. Stabilization of Zironia with Calcia and Magnesia. *J. Am. Ceram. Soc.* **35,** 107–113 (1952).

[10] Wolten, G. M. Diffusionless Phase Transformations in Zirconia and Hafnia. *J. Am. Ceram. Soc.* **46,** 418–422 (1963).

[11] Garvie, R. C. The occurrence of metastable tetragonal zirconia as a crystallite size effect. *J. Phys. Chem.* **69,** 1238–1243 (1965).

[12] Garvie, R. C. & Nicholson, P. S. Phase Analysis in Zirconia Systems. *J. Am. Ceram. Soc.* **55,** 303–305 (1972).

[13] Garvie, R. C., Hannink, R. H. & Pascoe, R. T. Ceramic steel? *Nature* **258,** 703–704 (1975).

[14] Rieth, P. H., Reed, J. S. & Naumann, A. W. Fabrication and flexural strength of ultrafine-grained yttria-stabilized zirconia. *Am. Ceram. Soc. Bull.* **55,** 717 (1976).

[15] Gupta, T. K., Bechtold, J. H., Kuznicki, R. C., Cadoff, L. H. & Rossing, B. R. Stabilization of tetragonal phase in polycrystalline zirconia. *J. Mater. Sci.* **12,** 2421–2426 (1977).

[16] Piconi, C., Burger, W., Richter, H. G., Cittadini, A., Maccauro, G., Covacci, V., Bruzzese, N., Ricci, G. A. & Marmo, E. Y-TZP ceramics for artificial joint replacements. *Biomaterials* **19,** 1489–1494 (1998).

[17] Piconi, C. & Maccauro, G. Zirconia as a ceramic biomaterial. *Biomaterials* **20,** 1–25 (1999).

[18] Christel, P., Meunier, A., Dorlot, J.-M., Crolet, J.-M., Witvoet, J., Sedel, L. & Boutin, P. Biomechanical Compatibility and Design of Ceramic Implants for Orthopedic Surgery. *Ann. N. Y. Acad. Sci.* **523,** 234–256 (1988).

[19] Denry, I. & Kelly, J. R. State of the art of zirconia for dental applications. *Dent. Mater.* **24,** 299–307 (2008).

[20] Kobayashi, K., Kuwajima, H. & Masaki, T. Phase change and mechanical properties of ZrO2–Y2O3 solid electrolyte after ageing. *Solid State Ion.* **3/4,** 489–493 (1981).

[21] Chevalier, J. & Gremillard, L. Ceramics for medical applications: A picture for the next 20 years. *J. Eur. Ceram. Soc.* **29,** 1245–1255 (2009).

[22] US Food and Drug Administration. *Steam re-sterilization causes deterioration of zirconia ceramic heads of total hip prostheses*. (1997).

[23] Maccauro, G., Piconi, C., Burger, W., Pilloni, L., De Santis, E., Muratori, E. & Learmonth, I. D. Fracture of a Y-TZP ceramic femoral head. *J. Bone Jt. Surgery-British Vol.* **86B,** 1192–1196 (2004).

[24] Chevalier, J. What future for zirconia as a biomaterial? *Biomaterials* **27,** 535–543 (2006).

[25] Lawson, S. Environmental Degradation of Zirconia Ceramics. *J. Eur. Ceram. Soc.* **15,** 485–502 (1995).

[26] Chevalier, J., Cales, B. & Drouin, J. M. Low-Temperature Aging of Y-TZP Ceramics. *J. Am. Ceram. Soc.* **82,** 2150–2154 (1999).

[27] Gaillard, Y., Jiménez-Piqué, E., Soldera, F., Mücklich, F. & Anglada, M. Quantification of hydrothermal degradation in zirconia by nanoindentation. *Acta Mater.* **56,** 4206–4216 (2008).

[28] Chevalier, J., Gremillard, L. & Deville, S. Low-Temperature Degradation of Zirconia and Implications for Biomedical Implants. *Annu. Rev. Mater. Res.* **37,** 1–32 (2007).

[29] Chevalier, J., Gremillard, L., Virkar, A. V. & Clarke, D. R. The tetragonal-monoclinic transformation in zirconia: Lessons learned and future trends. *J. Am. Ceram. Soc.* **92,** 1901–1920 (2009).

[30] Muñoz-Tabares, J. A., Jiménez-Piqué, E., Reyes-Gasga, J. & Anglada, M. Microstructural changes in ground 3Y-TZP and their effect on mechanical properties. *Acta Mater.* **59,** 6670–6683 (2011).

[31] Yoshimura, M. Phase stability of zirconia. *Am. Ceram. Soc. Bull.* **67,** 1950–1955 (1988).

[32] Pjetursson, B. E., Sailer, I., Zwahlen, M. & Hämmerle, C. H. F. A systematic review of the survival and complication rates of all-ceramic and metal-ceramic reconstructions after an observation period of at least 3 years. Part I: single crowns. *Clin. Oral Implants Res.* **18,** 73–85 (2007).

[33] Sailer, I., Pjetursson, B. E., Zwahlen, M. & Hämmerle, C. H. F. A systematic review of the survival and complication rates of all-ceramic and metal-ceramic reconstructions after an observation period of at least 3 years. Part II: fixed dental prostheses. *Clin. Oral Implants Res.* **18,** 86–96 (2007).

[34] Schley, J.-S., Heussen, N., Reich, S., Fischer, J., Haselhuhn, K. & Wolfart, S. Survival probability of zirconia-based fixed dental prostheses up to 5 yr: a systematic review of the literature. *Eur. J. Oral Sci.* **118,** 443–450 (2010).

[35] Raigrodski, A. J., Hillstead, M. B., Meng, G. K. & Chung, K.-H. Survival and complications of zirconia-based fixed dental prostheses: A systematic review. *J. Prosthet. Dent.* **107,** 170–177 (2012).

[36] Le, M., Papia, E. & Larsson, C. The clinical success of tooth- and implant-supported zirconia-based fixed dental prostheses. A systematic review. *J. Oral Rehabil.* **42,** 467–480 (2015).

[37] Beuer, F., Sachs, C., Groesser, J., Gueth, J.-F. & Stimmelmayr, M. Tooth-implant-supported posterior fixed dental prostheses with zirconia frameworks: 3-year clinical result. *Clin. Oral Investig.* **20,** 1079–1086 (2016).

[38] Beuer, F., Stimmelmayr, M., Gueth, J.-F., Edelhoff, D. & Naumann, M. In vitro performance of full-contour zirconia single crowns. *Dent. Mater.* **28,** 449–456 (2012).

[39] Preis, V., Behr, M., Hahnel, S., Handel, G. & Rosentritt, M. In vitro failure and fracture resistance of veneered and full-contour zirconia restorations. *J. Dent.* **40,** 921–928 (2012).

[40] Swain, M. V. Impact of oral fluids on dental ceramics: What is the clinical relevance? *Dent. Mater.* **30,** 33–42 (2014).

[41] Turp, V., Tuncelli, B., Sen, D. & Goller, G. Evaluation of hardness and fracture toughness, coupled with microstructural analysis, of zirconia ceramics stored in environments with different pH values. *Dent. Mater. J.* **31,** 891–902 (2012).

[42] Pauling, L. The principles determining the structure of complex ionic crystals. *J. Am. Chem. Soc.* **51,** 1010–1026 (1929).

[43] Cambridge, U. of. DoITPoMS TLP Library. Available at: http://www.doitpoms.ac.uk/tlplib/fuel-cells/sofc_electrolyte.php. (Accessed: 22nd January 2013)

[44] Kröger, F. A. & Vink, H. J. Relations between the Concentrations of Imperfections in Crystalline Solids. *Solid State Phys.* **3,** 307–435 (1956).

[45] Li, P., Chen, I. W. & Penner-Hahn, J. E. X-ray-absorption studies of zirconia polymorphs. II. Effect of Y2O3 dopant on ZrO2 structure. *Phys. Rev. B* **48,** 10074–10081 (1993).

[46] Li, P., Chen, I. & Penner-Hahn, J. E. Effect of Dopants on Zirconia Stabilization—An X-ray Absorption Study: I, Trivalent Dopants. *J. Am. Ceram. Soc.* **77,** 118–128 (1994).

[47] Fabris, S., Paxton, A. T. & Finnis, M. W. A stabilization mechanism of zirconia based on oxygen vacancies only. *Acta Mater.* **50,** 5171–5178 (2002).

[48] Ostanin, S., Salamatov, E., Craven, A. J., McComb, D. W. & Vlachos, D. Theory of the phases and atomistic structure of yttria-doped zirconia. *Phys. Rev. B* **66,** 132105 (2002).

[49] Bogicevic, a., Wolverton, C., Crosbie, G. & Stechel, E. Defect ordering in aliovalently doped cubic zirconia from first principles. *Phys. Rev. B* **64,** 1–14 (2001).

[50] Shannon, R. D. Revised effective ionic radii and systematic studies of interatomic distances in halides and chalcogenides. *Acta Crystallogr. Sect. A* **32,** 751–767 (1976).

[51] Li, P., Chen, I.-W. & Penner-Hahn, J. E. Effect of Dopants on Zirconia Stabilization—An X-ray Absorption Study: II, Tetravalent Dopants. *J. Am. Ceram. Soc.* **77,** 1281–1288 (1994).

[52] Li, P., Chen, I.-W. & Penner-Hahn, J. E. Effect of Dopants on Zirconia Stabilization—An X-ray Absorption Study: III, Charge-Compensating Dopants. *J. Am. Ceram. Soc.* **77,** 1289–1295 (1994).

[53] Yashima, M., Hirose, T., Kakihana, M., Suzuki, Y. & Yoshimura, M. Size and Charge Effects of Dopant M on the Unit-Cell Parameters of Monoclinic Zirconia Solid Solutions Zr0.98M0.02O2 -δ (M = Ce, La, Nd, Sm, Y, Er, Yb, Sc, Mg, Ca). *J. Am. Ceram. Soc.* **80,** 171–175 (1997).

[54] Duwez, P., Brown, F. H. & Odell, F. The Zirconia-Yttria System. *J. Electrochem. Soc.* **98,** 356 (1951).

[55] Scott, H. G. G. Phase relationships in the zirconia-yttria system. *J. Mater. Sci.* **10,** 1527–1535 (1975).

[56] Yashima, M., Kakihana, M. & Yoshimura, M. Metastable-stable phase diagrams in the zirconia-containing systems utilized in solid-oxide fuel cell application. *Solid State Ion.* **86–88,** 1131–1149 (1996).

[57] Jacobson, N. S., Liu, Z.-K., Kaufman, L. & Zhang, F. Thermodynamic Modeling of the YO1.5–ZrO2 System. *J. Am. Ceram. Soc.* **87,** 1559–1566 (2004).

[58] Chen, M., Hallstedt, B. & Gauckler, L. J. Thermodynamic modeling of the ZrO2–YO1.5 system. *Solid State Ion.* **170,** 255–274 (2004).

[59] Lakiza, S., Fabrichnaya, O., Zinkevich, M. & Aldinger, F. On the phase relations in the ZrO2–YO1.5–AlO1.5 system. *J. Alloys Compd.* **420,** 237–245 (2006).

[60] Fabrichnaya, O. & Aldinger, F. Assessment of thermodynamic parameters in the system ZrO2–Y2O3–Al2O3. *Zeitschrift für Met.* **95,** 27–39 (2004).

[61] Li, L., Van der Biest, O., Wang, P. L., Vleugels, J., Chen, W. W. & Huang, S. G. Estimation of the phase diagram for the ZrO2–Y2O3–CeO2 system. *J. Eur. Ceram. Soc.* **21,** 2903–2910 (2001).

[62] Grain, C. F. Phase Relations in the ZrO2-MgO System. *J. Am. Ceram. Soc.* **50,** 288–290 (1967).

[63] Garvie, R. C. The Cubic Field in the System CaO-ZrO2. *J. Am. Ceram. Soc.* **51,** 553–556 (1968).

[64] Stubican, V. S. & Ray, S. P. Phase Equilibria and Ordering in the System ZrO2-CaO. *J. Am. Ceram. Soc.* **60,** 534–537 (1977).

[65] Hellmann, J. R. & Stubican, V. S. Stable and Metastable Phase Relations in the System ZrO2-CaO. *J. Am. Ceram. Soc.* **66,** 260–264 (1983).

[66] Duran, P., Recio, P. & Rodriguez, J. M. Low temperature phase equilibria and ordering in the ZrO2-rich region of the system ZrO2-CaO. *J. Mater. Sci.* **22,** 4348–4356 (1987).

[67] Du, Y., Jin, Z. & Huang, P. Thermodynamic Calculation of the Zirconia–Calcia System. *J. Am. Ceram. Soc.* **75,** 3040–3048 (1992).

[68] Yin, Y. & Argent, B. B. Phase diagrams and thermodynamics of the systems ZrO2-CaO and ZrO2-MgO. *J. Phase Equilibria* **14,** 439–450 (1993).

[69] Kwon, S. Y. & Jung, I. H. Critical evaluation and thermodynamic optimization of the CaO-ZrO2 and SiO2-ZrO2 systems. *J. Eur. Ceram. Soc.* **37,** 1105–1116 (2017).

[70] Pyda, W. & Haberko, K. CaO-Containing Tetragonal ZrO2 Polycrystals (Ca-TZP). *Ceram. Int.* **13,** 113–118 (1987).

[71] Bailey, J. E. The Monoclinic-Tetragonal Transformation and Associated Twinning in Thin Films of Zirconia. *Proc. R. Soc.* **279,** 395–412 (1964).

[72] Kelly, P. M. & Rose, L. R. F. The martensitic transformation in ceramics – its role in transformation toughening. *Prog. Mater. Sci.* **47,** 463–557 (2002).

[73] Deville, S., Guénin, G. & Chevalier, J. Martensitic transformation in zirconia – Part I. Nanometer scale prediction and measurement of transformation induced relief. *Acta Mater.* **52,** 5697–5707 (2004).

[74] Deville, S., Guénin, G. & Chevalier, J. Martensitic transformation in zirconia – Part II. Martensite growth. *Acta Mater.* **52,** 5709–5721 (2004).

[75] Lange, F. F. Transformation toughening - Part 1 Size effects associated with the thermodynamics of constrained transformations. *J. Mater. Sci.* **17,** 225–234 (1982).

[76] Schmauder, S. & Schubert, H. Significance of Internal Stresses for the Martensitic Transformation in Yttria-Stabilized Tetragonal Zirconia Polycrystals During Degradation. *J. Am. Ceram. Soc.* **69,** 534–540 (1986).

[77] Lange, F. F. Transformation toughening - Part 2 Contribution to fracture toughness. *J. Mater. Sci.* **17,** 235–239 (1982).

[78] Butler, E. P. Transformation-toughened zirconia ceramics. *Mater. Sci. Technol.* **1,** 417–432 (1985).

[79] Kelly, J. R. & Denry, I. Stabilized zirconia as a structural ceramic: An overview. *Dent. Mater.* **24,** 289–298 (2008).

[80] Evans, A. G. Perspective on the Development of High-Toughness Ceramics. *J. Am. Ceram. Soc.* **73,** 187–206 (1990).

[81] Becher, P. F. & Swain, M. V. Grain-Size-Dependent Transformation Behavior in Polycrystalline Tetragonal Zirconia. *J. Am. Ceram. Soc.* **75,** 493–502 (1992).

[82] Lange, F. F. Transformation toughening - Part 3 Experimental observations in the ZrO2-Y2O3 system. *J. Mater. Sci.* **17,** 240–246 (1982).

[83] Tsukuma, K., Kubota, Y. & Tsukidate, T. Thermal and mechanical properties of Y2O3-stabilized tetragonal zirconia polycrystals; in: *Advances in Ceramics, vol. 12, Science and*

Technology of Zirconia II (eds. Claussen, N., Rühle, M. & Heuer, A. H.) 382–390 (American Ceramic Society, Columbus, OH, 1984).

[84] Watanabe, M., Iio, S. & Fuukura, I. Ageing behaviour of Y-TZP; in: *Advances in Ceramics, vol. 12, Science and Technology of Zirconia II* (eds. Claussen, N., Rühle, M. & Heuer, A. H.) 391–398 (The American Ceramic Society, Inc., Columbus, OH, 1984).

[85] Tsubakino, H., Hamamoto, M. & Nozato, R. Tetragonal-to-monoclinic phase transformation during thermal cycling and isothermal ageing in yttria-partially stabilized zirconia. *J. Mater. Sci.* **26,** 5521–5526 (1991).

[86] Cottom, B. A. & Mayo, M. J. Fracture toughness of nanocrystalline ZrO2-3mol% Y2O3 determined by Vickers indentation. *Scr. Mater.* **34,** 809–814 (1996).

[87] Eichler, J., Rödel, J., Eisele, U. & Hoffman, M. Effect of Grain Size on Mechanical Properties of Submicrometer 3Y-TZP: Fracture Strength and Hydrothermal Degradation. *J. Am. Ceram. Soc.* **90,** 2830–2836 (2007).

[88] Lange, F. F. Transformation toughening - Part 5 Effect of temperature and alloy on fracture toughness. *J. Mater. Sci.* **17,** 255–262 (1982).

[89] Michel, D., Mazerolles, L. & Perez Y Jorba, M. Fracture of metastable tetragonal zirconia crystals. *J. Mater. Sci.* **18,** 2618–2628 (1983).

[90] Virkar, A. V. & Matsumoto, R. L. K. Ferroelastic Domain Switching as a Toughening Mechanism in Tetragonal Zirconia. *J. Am. Ceram. Soc.* **69,** C-224-C-226 (1986).

[91] Ingel, R. P., Lewis, D., Bender, B. A. & Rice, R. W. Temperature Dependence of Strength and Fracture Toughness of ZrO2 Single Crystals. *Commun. Am. Ceram. Soc.* **65,** C150–C152 (1982).

[92] Ingel, R. P., Lewis, D., Bender, B. A. & Rice, R. W. Physical, Microstructural, and Thermomechanical Properties of ZrO2 Single Crystals; in: *Advances in Ceramics, vol. 12, Science and Technology of Zirconia II* (eds. Claussen, N., Rühle, M. & Heuer, A. H.) 408–414 (American Ceramic Society, Columbus, OH, 1984).

[93] Cain, M. G. & Lewis, M. H. Evidence of ferroelasticity in Y-tetragonal zirconia polycrystals. *Mater. Lett.* **9,** 309–312 (1990).

[94] Srinivasan, G. V., Jue, J.-F., Kuo, S.-Y. & Virkar, A. V. Ferroelastic Domain Switching in Polydomain Tetragonal Zirconia Single Crystals. *J. Am. Ceram. Soc.* 7**2,** 2098–2103 (1989).

[95] Sheu, T. -S, Tien, T. -Y & Chen, I. -W. Cubic-to-Tetragonal (t') Transformation in Zirconia-Containing Systems. *J. Am. Ceram. Soc.* 7**5,** 1108–1116 (1992).

[96] Chan, C.-J., Lange, F. F., Ruhle, M., Jue, J.-F. & Virkar, A. V. Ferroelastic Domain Switching in Tetragonal Zirconia Single Crystals-Microstructural Aspects. *J. Am. Ceram. Soc.* 7**4,** 807–813 (1991).

[97] Yoshimura, M., Noma, T., Kawabata, K. & Sōmiya, S. Role of H2O on the degradation process of Y-TZP; in: *Hydrothermal Reactions for Materials Science and Engineering*, ch. 7, 396–398 (Springer Netherlands, Dordrecht, 1989).

[98] Guo, X. Low Temperature Degradation Mechanism of Tetragonal Zirconia Ceramics in Water: Role of Oxygen Vacancies. *Solid State Ion.* **112,** 113–116 (1998).

[99] Guo, X. On the degradation of zirconia ceramics during low-temperature annealing in water or water vapor. *J. Phys. Chem. Solids* **60,** 539–546 (1999).

[100] Deville, S., Chevalier, J. & Gremillard, L. Influence of surface finish and residual stresses on the ageing sensitivity of biomedical grade zirconia. *Biomaterials* **27,** 2186–2192 (2006).

[101] Muñoz-Tabares, J. A. & Anglada, M. Quantitative Analysis of Monoclinic Phase in 3Y-TZP by Raman Spectroscopy. *J. Am. Ceram. Soc.* **93,** 1790–1795 (2010).

[102] Deville, S., Chevalier, J., Fantozzi, G., Bartolomé, J. F., Requena, J., Moya, J. S., Torrecillas, R. & Díaz, L. A. Low-temperature ageing of zirconia-toughened alumina ceramics and its implication in biomedical implants. *J. Eur. Ceram. Soc.* **23,** 2975–2982 (2003).

[103] Sato, T., Ohtaki, S., Endo, T. & Shimada, M. Transformation of Yttria-Doped Tetragonal ZrO2 Polycrystals by Annealing under Controlled Humidity Conditions. *J. Am. Ceram. Soc.* **68,** C-320-C-322 (1985).

[104] Guo, X. Property degradation of tetragonal zirconia induced by low-temperature defect reaction with water molecules. *Chem. Mater.* **16,** 3988–3994 (2004).

[105] Schubert, H. & Frey, F. Stability of Y-TZP during hydrothermal treatment: neutron experiments and stability considerations. *J. Eur. Ceram. Soc.* **25,** 1597–1602 (2005).

[106] Muñoz-Tabares, J. A., Jiménez-Piqué, E. & Anglada, M. Subsurface evaluation of hydrothermal degradation of zirconia. *Acta Mater.* **59,** 473–484 (2011).

[107] Avrami, M. Kinetics of Phase Change. II Transformation-Time Relations for Random Distribution of Nuclei. *J. Chem. Phys.* **8,** 212 (1940).

[108] Lawson, S. & Smith, P. A. A New Technique for Monitoring Aging in Yttria-Tetragonal Zirconia Polycrystals. *J. Am. Ceram. Soc.* **76,** 3170–3172 (1993).

[109] Keuper, M., Eder, K., Berthold, C. & Nickel, K. G. Direct evidence for continuous linear kinetics in the low-temperature degradation of Y-TZP. *Acta Biomater.* **9,** 4826–4835 (2013).

[110] Keuper, M., Berthold, C. & Nickel, K. G. Long-time aging in 3 mol.% yttria-stabilized tetragonal zirconia polycrystals at human body temperature. *Acta Biomater.* **10,** 951–959 (2014).

[111] Vleugels, J. J., Yuan, Z. X. & Van der Biest, O. Mechanical properties of Y2O3/Al2O3-coated Y-TZP ceramics. **22,** 873–881 (2002).

[112] Tsubakino, H., Sonoda, K. & Nozato, R. Martensite transformation behaviour during isothermal ageing in partially stabilized zirconia with and without alumina addition. *J. Mater. Sci. Lett.* **12,** 196–198 (1993).

[113] Kim, D.-J., Jung, H.-J. & Cho, D.-H. Phase transformations of Y2O3 and Nb2O5 doped tetragonal zirconia during low temperature aging in air. *Solid State Ion.* **80,** 67–73 (1995).

[114] Chevalier, J., Grandjean, S., Kuntz, M. & Pezzotti, G. On the kinetics and impact of tetragonal to monoclinic transformation in an alumina/zirconia composite for arthroplasty applications. *Biomaterials* **30,** 5279–5282 (2009).

[115] Lughi, V. & Sergo, V. Low temperature degradation -aging- of zirconia: A critical review of the relevant aspects in dentistry. *Dent. Mater.* **26,** 807–820 (2010).

[116] Zhang, F., Vanmeensel, K., Inokoshi, M., Batuk, M., Hadermann, J., Van Meerbeek, B., Naert, I. & Vleugels, J. Critical influence of alumina content on the low temperature degradation of 2–3mol% yttria-stabilized TZP for dental restorations. *J. Eur. Ceram. Soc.* **35,** 741–750 (2015).

[117] Zhang, F., Inokoshi, M., Vanmeensel, K., Van Meerbeek, B., Naert, I. & Vleugels, J. Lifetime estimation of zirconia ceramics by linear ageing kinetics. *Acta Mater.* **92,** 290–298 (2015).

[118] Zhang, F., Batuk, M., Hadermann, J., Manfredi, G., Mariën, A., Vanmeensel, K., Inokoshi, M., Van Meerbeek, B., Naert, I. & Vleugels, J. Effect of cation dopant radius on the hydrothermal stability of tetragonal zirconia: Grain boundary segregation and oxygen vacancy annihilation. *Acta Mater.* **106,** 48–58 (2016).

[119] Nasrallah, M. M. & Douglass, D. L. Ionic and Electronic Conductivity in Y2O3-Doped Monoclinic ZrO2. *J. Electrochem. Soc.* **121,** 255 (1974).

[120] Badwal, S. P. S. & Swain, M. V. ZrO2-Y2O3: electrical conductivity of some fully and partially stabilized single grains. *J. Mater. Sci. Lett.* **4,** 487–489 (1985).

[121] Weller, M. & Schubert, H. Internal Friction, Dielectric Loss, and Ionic Conductivity of Tetragonal ZrO2-3% Y2O3 (Y-TZP). *J. Am. Ceram. Soc.* **69,** 573–577 (1986).

[122] Badwal, S. P. S. & Drennan, J. Grain boundary resistivity in Y-TZP materials as a function of thermal history. *J. Mater. Sci.* **24,** 88–96 (1989).

[123] Manning, P., Sirman, J. D., De Souza, R. A. & Kilner, J. A. The kinetics of oxygen transport in 9.5 mol% single crystal yttria stabilised zirconia. *Solid State Ion.* **100,** 1–10 (1997).

[124] Lughi, V. & Clarke, D. R. Low-temperature transformation kinetics of electron-beam deposited 5 wt.% yttria-stabilized zirconia. *Acta Mater.* **55,** 2049–2055 (2007).

[125] Rogers, W. J. Steam and dry heat sterilization of biomaterials and medical devices; in: *Sterilisation of Biomaterials and Medical Devices* (eds. Lerouge, S. & Simmons, A.) 20–55 (Woodhead Publishing Limited, Cambridge, 2012).

[126] ANSI/AAMI/ISO TIR17665-2:2009. *Sterilization of health care products — Moist heat — Part 2: Guidance on the application of ANSI/AAMI/ISO 17665-1*. (Association for the Advancement of Medical Instrumentation, 2009).

[127] Olagnon, C., Chevalier, J. & Pauchard, V. Global description of crack propagation in ceramics. *J. Eur. Ceram. Soc.* **26,** 3051–3059 (2006).

[128] Deville, S., Gremillard, L., Chevalier, J. & Fantozzi, G. A critical comparison of methods for the determination of the aging sensitivity in biomedical grade yttria-stabilized zirconia. *J. Biomed. Mater. Res. - Part B Appl. Biomater.* 7**2,** 239–245 (2005).

[129] Chevalier, J., Deville, S., Münch, E., Jullian, R. & Lair, F. Critical effect of cubic phase on aging in 3 mol% yttria-stabilized zirconia ceramics for hip replacement prosthesis. *Biomaterials* **25,** 5539–5545 (2004).

[130] Inokoshi, M., Zhang, F., De Munck, J., Minakuchi, S., Naert, I., Vleugels, J., Van Meerbeek, B., Vanmeensel, K., Munck, J. De, Minakuchi, S., Naert, I., Vleugels, J., Meerbeek, B. Van & Vanmeensel, K. Influence of sintering conditions on low-temperature degradation of dental zirconia. *Dent. Mater.* **30,** 669–678 (2014).

[131] Kountouros, P. & Petzow, G. *Science and Technology of Zirconia V*. (eds. Badwal, S. P. S., Bannister, M. J. & Hannink, R. H. J.) (Technomic, Lancaster, 1993).

[132] Guo, X. & He, J. Hydrothermal degradation of cubic zirconia. *Acta Mater.* **51,** 5123–5130 (2003).

[133] Guo, X. Physical origin of the intrinsic grain-boundary resistivity of stabilized-zirconia: Role of the space-charge layers. *Solid State Ion.* **81,** 235–242 (1995).

[134] Guo, X. Solute Segregations at the Space-Charge Layers of Stabilized Zirconia: An Opportunity for Ameliorating Conductivity. *J. Eur. Ceram. Soc.* **16,** 575–578 (1996).

[135] Guo, X. Space-charge conduction in yttria and alumina codoped-zirconia. *Solid State Ion.* **96,** 247–254 (1997).

[136] Guo, X. & Waser, R. Space charge concept for acceptor-doped zirconia and ceria and experimental evidences. *Solid State Ion.* **173,** 63–67 (2004).

[137] Guo, X. & Maier, J. Grain Boundary Blocking Effect in Zirconia: A Schottky Barrier Analysis. *J. Electrochem. Soc.* **148,** E121–E126 (2001).

[138] Guo, X. & Zhang, Z. Grain size dependent grain boundary defect structure: Case of doped zirconia. *Acta Mater.* **51,** 2539–2547 (2003).

[139] Badwal, S. P. S. Grain boundary resistivity in zirconia-based materials: effect of sintering temperatures and impurities. *Solid State Ion.* **76,** 67–80 (1995).

[140] ISO 13356:2008. *Implants for surgery - Ceramic materials based on yttria-stabilized tetragonal zirconia (Y-TZP)*. (2013).

[141] Sato, T. & Shimada, M. Transformation of Ceria-Doped Tetragonal Zirconia Polycrystals by Annealing in Water. *Am. Ceram. Soc. Bull.* **64,** 1382–1384 (1985).

[142] Sato, T., Ohtaki, S., Endo, T. & Shimada, M. Improvement of thermal stability of Yttria-doped tetragonal zirconia polycrystals by alloying with various oxides. *Int. J. High Technol. Ceram.* **2,** 167–177 (1986).

[143] Duh, J.-G., Dai, H.-T. & Hsu, W.-Y. Synthesis and sintering behaviour in CeO2-ZrO2 ceramics. *J. Mater. Sci.* **23,** 2786–2791 (1988).

[144] Duh, J.-G., Dai, H.-T. & Chiou, B.-S. Sintering, Microstructure, Hardness, and Fracture Toughness Behavior of Y2O3-CeO2-ZrO2. *J. Am. Ceram. Soc.* **71,** 813–819 (1988).

[145] Boutz, M. M. R., Winnubst, A. J. A., Van Langerak, B., Olde Scholtenhuis, R. J. M., Kreuwel, K. & Burggraaf, A. J. The effect of ceria co-doping on chemical stability and fracture toughness of Y-TZP. *J. Mater. Sci.* **30,** 1854–1862 (1995).

[146] Theunissen, G. S. A. M., Winnubst, A. J. A. & Burggraaf, A. J. Effect of dopants on the sintering behaviour and stability of tetragonal zirconia ceramics. *J. Eur. Ceram. Soc.* **9,** 251–263 (1992).

[147] Lin, J.-D. & Duh, J.-G. Correlation of mechanical properties and composition in tetragonal CeO2-Y2O3-ZrO2 ceramic system. *Mater. Chem. Phys.* 7**8,** 246–252 (2002).

[148] Lin, J. D. & Duh, J. G. Fracture toughness and hardness of ceria- and yttria-doped tetragonal zirconia ceramics. *Mater. Chem. Phys.* 7**8,** 253–261 (2003).

[149] Huang, S. G., Vleugels, J., Li, L., Van der Biest, O. & Wang, P. L. Composition design and mechanical properties of mixed (Ce,Y)-TZP ceramics obtained from coated starting powders. *J. Eur. Ceram. Soc.* **25,** 3109–3115 (2005).

[150] Nakahira, A., Murakami, T., Kudou, T., Matsushita, T. & Honma, T. Fabrication and evaluation of high performance 12Ce-ZrO2/3Y-ZrO2 composites for an implant. *J. Ceram. Soc. Japan* **11,** 1076–1080 (2006).

[151] Nakahira, A., Murakami, T., Ohta, M., Honma, T. & Kudo, T. Ce and Y Local Structures of High-performance ZrO2 Composites Codoped with Ce and Y for Implant Applications. *Chem. Lett.* **35,** 874–875 (2006).

[152] Zhang, F., Vanmeensel, K., Inokoshi, M., Batuk, M., Hadermann, J., Van Meerbeek, B., Naert, I. & Vleugels, J. 3Y-TZP ceramics with improved hydrothermal degradation resistance and fracture toughness. *J. Eur. Ceram. Soc.* **34,** 2453–2463 (2014).

[153] Zhang, F., Vanmeensel, K., Batuk, M., Hadermann, J., Inokoshi, M., Van Meerbeek, B., Naert, I. & Vleugels, J. Highly-translucent, strong and aging-resistant 3Y-TZP ceramics for dental restoration by grain boundary segregation. *Acta Biomater.* **16,** 215–222 (2015).

[154] Swab, J. J. Low temperature degradation of Y-TZP materials. *J. Mater. Sci.* **26,** 6706–6714 (1991).

[155] Sato, T. & Shimada, M. Crystalline Phase Change in Yttria-Partially-Stabilized Zirconia by Low-Temperature Annealing. *J. Am. Ceram. Soc.* **67,** C-212-C-213 (1984).

[156] Sato, T. & Shimada, M. Transformation of Yttria-Doped Tetragonal ZrO2 Polycrystals by Annealing in Water. *J. Am. Ceram. Soc.* **68,** 356–356 (1985).

[157] Ruiz, L. & Readey, M. J. Effect of heat-treatment on grain size, phase assemblage, and mechanical properties of 3 mol% Y-TZP. *J. Am. Ceram. Soc.* 7**9,** 2331–2340 (1996).

[158] Bravo-Leon, A., Morikawa, Y., Kawahara, M. & Mayo, M. J. Fracture toughness of nanocrystalline tetragonal zirconia with low yttria content. *Acta Mater.* **50,** 4555–4562 (2002).

[159] Wei, C. & Gremillard, L. The influence of stresses on ageing kinetics of 3Y- and 4Y-stabilized zirconia. *J. Eur. Ceram. Soc.* (2017).

[160] Kosmač, T., Oblak, Č. & Marion, L. The effects of dental grinding and sandblasting on ageing and fatigue behavior of dental zirconia (Y-TZP) ceramics. *J. Eur. Ceram. Soc.* **28,** 1085–1090 (2008).

[161] Kim, J.-W., Covel, N. S., Guess, P. C., Rekow, E. D. & Zhang, Y. Concerns of Hydrothermal Degradation in CAD/CAM Zirconia. *J. Dent. Res.* **89,** 91–95 (2010).

[162] Lee, T. H., Lee, S. H., Her, S. B., Chang, W. G. & Lim, B. S. Effects of surface treatments on the susceptibilities of low temperature degradation by autoclaving in zirconia. *J. Biomed. Mater. Res. - Part B Appl. Biomater.* **100 B,** 1334–1343 (2012).

[163] Inokoshi, M., Vanmeensel, K., Zhang, F., De Munck, J., Eliades, G., Minakuchi, S., Naert, I., Van Meerbeek, B. & Vleugels, J. Aging resistance of surface-treated dental zirconia. *Dent. Mater.* **31,** 182–194 (2015).

[164] Muñoz-Saldaña, J., Balmori-Ramírez, H., Jaramillo-Vigueras, D., Iga, T. & Schneider, G. A. Mechanical properties and low-temperature aging of tetragonal zirconia polycrystals processed by hot isostatic pressing. *J. Mater. Res.* **18,** 2415–2426 (2003).

[165] Chevalier, J., Loh, J., Gremillard, L., Meille, S. & Adolfson, E. Low-temperature degradation in zirconia with a porous surface. *Acta Biomater.* **7,** 2986–2993 (2011).

[166] Sata, T. & Yoshimura, M. Reduction Process from CeO2 to Ce2O3 in Hydrogen. *Bull. Tokyo Inst. Technol.* **84,** 13–23 (1968).

[167] Moya, J. S., Moreno, R., Requena, J. & Soria, J. Black Color in Partially Stabilized Zirconia. *J. Am. Ceram. Soc.* **71,** 479–480 (1988).

[168] Zhu, H.-Y., Hirata, T. & Muramatsu, Y. Phase Separation in 12 mol% Ceria-Doped Zirconia Induced by Heat Treatment in H2 and Ar. *J. Am. Ceram. Soc.* **75,** 2843–2848 (1992).

[169] Zhu, H.-Y. & Hirata, T. Ce3d and Zr3d X-ray photoelectron spectroscopy spectra of ZrO2-12 mol% CeO2 after heat-treatments and Ar+ etching. *J. Mater. Sci. Lett.* **12,** 749–751 (1993).

[170] Orera, V. M., Merino, R. I. & Peña, F. Ce3+↔Ce4+ conversion in ceria-doped zirconia single crystals induced by oxido-reduction treatments. *Solid State Ion.* **72,** 224–231 (1994).

[171] Zhao, C., Vleugels, J., Groffils, C., Luypaert, P. J. & Van Der Biest, O. Hybrid sintering with a tubular susceptor in a cylindrical single-mode microwave furnace. *Acta Mater.* **48,** 3795–3801 (2000).

[172] Vleugels, J. & Biest, O. Van Der. Engineering the toughness of CeO2-stabilised ZrO2. *Key Eng. Mater.* **213,** 273–276 (2002).

[173] Matsuzawa, M., Abe, M., Horibe, S. & Sakai, J. The effect of reduction on the mechanical properties of CeO2 doped tetragonal zirconia ceramics. *Acta Mater.* **52,** 1675–1682 (2004).

[174] Huang, S. G., Vanmeensel, K., Van Der Biest, O. & Vleugels, J. Influence of CeO2 reduction on the microstructure and mechanical properties of pulsed electric current sintered Y2O3-CeO2 co-stabilized ZrO2 ceramics. *J. Am. Ceram. Soc.* **90,** 1420–1426 (2007).

[175] Tsukuma, K. & Shimada, M. Strength, fracture toughness and Vickers hardness of CeO2-stabilized tetragonal ZrO2 polycrystals (Ce-TZP). *J. Mater. Sci.* **20,** 1178–1184 (1985).

[176] Tsukuma, K. Mechanical properties and thermal stability of CeO2 containing tetragonal zirconia polycrystals. *Am. Ceram. Soc. Bull.* **65,** 1386–1389 (1986).

[177] Takemura, A., Nakahira, A., Sekino, T., Koyama, T. & Kouichi, N. Effects of Oxide Doping on Microstructure and Mechanical Properties of Ce-TZP. *J. Soc. Mater. Sci. Japan* **43,** 606–612 (1994).

[178] Zhao, C., Vleugels, J., Vandeperre, L., Basu, B. & Van Der Biest, O. Y–TZP/Ce–TZP Functionally Graded Composite. *J. Mater. Sci. Lett.* **7,** 1453–1455 (1998).

[179] Marro, F. G., Valle, J., Mestra, Á. & Anglada, M. Surface modification of 3Y-TZP with cerium oxide. *J. Eur. Ceram. Soc.* **31,** 331–338 (2011).

[180] Camposilvan, E., Marro, F. G., Mestra, Á. & Anglada, M. Development of a novel zirconia dental post resistant to hydrothermal degradation. *IOP Conf. Ser. Mater. Sci. Eng.* **31,** 12016 (2012).

[181] Tsubakino, H., Nozato, R. & Hamamoto, M. Effect of Alumina Addition on the Tetragonal-to-Monoclinic Phase Transformation in Zirconia-3 mol% Yttria. *J. Am. Ceram. Soc.* **74,** 440–443 (1991).

[182] Nogiwa-Valdez, A. A., Rainforth, W. M., Zeng, P. & Ross, I. M. Deceleration of hydrothermal degradation of 3Y-TZP by alumina and lanthana co-doping. *Acta Biomater.* **9,** 6226–6235 (2013).

[183] Matsui, K., Yoshida, H. & Ikuhara, Y. Nanocrystalline, Ultra-Degradation- Resistant Zirconia: Its Grain Boundary Nanostructure and Nanochemistry. *Sci. Rep.* **4,** 1–6 (2014).

[184] Theunissen, G. S. A. M., Winnubst, A. J. A. & Burggraaf, A. J. Segregation aspects in the ZrO2-Y2O3 ceramic system. *J. Mater. Sci. Lett.* **8,** 55–57 (1989).

[185] Boutz, M. M. R., Winnubst, A. J. A. & Burggraaf, A. J. Yttria-ceria stabilized tetragonal zirconia polycrystals: Sintering, grain growth and grain boundary segregation. *J. Eur. Ceram. Soc.* **13,** 89–102 (1994).

[186] Hwang, S.-L. & Chen, I.-W. Grain size control of tetragonal zirconia polycrystals using the space charge concept. *J. Am. Ceram. Soc.* **77,** (1990).

[187] Allemann, J. A., Michel, B., Märki, H.-B., Gauckler, L. J. & Moser, E. M. Grain growth of differently doped zirconia. *J. Eur. Ceram. Soc.* **15,** 951–958 (1995).

[188] Chen, I. W. Mobility control of ceramic grain boundaries and interfaces. *Mater. Sci. Eng. A* **166,** 51–58 (1993).

[189] Park, J. H. & Moon, S. W. Stability and sinterability of tetragonal zirconia polycrystals costabilized by CeO2 and various oxides. *J. Mater. Sci. Lett.* **11,** 1046–1048 (1992).

[190] Nawa, M., Bamba, N., Sekino, T. & Niihara, K. The effect of TiO2 addition on strengthening and toughening in intragranular type of 12Ce-TZP/Al2O3 nanocomposites. *J. Am. Ceram. Soc.* **18,** 209–219 (1998).

[191] Arin, M., Goller, G., Vleugels, J. & Vanmeensel, K. Production and characterization of ZrO2 ceramics and composites to be used for hip prosthesis. *J. Mater. Sci.* **43,** 1599–1611 (2007).

[192] Gadow, R. & Kern, F. Novel Zirconia-Alumina Nanocomposites Combining High Strength and Toughness. *Adv. Eng. Mater.* **12,** 1220–1223 (2010).

[193] Cutler, R. a, Mayhew, R. J., Prettyman, K. M. & Virkar, A. V. High-Toughness Ce-TZP/Al2O3 Ceramics with Improved Hardness and Strength. *J. Am. Ceram. Soc.* **74,** 179–186 (1991).

[194] Nawa, M., Nakamoto, S., Sekino, T. & Niihara, K. Tough and strong Ce-TZP/Alumina nanocomposites doped with titania. *Ceram. Int.* **24,** 497–506 (1998).

[195] Quénard, O., Laurent, C., Peigney, A. & Rousset, A. Zirconia-spinel composites. Part II: mechanical properties. *Mater. Res. Bull.* **35,** 1979–1987 (2000).

[196] Yang, B., Chen, X. M. & Liu, X. Q. Effect of BaTiO3 addition on structures and mechanical properties of 3Y-TZP ceramics. *J. Eur. Ceram. Soc.* **20,** 1153–1158 (2000).

[197] Morita, K., Hiraga, K., Kim, B.-N., Yoshida, H. & Sakka, Y. Synthesis of dense nanocrystalline ZrO2–MgAl2O4 spinel composite. *Scr. Mater.* **53,** 1007–1012 (2005).

[198] Chen, X. M., Liu, X. Q., Liu, F. & Zhang, X. Bin. 3Y-TZP ceramics toughened by Sr2Nb2O7 secondary phase. *J. Eur. Ceram. Soc.* **21,** 477–481 (2001).

[199] Ganesh, I. & Ferreira, J. M. F. Synthesis and characterization of MgAl2O4-ZrO2 composites. *Ceram. Int.* **35,** 259–264 (2009).

[200] Nevarez-Rascon, A., Aguilar-Elguezabal, A., Orrantia, E. & Bocanegra-Bernal, M. H. Al2O3(w)–Al2O3(n)–ZrO2 (TZ-3Y)n multi-scale nanocomposite: An alternative for different dental applications? *Acta Biomater.* **6,** 563–570 (2010).

[201] Apel, E., Ritzberger, C., Courtois, N., Reveron, H., Chevalier, J., Schweiger, M., Rothbrust, F., Rheinberger, V. M. & Höland, W. Introduction to a tough, strong and stable Ce-TZP/MgAl2O4 composite for biomedical applications. *J. Eur. Ceram. Soc.* **32,** 2697–2703 (2012).

[202] Pelleg, J. *Mechanical Properties of Ceramics*. (ed. Gladwell, G. M. L.) (Springer International Publishing, Cham, 2014).

[203] Marshall, D. B., Ratto, J. J. & Lange, F. F. Enhanced Fracture Toughness in Layered Microcomposites of Ce-ZrO2 and Al2O3. *J. Am. Ceram. Soc.* **74,** 2979–2987 (1991).

[204] Bermejo, R., Torres, Y., Sánchez-Herencia, A. J., Baudín, C., Anglada, M. J. & Llanes, L. Residual stresses, strength and toughness of laminates with different layer thickness ratios. *Acta Mater.* **54,** 4745–4757 (2006).

[205] Bermejo, R., Torres, Y., Baudín, C., Sánchez-Herencia, A. J., Pascual, J., Anglada, M. J. & Llanes, L. Threshold strength evaluation on an Al2O3–ZrO2 multilayered system. *J. Eur. Ceram. Soc.* **27,** 1443–1448 (2007).

[206] Bermejo, R., Baudín, C., Moreno, R., Llanes, L. & Sánchez-Herencia, A. J. Processing optimisation and fracture behaviour of layered ceramic composites with highly compressive layers. *Compos. Sci. Technol.* **67,** 1930–1938 (2007).

[207] Lange, F. F. Transformation toughening - Part 4 Fabrication, fracture toughness and strength of Al2O3-ZrO2 composites. *J. Mater. Sci.* **17,** 247–254 (1982).

[208] Schneider, J., Begand, S., Kriegel, R., Kaps, C., Glien, W. & Oberbach, T. Low-Temperature Aging Behavior of Alumina-Toughened Zirconia. *J. Am. Ceram. Soc.* **91,** 3613–3618 (2008).

[209] Kern, F. & Gadow, R. Alumina toughened zirconia from yttria coated powders. *J. Eur. Ceram. Soc.* **32,** 3911–3918 (2012).

[210] Pecharromán, C., Bartolomé, J. F., Requena, J., Moya, J. S., Deville, S., Chevalier, J., Fantozzi, G. & Torrecillas, R. Percolative Mechanism of Aging in Zirconia-Containing Ceramics for Medical Applications. *Adv. Mater.* **15,** 507–511 (2003).

[211] Irwin, G. R. Analysis of Stresses and Strains Near the End of a Crack Traversing a Plate. *J. Appl. Mech.* **24,** 361–364 (1957).

[212] Strecker, K., Ribeiro, S. & Hoffmann, M.-J. Fracture toughness measurements of LPS-SiC: a comparison of the indentation technique and the SEVNB method. *Mater. Res.* **8,** 121–124 (2005).

[213] Wachtman, J. B., Cannon, W. R. & Matthewson, M. J. *Mechanical Properties of Ceramics*. (John Wiley & Sons, Inc., 2009).

[214] Niihara, K., Morena, R. & Hasselman, D. P. . Evaluation of Klc of brittle solids by the indentation method with low crack-to-indent ratios. *J. Mater. Sci. Lett.* **1,** 13–16 (1982).

[215] Munz, D. & Fett, T. *Ceramics: Mechanical Properties, Failure Behaviour, Materials Selection*. (eds. Hull, R., Osgood, Jr., R. M., Sakaki, H. & Zunger, A.) (Springer-Verlag, Berlin - Heidelberg, 1999).

[216] Anstis, G. R., Chantikul, P., Lawn, B. R. & Marshall, D. B. A Critical Evaluation of Indentation Techniques for Measuring Fracture Toughness: I, Direct Crack Measurements. *J. Am. Ceram. Soc.* **64,** 533–538 (1981).

[217] Quinn, G. D. & Bradt, R. C. On the Vickers Indentation Fracture Toughness Test. *J. Am. Ceram. Soc.* **90,** 673–680 (2007).

[218] ASTM C 1421 – 01b. *Standard Test Methods for Determination of Fracture Toughness of Advanced Ceramics at Ambient Temperature*. (2002).

[219] Quinn, G. D., Kübler, J. J. & Gettings, R. J. *Fracture Toughness of Advanced Ceramics by the Surface Crack in Flexure (SCF) Method: A VAMAS Round Robin. VAMAS Report No. 17.* (Gaithersburg, MD, 1994).

[220] ISO 18756:2003. *Fine ceramics (advanced ceramics, advanced technical ceramics) -- Determination of fracture toughness of monolithic ceramics at room temperature by the surface crack in flexure (SCF) method*. (2003).

[221] Cesar, P. F., Della Bona, A., Scherrer, S. S., Tholey, M., van Noort, R., Vichi, A., Kelly, R. & Lohbauer, U. ADM guidance—Ceramics: Fracture toughness testing and method selection. *Dent. Mater.* **33,** 575–584 (2017).

[222] Himsolt, G., Munz, D. & Fett, T. A Modified Chevron Specimen for Ceramic Materials. *Commun. Am. Ceram. Soc.* **70,** C133–C135 (1987).

[223] Nishida, T., Hanaki, Y. & Pezzotti, G. Effect of Notch-Root Radius on the Fracture Toughness of a Fine-Grained Alumina. *J. Am. Ceram. Soc.* **77,** 606–608 (1994).

[224] Primas, R. J. & Gstrein, R. ESIS TC 6 Round Robin On Fracture Toughness. *Fatigue Fract. Eng. Mater. Struct.* **20,** 513–532 (1997).

[225] Damani, R. J., Gstrein, R. & Danzer, R. Critical notch-root radius effect in SENB-S fracture toughness testing. *J. Eur. Ceram. Soc.* **16,** 695–702 (1996).

[226] Nishida, T., Pezzotti, G., Mangialardi, T. & Paolini, A. E. Fracture mechanics evaluation of ceramics by stable crack propagation in bend bar specimens; in: *Fracture Mechanics of Ceramics* (eds. Bradt, R. C., Hasselman, D. P. H., Munz, D., Sakai, M. & Shevchenko, V. Y.), ch. **11**, 107–114 (Plenum Press, New York, NY, 1996).

[227] Kübler, J. Fracture toughness of ceramics using the SEVNB method: Preliminary results. in: *Ceramic Engineering & Science Proceedings, Volume 18* (ed. Wachtman, J. B.) 155–162 (American Ceramic Society, Westerville, OH, 1997).

[228] Kübler, J. *Fracture Toughness of Ceramics using the SEVNB Method; Round Robin. VAMAS Report No. 37, ESIS Document D2-99. ECF13, San Sebastian 2000* (EMPA, Dübendorf, 1999).

[229] Fett, T. Estimated stress intensity factors for semi-elliptical cracks in front of narrow circular notches. *Eng. Fract. Mech.* **64,** 357–362 (1999).

[230] Fett, T. Influence of a finite notch root radius on the measured R-curves. *J. Mater. Sci.* **39,** 1061–1063 (2004).

[231] Moreno, P., Méndez, C., García, A., Arias, I. & Roso, L. Femtosecond laser ablation of carbon reinforced polymers. *Appl. Surf. Sci.* **252,** 4110–4119 (2006).

[232] Salazar, A., Rodríguez, J., Segovia, A. & Martínez, A. B. Relevance of the femtolaser notch sharpening to the fracture of ethylene–propylene block copolymers. *Eur. Polym. J.* **46,** 1896–1907 (2010).

[233] Salazar, A., Rodríguez, J., Segovia, A. & Martínez, A. B. Influence of the notch sharpening technique on the fracture toughness of bulk ethylene–propylene block copolymers. *Polym. Test.* **29,** 49–59 (2010).

[234] Bärsch, N., Werelius, K., Barcikowski, S., Liebana, F., Stute, U. & Ostendorf, A. Femtosecond laser microstructuring of hot-isostatically pressed zirconia ceramic. *J. Laser Appl.* **19,** 107 (2007).

[235] Bärsch, N., Barcikowski, S. & Baier, K. Ultrafast-Laser-Processed Zirconia and its Adhesion to Dental Cement. *J. Laser Micro/Nanoengineering* **3,** 78–83 (2008).

[236] Parry, J. P., Shephard, J. D., Hand, D. P., Moorhouse, C., Jones, N. & Weston, N. Laser Micromachining of Zirconia (Y-TZP) Ceramics in the Picosecond Regime and the Impact on Material Strength. *Int. J. Appl. Ceram. Technol.* **8,** 163–171 (2011).

[237] Delgado-Ruíz, R. A., Calvo-Guirado, J. L., Moreno, P., Guardia, J., Gomez-Moreno, G., Mate-Sánchez, J. E., Ramirez-Fernández, P. & Chiva, F. Femtosecond laser microstructuring of zirconia dental implants. *J. Biomed. Mater. Res. Part B* **96,** 91–100 (2011).

[238] Hertel, I. V., Stoian, R., Ashkenasi, D., Rosenfeld, A. & Campbell, E. E. B. On the physics of material processing with femtosecond lasers. *RIKEN Rev.* **32,** 23–30 (2001).

[239] Samant, A. N. & Dahotre, N. B. Laser machining of structural ceramics—A review. *J. Eur. Ceram. Soc.* **29,** 969–993 (2009).

[240] Lucas, L. & Zhang, J. Femtosecond laser micromachining: A back-to-basics primer. *Industrial Laser Solutions* 1–22 (2012).

[241] Ritchie, R. O., Koester, K. J., Ionova, S., Yao, W., Lane, N. E. & Ager, J. W. Measurement of the toughness of bone: A tutorial with special reference to small animal studies. *Bone* **43,** 798–812 (2008).

[242] Marshall, D. B. & Swain, M. V. Crack Resistance Curves in Magnesia-Partially-Stabilized Zirconia. *J. Am. Ceram. Soc.* **71,** 399–407 (1988).

[243] Eichler, J., Hoffman, M., Eisele, U. & Rödel, J. R-curve behaviour of 2Y-TZP with submicron grain size. *J. Eur. Ceram. Soc.* **26,** 3575–3582 (2006).

[244] Fett, T. Influence of a finite notch root radius on fracture toughness. *J. Eur. Ceram. Soc.* **25,** 543–547 (2005).

[245] Ritchie, R. O. The conflicts between strength and toughness. *Nat. Mater.* **10,** 817–822 (2011).

[246] Anderson, T. L. Fracture Testing of Nonmetals - Ceramics; in: *Fracture Mechanics. Fundamentals and Applications*, ch. **8**, 378–382 (Taylor & Francis Group, Boca Raton, FL, 2005).

[247] Kendall, K., Alford, N. M., Tan, S. R., Birchall, D., Group, I. S., Box, P. O. & Heath, T. Influence of toughness on Weibull modulus of ceramic bending strength. *J. Mater. Res.* **1,** 120–123 (1986).

[248] Attaoui, H. El, Saâdaoui, M., Chevalier, J. & Fantozzi, G. Static and cyclic crack propagation in Ce-TZP ceramics with different amounts of transformation toughening. *J. Eur. Ceram. Soc.* **27,** 483–486 (2007).

[249] Swain, M. V. & Rose, L. R. F. Strength Limitations of Transformation-Toughened Zirconia Alloys. *J. Am. Ceram. Soc.* **69,** 511–518 (1986).

[250] Griffith, A. A. The Phenomena of Rupture and Flow in Solids. *Philos. Trans. R. Soc. A Math. Phys. Eng. Sci.* **221,** 163–198 (1921).

[251] Zhigilei, L. V, Kodali, P. B. S. & Garrison, B. J. On the threshold behavior in laser ablation of organic solids. *Chem. Phys. Lett.* **276,** 269–273 (1997).

[252] Stoian, R., Ashkenasi, D., Rosenfeld, A. & Campbell, E. E. B. Coulomb explosion in ultrashort pulsed laser ablation of Al2O3. *Phys. Rev. B - Condens. Matter Mater. Phys.* **62,** 13167–13173 (2000).

[253] Lube, T., Danzer, R., Dusza, J., Erauw, J.-P., Klemm, H. & Sglavo, V. M. Strength and Fracture Toughness of the ESIS Silicon Nitride Reference Material. *Ceramics* 409–416 (2002).

[254] Lube, T. & Dusza, J. A silicon nitride reference material—A testing program of ESIS TC6. *J. Eur. Ceram. Soc.* **27,** 1203–1209 (2007).

[255] Fischer, H., Waindich, A. & Telle, R. Influence of preparation of ceramic SEVNB specimens on fracture toughness testing results. *Dent. Mater.* **24,** 618–622 (2008).

[256] Heiroth, S., Koch, J., Lippert, T., Wokaun, A., Günther, D., Garrelie, F. & Guillermin, M. Laser ablation characteristics of yttria-doped zirconia in the nanosecond and femtosecond regimes. *J. Appl. Phys.* **107,** 14908 (2010).

[257] Hu, H., Wang, X., Zhai, H., Zhang, N. & Wang, P. Generation of multiple stress waves in silica glass in high fluence femtosecond laser ablation. *Appl. Phys. Lett.* **97,** 61117 (2010).

[258] Ortiz, M. Microcrack coalescence and macroscopic crack growth initiation in brittle solids. *Int. J. Solids Struct.* **24,** 231–250 (1988).

[259] Casellas, D., Feder, A., Llanes, L. & Anglada, M. Fracture toughness and mechanical strength of Y-TZP/PSZ ceramics. *Scr. Mater.* **45,** 213–220 (2001).

[260] Roa, J. J., Aboulfadl, H., Barrirero, J., Turon-Vinas, M., Mücklich, F. & Anglada, M. Chemical segregation in a 12Ce-ZrO2/3Y-ZrO2 ceramic composite. *Mater. Charact.* **132,** 83–91 (2017).

[261] Zhao, W., Rao, P. & Ling, Z. A new method for the preparation of ultra-sharp V-notches to measure fracture toughness in ceramics. *J. Eur. Ceram. Soc.* **34,** 4059–4062 (2014).

[262] Wang, A., Hu, P., Zhang, X., Han, W., Chen, G. & Han, J. Accurate measurement of fracture toughness in structural ceramics. *J. Eur. Ceram. Soc.* **37,** 4207–4212 (2017).

[263] Carlton, H. D., Elmer, J. W., Freeman, D. C., Schaeffer, R. D., Derkach, O. & Gallegos, G. F. Laser notching ceramics for reliable fracture toughness testing. *J. Eur. Ceram. Soc.* **36,** 227–234 (2016).

[264] Theunissen, G. S. A. M., Winnubst, A. J. A. & Burggraaf, A. J. Surface and grain boundary analysis of doped zirconia ceramics studied by AES and XPS. *J. Mater. Sci.* **27,** 5057–5066 (1992).

ARTICLE I

Fracture toughness of zirconia from a shallow notch produced by ultra-short pulsed laser ablation

APPENDED MANUSCRIPT

Effect of calcia co-doping on ceria-stabilized zirconia

Turon-Vinas, M., Zhang, F., Vleugels, J. & Anglada, M. Effect of calcia co-doping on ceria-stabilized zirconia. *Submitted to J. Eur. Ceram. Soc.* (2017)

Effect of calcia co-doping on ceria-stabilized zirconia

Abstract

Ceria-stabilized zirconia ceramics are characterized by excellent hydrothermal stability and high fracture toughness, but the fracture strength and hardness are lower than that of conventional 3Y-TZP, which is sensitive to low temperature degradation in humid environments. In the present work, the influence of small concentrations of calcia on the microstructure, mechanical properties and hydrothermal ageing resistance of 10 and 12 mol% CeO_2 stabilized ZrO_2 has been assessed. The addition of only 1 mol% of CaO had a strong refining effect on the microstructure resulting in an increased hardness and strength but reduced stress activated tetragonal-to-monoclinic transformability. The addition of 3 mol% CaO addition however enhanced the transformability with respect to 1 mol% CaO and, preserved the high resistance to hydrothermal degradation of the Ce-TZP.

Keywords: zirconia, ceria, calcia, transformability, co-doping

1. Introduction

Tetragonal polycrystalline zirconia stabilized with 3 mol% of yttria (3Y-TZP) is widely used in dentistry owing to its biocompatibility, aesthetic appearance and excellent mechanical properties, which are related to its relatively high fracture toughness, K_{Ic}, and small grain size [1], [2]. The stabilization of the tetragonal phase at room temperature is possible by the yttrium (Y^{3+}) substitution of zirconium (Zr^{4+}) and concomitant formation of charge neutralizing oxygen vacancies. The main mechanism for the high K_{Ic} is transformation toughening, i.e. the transformation of the tetragonal ZrO_2 phase (*t*) into the monoclinic phase (*m*) by the tensile stresses around the crack tip. This is accompanied by a local volume expansion that induces a reaction compressive stress, reducing in this way the stress intensity factor at the crack tip [3]. However, the $t \rightarrow m$ phase transformation can also occur spontaneously at the surface in contact with humid environments inducing surface microcracking and an increase in roughness. This phenomenon, referred to as low-temperature degradation (LTD), is the main issue for the long-term reliability of 3Y-TZP in humid environmental applications [4]. The exact mechanism responsible for LTD is still not fully understood, but it is related to the annihilation of oxygen vacancies induced by the diffusion of water species from the surface in humid environments [5], [6].

Tetragonal zirconia can also be stabilized at room temperature by cerium, Ce^{4+}, instead of Y^{3+} cations, without inducing oxygen vacancies. However, ceria stabilized zirconia (Ce-TZP) has a substantially larger grain size than 3Y-TZP, which is partly due to the need of higher sintering temperatures and/or longer times for full densification. The grain growth of Ce-TZP at low temperatures is slow due to the slow diffusion kinetics of $Ce^{3+/4+}$ (compared to Y^{3+}), requiring higher sintering temperatures, producing a larger and broader grain size distribution due to the absence of an effective grain growth retarding mechanism as it occurs in 3Y-TZP [7]. Dense 7 to 16 mol% CeO_2 stabilized zirconia ceramics with different grain sizes were fabricated and evaluated in terms of hardness, strength and fracture toughness by Tsukuma et al. [8]. They found a high fracture toughness, but also low hardness and fracture strength, which was associated with the relatively

large micrometer grain size and high transformability under stress of the metastable tetragonal phase.

As the mechanical properties strongly depend on the grain size, it is expected that limiting the grain growth during sintering will decrease the high t-m transformability and increase the strength and hardness of Ce-TZP. In principle, this can be achieved by the addition of specific solutes which might segregate to the grain boundaries during sintering, reducing their mobility by a solute drag mechanism [7], [9], [10].

The effect of solutes has been previously investigated mainly in 3Y-TZP, where the addition of specific additives or impurities such as Al_2O_3, TiO_2 or Fe_2O_3 was established to be beneficial, acting as sintering aids or affecting *t*-phase stability and ageing resistance [11]. For instance, small amounts of homogeneously distributed alumina (less than 0.5 wt.%) can improve the LTD resistance [12], [13]. Recent studies suggest that the ageing resistance of t-ZrO_2 can be enhanced even more by co-doping a 3Y-TZP with small amounts of both alumina and lanthania [14] or alumina and germania [15].

One of the first studies on the influence of different oxides on the grain size of 3Y-TZP was carried out by Sato et al. [16]. They co-doped 3Y-TZP with 0-12 mol% of either CaO, MgO, CeO_2 or TiO_2 revealing that alloying with TiO_2 accelerated the grain growth and suppressed densification, but alloying with less than 6 mol% of CeO_2 caused no significant changes in grain size. CaO was the most effective oxide in reducing the tetragonal grain size, and cubic zirconia phase was already detected with only 2 mol% CaO addition [16].

In ceria-doped zirconia, partial substitution of ceria by yttria also resulted in a reduced grain size and in a more stabilized tetragonal structure, which increased the hardness but decreased the fracture toughness [17]–[21]. As Y_2O_3 is more effective than CeO_2 with respect to a grain size refinement and tetragonal stability, co-doping zirconia with proper proportions of ceria and yttria results in a reduced grain size with respect to a Ce-TZP and a better LTD resistance than Y-TZP ceramics [7], [16]–[18].

Grain growth in zirconia is strongly related to the composition and phase content, as observed in zirconia doped with Y_2O_3, where the grain growth of cubic grains can be two orders of magnitude faster than that of tetragonal grains alloyed with the same cation, but it can be strongly suppressed if both phases coexist [22]. Grain growth depends strongly on the ionic radius and valence of the solutes. Oversized divalent and trivalent ions (such as Y^{3+} and Gd^{3+}) reduce the grain growth efficiently, but other oversized solutes with the same valence as zirconium, like Ce^{4+}, have no effect [23]–[25]. The resistance to grain boundary mobility is related to the segregation of these ions at the grain boundaries and it increases with a higher solute concentration and a larger valence difference between the solute and the host cation [22], [26].

The cation radius of the dopant also influences the ageing resistance of 3Y-TZP, obtaining an enhanced LTD resistance with large as well as with small cation trivalent dopants due to the stronger bond of the $[M'_{Zr} \cdot V_o^{\cdot\cdot}]$ defect clusters in the space charge layer at the grain boundaries, without affecting the mechanical properties [27].

In the present work, Ca^{2+} has been used as a co-doping ion (up to 3 mol% CaO) in ceria-doped zirconia (10Ce-ZrO_2 and 12Ce-ZrO_2) in order to refine its microstructure and increase the mechanical properties. The selection of Ca^{2+} is justified by its low valence and very large ionic size (ionic radius of Ca^{2+} and Zr^{4+} are 112 and 84 pm respectively), which is expected to substantially reduce the grain size and increase the hardness and strength of ceria-stabilized zirconia ceramics.

2. Experimental procedure

2.1. Sample preparation

Commercial co-precipitated ceria-stabilized zirconia powders with 10 and 12 mol% ceria (CEZ-10 and CEZ-12, Daiichi Kigenso Kagaku Kogyo) containing 0.25 wt% Al_2O_3 were mixed with different amounts of CaO (ReagentPlus® 99.9%, 15 – 35 μm

particle size, Sigma-Aldrich) in ethanol using 5 mm diameter zirconia balls (grade TZ-3Y, Tosoh) on a multidirectional mixer (Turbula T2F, WAB) for 24h. The dried powders were sieved (315 μm mesh) and shaped by uniaxial pressing at 50 MPa followed by cold isostatic pressing at 250 MPa (EPSI). The green samples were sintered in a high-temperature furnace (LHT 02/17, Nabertherm) for 2h at 1500°C with a heating rate of 10°C/min. This temperature and time were selected in order to improve the densification of the calcia-containing ceramics, as a reduction of grain boundary mobility was expected, which could affect their sinterability. The different compositions will be designated by X-Y where X and Y are the molar concentration of ceria and calcia respectively.

The sintered ceramics were either in the form of discs of ~13.5 mm diameter and ~1.5 mm thick or prismatic bars with dimensions ~3x4x45 mm. All samples were ground and polished following the standard methods up to 3 μm diamond paste with a final polishing step using a 0.5 μm silica suspension on the surfaces to be analysed.

The density of the samples was measured by the Archimedes method in ethanol.

2.2. Microstructural characterization

The grain size distribution was determined by the linear intercept method on more than 1000 grains per condition from micrographs obtained by scanning electron microscopy (SEM, XL-30FEG, FEI). The reported values are as-measured without any correction factor.

X-ray diffraction analysis (XRD, 3003-TT, Seifert) was performed on polished surfaces using Cu K_α radiation at 40 kV and 40 mA, with a scan speed of 2 s/step and a scan step size of 0.02° in the 20–90° 2θ range. In order to quantify the different phases, Rietveld refinements were performed using TOPAS-Academic software (Bruker AXS). The phases were refined as: monoclinic zirconia (*m*) with space group P21/c, tetragonal zirconia (*t*) with space group $P4_2/nmc$ and cubic zirconia (*c*) with space group Fm-3m.

Hydrothermal degradation tests were performed in an autoclave in full steam atmosphere at 134 °C and 0.2 MPa pressure during 30 hours. The surface monoclinic content (V_m) was measured by XRD analysis, and calculated according to the equation proposed by Garvie et al. [28] and modified by Toraya et al. [29]:

$$V_m = \frac{1.311[I_m(\bar{1}11) + I_m(111)]}{1.311[I_m(\bar{1}11) + I_m(111)] + I_t(101)} \quad (1)$$

with I_m and I_t the intensity of the monoclinic and tetragonal peaks respectively.

High-resolution scanning transmission electron microscopy (HRSTEM) combined with energy dispersive X-ray spectroscopy (EDS) was used to analyse thin foils on an aberration-corrected transmission electron microscope (ARM200F, JEOL) operating at 200 kV, using a high-angle annular dark-field (HAADF) detector. Thin-foil preparation for TEM analysis involved mechanical thinning with diamond lapping films and polishing down to 100 μm before final preparation to electron transparency using a JEOL Cryo Ion Slicer at 6 kV.

2.3. Mechanical characterization

The biaxial strength was measured on discs (5-8 specimens per condition) in biaxial flexure with a ball-on-three-balls testing fixture with 6 mm diameter balls using a servo-hydraulic testing machine (8511, Instron) [30], [31]. The maximum biaxial stress (σ_{max}) was calculated using the equation proposed by Fett et al. [32]:

$$\sigma_{max} \cong \frac{3F(1+\upsilon)}{4\pi t^2}\left[2\ln\left(\frac{R}{\alpha t}\right) + \frac{1-\upsilon}{1+\upsilon}\left(\frac{R}{R_D}\right)^2\right] \quad (2)$$

where F is the applied load, υ the Poisson ratio (0.28), t the thickness of the disc, R_D the disc radius, R the flexure radius (~0.35 mm) and $\alpha = 0.2$.

The fracture toughness was measured from small cracks in single-edge V-notched prismatic specimens (SEVNB) with a starting notch generated by ultra-short pulsed laser ablation (UPLA) (Ti : Sapphire, 120 fs, 795 nm, 1 kHz). The pulse energy used was 7–8 μJ

(depending on the composition), and a scanning speed of 50 μm/s. Four or six passes were needed to achieve the desired notch depth of about 40 μm. Five V-notched bar specimens per condition were tested in a servo-hydraulic testing machine (model 8511, Instron) using a four-point bending test configuration with spans of 40/20 mm under a constant stress rate of ~100 MPa/s. The full description and assessment of the method is described elsewhere [33]–[36].

The Vickers indentation fracture toughness test (IF) was also used by indenting with a load of 294 N and measuring the radial crack patterns by means of laser scanning confocal microscopy (LEXT OLS3100, Olympus). This was carried out with the only objective to compare the results with those obtained by using single-edge cracked prismatic specimens, since the limitations of the indentation method are well known [37]. The equation used to calculate the indentation toughness was that of Niihara et al. for Palmqvist cracks [38]:

$$K_{Ic} = 0.018H\sqrt{a}\left(\frac{E}{H}\right)^{0.4}\left(\frac{c-a}{a}\right)^{-1/2} \qquad (3)$$

where H is the Meyer's hardness, E the elastic modulus (taken as 200 GPa from [39]), a half of the diagonal of the indentation imprint and c the distance between the center of the indentation and the crack tip. For small indentation cracks, this equation can be used as far as $0.25 \lesssim (c\text{-}a)/a \lesssim 2.5$. However, in high toughness zirconia ceramics the transformation induced upon indentation takes place up to a distance of about a from the border of the imprint, so that indentation cracks shorter than $(c\text{-}a)/a \lesssim 1$ are severely affected by the transformation. Therefore, the indentation method was only used when $(c\text{-}a)/a$ was between 1 and 2.5. The Meyer's hardness was measured by a Vickers indenter with a load of 98.1 N.

Confocal micro-Raman spectroscopy (inVia Qontor, Renishaw) was used to estimate the amount of monoclinic phase and to compare the phase transformability of the different ceramic compositions. A Nd:YAG laser (wavelength 532nm) was used, with a spectrum integration time of 1 s. Single point measurements on the fracture surfaces of discs and bars and 2D mappings around Vickers indentations were performed. The monoclinic phase content was quantified applying the formula proposed by Katagiri et al. [40] and assessed by Tabares et al. [41].

Fracture surfaces were investigated using a SEM coupled with a focused ion beam (dual beam SEM/FIB) (Neon 40, Zeiss).

Table 1. Composition, density, grain size and constituent phases of the ceramics sintered for 2 h at 1500 °C.

Designation	CeO_2 (mol%)	CaO (mol%)	Density (g/cm^3)	Avg. grain size (μm)	Monoclinic phase (wt%)	Tetragonal phase (wt%)	Cubic phase (wt%)
10-0	10	0	--	1.99±0.75	76.7	20.5	< 3
10-1	10	1	6.14±0.04	0.53±0.23	<1	91.8	8.2
10-3	10	3	5.99±0.03	0.64±0.35	<1	65.1	34.9
12-0	12	0	6.19±0.02	1.27±0.74	<1	97.0	< 3
12-1	12	1	6.17±0.01	0.60±0.24	<1	89.9	10.1
12-3	12	3	6.07±0.01	0.65±0.31	<1	61.8	38.2

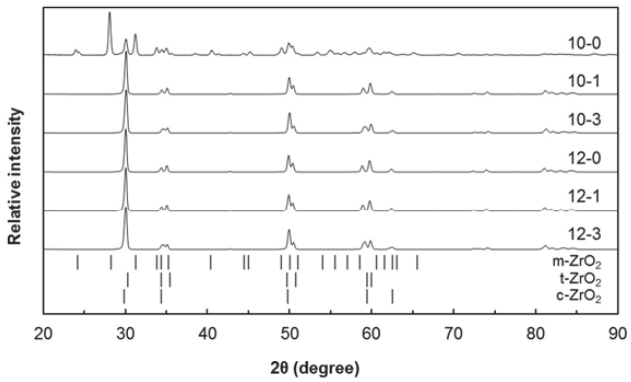

Figure 1. XRD patterns of polished surfaces of 10 and 12CeO_2-ZrO2 with 0, 1 or 3 mol% CaO addition. The main peaks of the monoclinic (m-ZrO_2), tetragonal (t-ZrO_2) and cubic (c-ZrO_2) phases are marked.

3. Results

3.1. Microstructure

Table 1 summarizes the microstructural and constituent phase characteristics in the CaO co-doped Ce-ZrO_2 ceramics. After sintering, monoclinic ZrO_2 was only detected in the 10-0, as shown in the XRD pattern presented in Fig. 1. Hence, because of the presence of monoclinic phase, this specific composition was discarded for further analysis.

Rietveld analysis revealed an increasing cubic ZrO_2 content upon calcia addition, which is reflected in a slight change of shape of the peaks around 35° and 60° 2θ in Fig. 1 (more remarkable in 10-3 and 12-3 compositions). Calcia is a strong stabilizer of the tetragonal phase in pure zirconia up to about 5 mol% CaO, where cubic ZrO_2 starts to form under equilibrium conditions. Therefore, it is expected that when used as a co-dopant in 10 or 12 mol% CeO_2, relatively small concentrations of calcia may already induce the cubic ZrO_2 phase formation. However, no information on the ternary ZrO_2-CeO_2-CaO equilibrium phase diagram seems to be available in literature. It should also be noted that the stabilization mechanisms of both dopants are different: while CaO stabilizes the tetragonal phase by introducing anionic oxygen vacancies similarly to Y_2O_3, whereas CeO_2 stabilizes the t-ZrO_2 phase by dilating the cation network decreasing the strain energy and the relief of oxygen overcrowding [42], [43].

Calcia addition contracts both the tetragonal and cubic ZrO_2 unit cells, as shown in Fig. 2a and b. Although Ca^{2+} is larger than Ce^{4+} (112 pm and 97 pm respectively), the lattice contraction can be explained by the formation of oxygen vacancies [23]. For the 12Ce-ZrO_2 grades, the more thermodynamically stable t-ZrO_2 phase, i.e. the t-ZrO_2 phase with the lowest tetragonality or phase transformability, appears to be the one formed in the 1 mol% calcia-doped ceramic, but the transformability is increased with further CaO addition (see Fig. 2c). For the 10Ce-ZrO_2 grades, the transformability of the tetragonal phase increased when the amount of CaO is increased from 1 to 3 mol%. It should be mentioned however that most of the t-ZrO_2 phase in the 10-0 already spontaneously transformed after cooling and only those t-ZrO_2 grains with the lowest tetragonality remained.

Grain size measurements clearly showed that the large grains observed in the 10-0 and 12-0 disappeared with the addition of small amounts of calcia (≥ 1 mol%), which narrows and shifts the grain size distribution to smaller values (Fig. 3). The reduction in grain size was already strong with only 1 mol% CaO addition. When co-doping with 3 mol% CaO, larger grains (pointed out by the arrows in Fig. 3) can be identified in a finer grained matrix, which

are attributed to the presence of higher volume fractions of larger cubic ZrO_2 grains, as revealed by Rietveld analysis (see Table 1).

TEM-EDS elemental mappings of the 12-1 ceramic revealed a slight segregation of especially Ca but also Al and Ce to the grain boundaries (as illustrated in Fig. 4a), with a local grain boundary depletion of Zr. A substantially higher concentration of both Ca and Ce can be found in some grains, as shown in Fig. 4b. Diffraction analysis of the same grains revealed that the dopant-rich larger grain has a cubic crystal structure, whereas the smaller grains with lower Ca and Ce stabiliser contents have a tetragonal crystal structure (see Fig. 4c).

TEM-EDS point analysis were performed in different grains and on grain boundaries. A summary of the measured average composition, averaged over 3–5 point analysis measurements on 10 different grains, is provided in Table 2.

Fig. 5 shows the XRD patterns of polished surfaces after 30 hours hydrothermal autoclave testing in steam at 134 °C, which theoretically corresponds to more than a human lifespan under *in vivo* conditions [44]. Only the 10-3 grade shows a small amount of monoclinic ZrO_2 phase, as estimated by Equation 1 to be about 8 vol%.

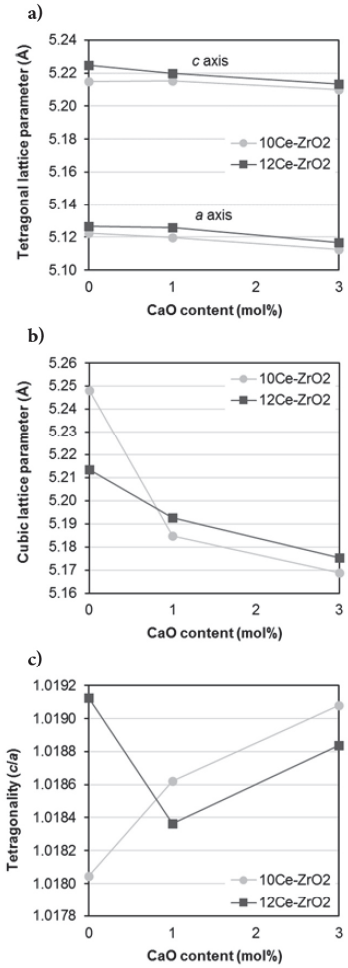

Figure 2. Lattice parameters of the (a) tetragonal and (b) cubic ZrO_2 phase, and (c) tetragonality of the t-ZrO_2 phase in the 10Ce and 12Ce-ZrO_2 doped with different amounts of calcia. The tetragonal data are presented using pseudo-cubic (distorted fluorite) unit cell.

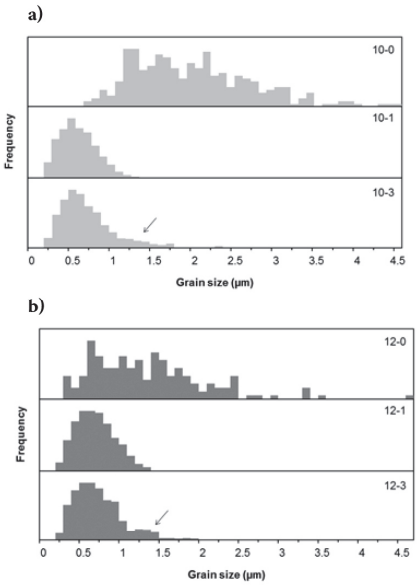

Figure 3. Grain size distribution histograms of (a) 10Ce-ZrO_2 and (b) 12Ce-ZrO_2 with 0, 1 and 3 mol% CaO addition. The arrows indicate the appearance of a bimodal distribution.

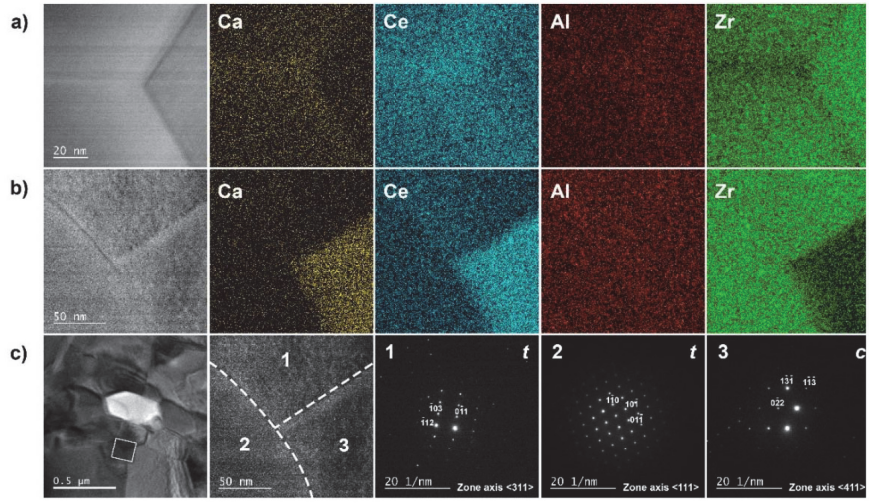

Figure 4. HRSTEM EDS elemental mappings of the a) and b) 12-1 sample. c) TEM diffraction analysis of the same region as in b).

Table 2. Average concentration (in mol%) as determined by TEM-EDS point analysis inside tetragonal and cubic ZrO_2 grains and on the t-t and t-c grain boundaries (GB) in the 12-1 sample.

	CaO (mol%)	CeO_2 (mol%)	Al_2O_3 (mol%)	ZrO_2 (mol%)
t grains	0.4 ±0.2	9.1 ±0.2	0.8 ±0.2	89.4 ±0.3
c grains	2.2 ±0.2	13.9 ±0.4	1.4 ±0.1	82.3 ±0.3
t-t GB	1.2 ±0.5	10.3 ±0.8	1.3 ±0.2	86.9 ±1.3
t-c GB	2.5 ±0.3	12.7 ±0.8	1.8 ±0.1	82.8 ±1.0

3.2. Mechanical properties

Table 3 summarises of the mechanical properties of the different compositions. The influence of CaO co-stabilization is strong as revealed by the increased hardness upon only 1 mol% calcia addition, as shown in Fig. 6. This effect can be attributed to the strong reduction in grain size. The difference in hardness between 10-1 and 10-3 and between 12-1 and 12-3 is negligible, but the 12Ce-ZrO_2 grades are harder than the 10Ce-ZrO_2 ones.

The biaxial tensile strength is highest for the 1 mol% CaO co-doped 10 and 12Ce-ZrO_2, with a fracture strength around 900 MPa (see Fig. 7a). However, the average amount of monoclinic ZrO_2 phase on the fracture surfaces of the broken discs is reduced by the addition of 1 mol% CaO, but increases at 3 mol% CaO for both CeO_2 contents (Fig. 7b).

The evolution of the t-ZrO2 phase transformability with calcia addition was also studied by means of micro-Raman spectroscopy around Vickers indentations. Fig. 8 shows the m-ZrO_2 content maps for the different ceramic grades confirming the trend in m-ZrO_2 volume measured on the fracture disc surfaces (Fig. 7b).

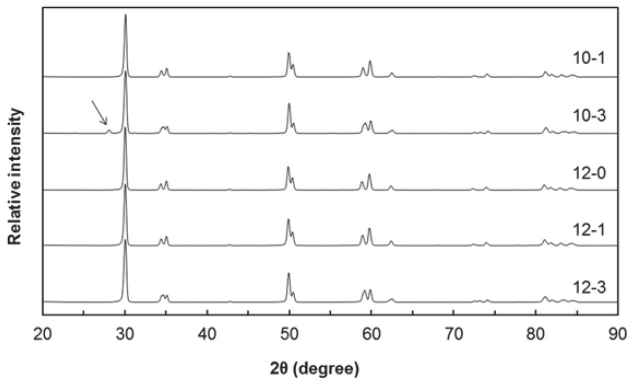

Figure 5. XRD patterns of the surface of the different ceramic compositions after hydrothermal testing for 30 h. The arrow points at a small monoclinic peak detected on the 10-3 grade.

For some compositions, i.e. 10-1, 10-3 and 12-0, no cracks were formed or they were extremely short for using the indentation fracture toughness equation (Equation 4). The 10-0 composition was not investigated since the material was mostly monoclinic. For 12-0, no cracks were formed even with an indentation load of 294 N, due to its high transformability. Well-developed crack radial patterns, suitable for applying Niihara's equation for indentation fracture toughness measurements, were only formed with the 12-1 and 12-3 grades. Even though the addition of calcia also reduces the t-m transformability of 10-0, the indentation cracks were still very small and did not fulfil the criteria imposed by Niihara's equation of $(c\text{-}a)/a > 0.25$.

The lack of reliability of the indentation fracture toughness testing method has been extensively discussed in literature [37]. It has been stated that it is not a reliable technique to measure the fracture toughness of ceramics, and therefore other standardized methods should be used. However, the use of the indentation fracture toughness is justified here in order to compare with literature values. On the other hand, measuring the transformation zone around the Vickers imprints gives a very useful measurement of the degree of t-m transformability, but not necessarily of the fracture toughness.

Table 3. Mechanical properties of 10 and 12Ce-ZrO_2 ceramics with 0, 1 and 3 mol% calcia.

Designation	Grain size (μm)	Hardness (GPa)	Biaxial tensile strength (MPa)	SEVNB fracture toughness (MPa√m)	Monoclinic content on fracture surface of discs (vol%)
10-0	1.99±0.75	6.2±0.1	--	--	>70
10-1	0.53±0.23	11.9±0.1	922±77	4.3±0.1	8.5±1.9
10-3	0.64±0.35	12.2±0.1	678±30	4.4±0.1	20.0±2.1
12-0	1.27±0.74	9.6±0.1	591±53	4.5±0.1	32.6±5.7
12-1	0.60±0.24	12.7±0.1	899±151	3.9±0.1	< 3
12-3	0.65±0.31	12.9±0.2	680±44	3.8±0.1	15.1±5.0

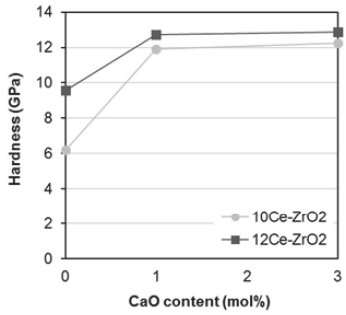

Figure 6. Meyers hardness measured by 98.1 N Vickers indentation.

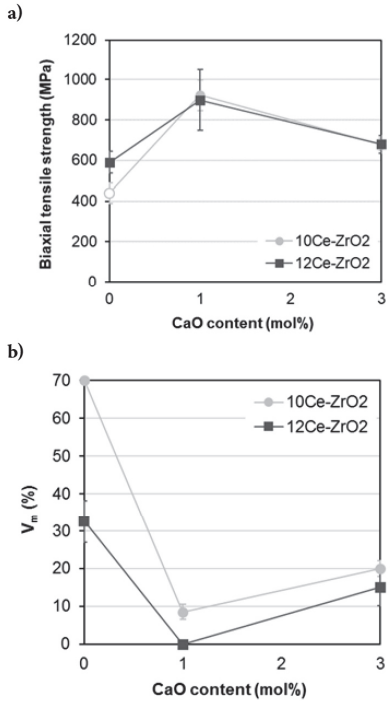

Figure 7. a) Biaxial tensile strength (the value for 10-0 is taken from [39]) and b) volume fraction of monoclinic ZrO_2 phase on fracture surfaces.

From the strength point of view, the important parameters are the size of the processing defects and the material's fracture toughness which determines the strength. Since the processing defects are usually very small, the fracture toughness was determined from artificial small defects in the form of shallow single edge cracks with a total depth of about 40 μm, machined by UPLA as described in section 2.3. In this method, the notch is only about 20 μm deep and extremely sharp with a typical radius of less than 1 μm and there is also a narrow highly microcracked zone in the direction of the notch and with nearly the same length as the notch. Because of the very high microcrack density, the initial crack length can be taken as the length of the notch plus the length of the microcracked zone [33], [34], [36].

The K_{Ic} values obtained from these short straight edge cracks are summarized in Fig. 9. It should be noted that these values do not correspond to the often recalled plateau levels of K_{Ic} for 10 and 12Ce-ZrO_2 ceramics (about 15 and 7 MPa√m respectively [45]), which are obtained from larger cracks, but they rather represent the effective fracture toughness of small and not initially shielded cracks [35]. Moreover, for the 12-1 and 12-3 grades, the values measured (3.9 and 3.8 MPa√m respectively) are significantly smaller than those obtained by indentation fracture toughness (5.7 and 5.5 MPa√m respectively).

The fracture surfaces of the notched specimens were investigated by means of SEM, as shown in Fig. 10. Upon adding CaO, the clean intergranular fracture in the 10-0 and 12-0 grades changed to a partially transgranular fracture. Larger cubic ZrO_2 grains that were pulled out during fracture can be clearly observed, as marked by the white arrows in Fig. 10, leaving an intergranular fracture. The area of fracture surface corresponding to cubic grains increased with the amount of CaO addition as expected from the larger presence of this phase. Fig. 10 clearly illustrates the strongly reduced grain size upon adding 1 or 3 mol% CaO for both the 10 and 12 mol% CeO_2 ceramic grades. The 3 mol% CaO co-stabilized ceramics clearly have a bimodal grain size distribution with larger c-ZrO_2 grains in a smaller grained t-ZrO_2 matrix.

On a final note, the as sintered ceramics showed an increasing greenish shade with increasing calcia content, being more notorious in the bulk. The typical yellowish coloration of Ce-TZP ceramics, both on the

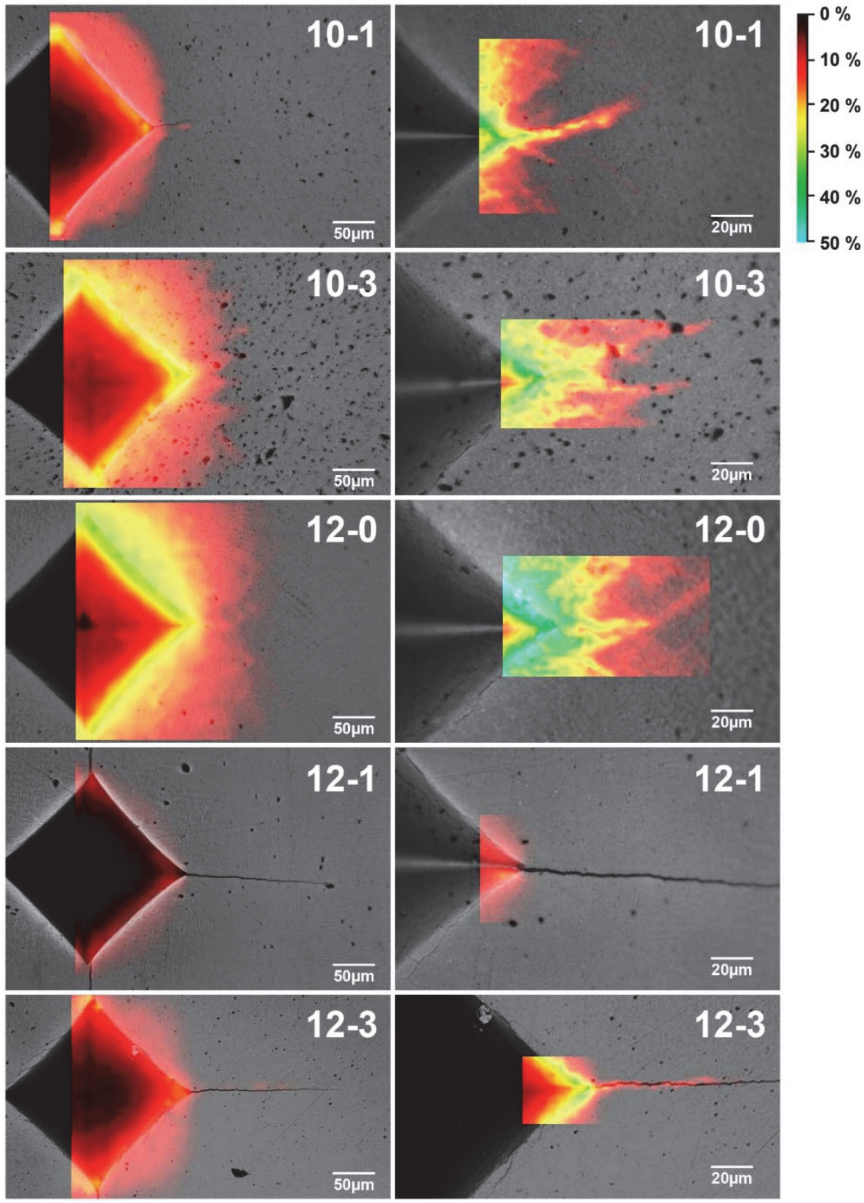

Figure 8. Monoclinic phase content maps around 98.1 N Vickers indentations obtained by micro-Raman spectroscopy.

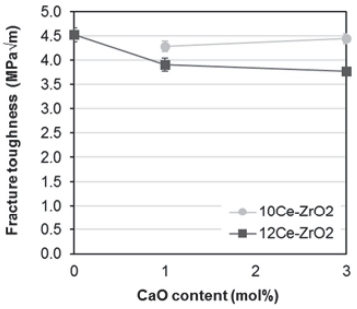

Figure 9. Fracture toughness as measured by SEVNB.

surface and in the bulk, could be obtained by an additional conventional heat treatment (1200 ºC for 1h) in a tubular furnace with air ventilation (ST-18, Hobersal), as seen in Fig. 11. The change in color could be attributed to a partial ceria reduction during the sintering process due to a lack of oxygen supply, as different colorations have been reported in literature when sintering Ce-TZP ceramics in different atmospheres and in reduced partial oxygen pressure. This effect seems to be related to the production of vacancies due to an oxygen deficiency [46]–[54]. Thus, it seems that ceria-stabilized zirconia ceramics are very sensitive to the oxygen supply in the furnace during sintering, being able to reduce even in air in conventional sintering furnaces, typically resulting in a color gradient with a darker bulk and a brighter surface. No difference in mechanical properties were observed by Vickers indentation evaluation of as-sintered (greenish) and heat-treated (yellowish) ceramics.

4. Discussion

The high amount of monoclinic ZrO_2 content in the 10-0 grade can be explained by the increase in grain size during sintering at 1500 ºC. This sintering temperature was used for all compositions in order to reach nearly full densification of the calcia-doped compositions. However, it produced large grains in the 10-0 specimens, which caused thermally-induced spontaneous transformation during cooling due to the relatively low stabilizer content [7], [17]. Spontaneous transformation to monoclinic after sintering has also been reported in literature for the same composition even at lower sintering temperatures, implying the M_s temperature of this material is above room temperature [45]. Moreover, the possible partial reduction of ceria (from Ce^{4+} to Ce^{3+}) during sintering can decrease the amount of dopant in the grains due to Ce^{3+} segregation to the grain boundaries [52], [55], [56], making them more prone to spontaneous transformation during cooling, producing micro- and macrocracks that affect the mechanical properties. It has been reported that the t-m transformation can be promoted in Ce-ZrO_2 ceramics by ceria reduction, obtaining mechanical properties which are sensitive to the sintering atmosphere and annealing temperature and time [56], [57]. It is remarkable that the addition of only 1 mol% calcia, which enhances the stability of the tetragonal phase, reduces the grain size and increases the cubic volume fraction as determined by Rietveld analysis. In the 10-1 and 12-1 compositions, the increase in cubic ZrO_2 phase content is rather small, only about 5 and 7% respectively. The substantially reduced grain size from 1.3–2.0 μm for the compositions without calcia to about 0.6 μm for the specimens with 1 mol% CaO (see Table 1) is the main reason for the increase in hardness, with a concomitant further stabilization of the tetragonal phase, making t-m transformation more difficult [58]. This is clearly revealed in the analysis of the t-m transformation of 10-1 and 12-1 by micro-Raman around Vickers indentations (Fig. 8), on the fracture surfaces of discs (Fig. 7b), as well as on the fracture surface of SEVNB specimens (not shown here), where the amount of monoclinic phase is practically absent or strongly reduced. Not only the grain size influenced the transformability of the t-ZrO_2 grains, but also the presence of Ca^{2+} decreased the tetragonality and concomitant transformability of the t-ZrO_2 phase compared to that in 12Ce-ZrO_2 (see Fig. 2c).

The partition between tetragonal and cubic ZrO_2 phases that occurred upon calcia addition produces an inhomogeneity in the dopant distribution. In these compositions, the cubic ZrO_2 phase is highly enriched

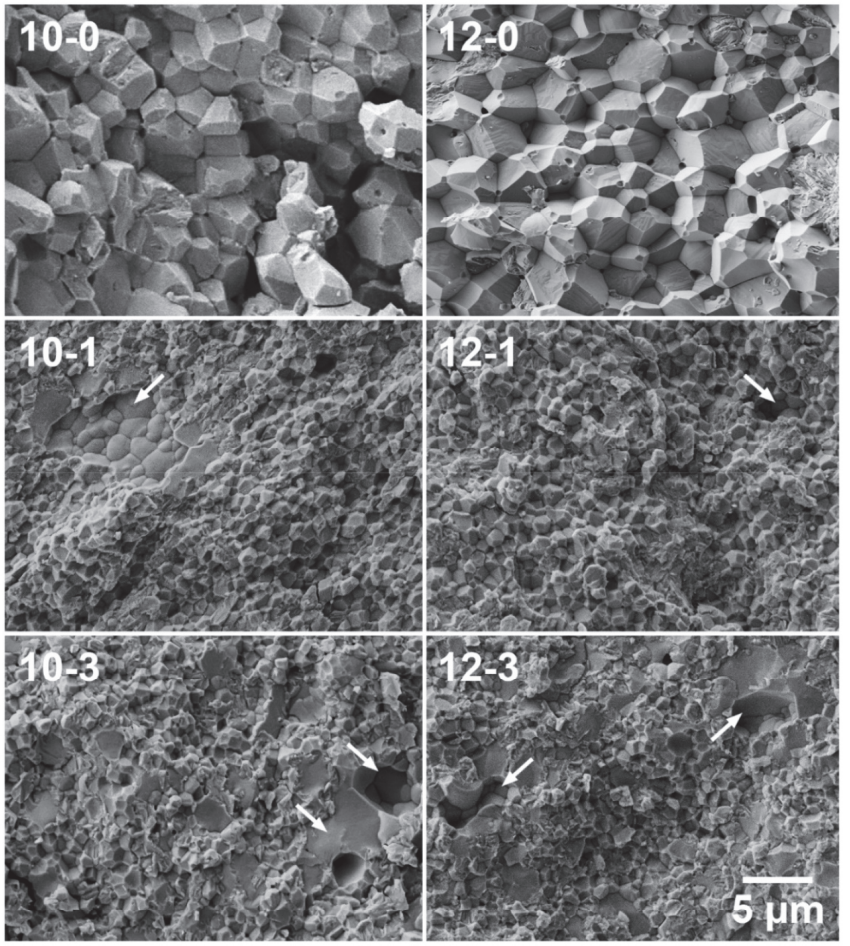

Figure 10. SEM images of fracture surfaces of notched specimens. Arrows point at cubic grains pulled out during the fracture.

in Ce and Ca solutes while the overall stabilizer in Ce and Ca solutes while the overall stabilizer content in the tetragonal neighbouring grains is lowered (see Table 2). This has been directly observed by TEM in 12-1 (see Fig. 4 and Table 2) with a Ca concentration in the cubic grains of more than five times higher than in the tetragonal grains. As the cubic ZrO_2 volume fraction increases considerably in the compositions with 3 mol% CaO addition (see Table 1), this effect is expected to be even more significant in these compositions, as more cubic grains will be formed and the amount of poorly doped tetragonal grains will be higher. This is reflected in an increased transformability of the tetragonal phase (see Fig. 2c, Fig. 7b and Fig.8), which translates in a higher fracture toughness (see Fig. 9). The presence of a higher fraction of the intrinsically harder c-ZrO_2 phase compensates the higher transformability of the tetragonal phase in 10-3 and 12-3, so that their hardness is comparable to the 10-1 and 12-1 respectively.

The biaxial tensile strength increased from ~600

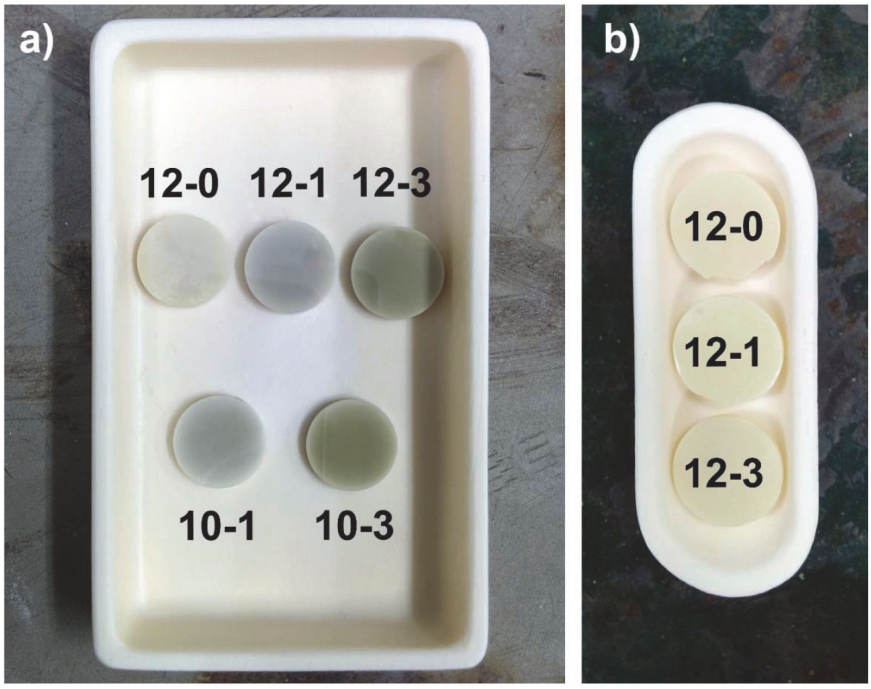

Figure 11. Color appearance of the ceramics (a) as-sintered and (b) after a heat treatment with air ventilation at 1200 ºC for 1h.

to ~900 MPa upon 1 mol% CaO addition because of the reduction in grain size and transformability. Further addition of calcia up to 3 mol% reduced the bending strength to about 700 MPa. This is in line with the increase in transformability of the tetragonal phase and the presence of a considerable amount of cubic phase in the form of large grains in 10-3 and 12-3 grades, as revealed in the fracture surfaces (see Fig. 10). It should be noted that an increased amount of residual porosity with calcia addition was observed in the SEM images, which may also affect the mechanical properties.

The indentation fracture toughness could only be measured for the 12-1 and 12-3 compositions, in which cracks had suitable lengths to comply with the requirements of Niihara's equation [59]. The fracture resistance of 5.7 MPa$\sqrt{m}$ for the 12-1 grade and 5.5 MPa$\sqrt{m}$ for 12-3 are in line with the reported indentation fracture toughness of ~5.5 MPa$\sqrt{m}$ [21] for 3Y-TZP with a similar grain size, calculated according to Niihara's equation.

It can be noticed that the fracture toughness obtained from the notched specimens for the base materials without calcia was rather low compared with the high values often quoted by other methods [45]. Because of the specific dimensions of the initially unshielded small crack, it is uncertain whether fracture is controlled by the R-curve of short or long cracks. From the low and similar K_{Ic} measured for both materials, it is most likely that fracture was mainly controlled by the intrinsic fracture toughness. If there is any stable crack extension before unstable fracture, it should have been very limited. This may occur in 3Y-TZP where the R-curve has a relatively low plateau and a high steepness, with the plateau being reached after very short crack extensions of about 20 μm [60]. In contrast, considering the well-known high plateau levels of the R curves of 12Ce-

ZrO_2 [35], [45], [61], the low K_{Ic} measured here may indicate that these curves are not sufficiently steep to have a significant role in the control of fracture of these artificial cracks with the present specific dimensions. This explains the similar values of K_{Ic} for the different zirconia ceramics.

On the other side, the short edge artificial cracks used were long enough to control the fracture during testing of all the investigated compositions. That is, the fracture was not controlled by the critical transformation stress on the surface of the flexure specimens, since the fracture stress applied on the tensile surface in the precracked specimens (~315 MPa) is lower than the reported values for the critical stress for t-m transformation (around 600 MPa in 11 mol% CeO_2 [8]).

In the discs with natural defects, the relative low strength of 12-0 it may be indicative of the strength being controlled by the t-m transformation due to its high transformability. The strong reduction in transformability with 1 mol% calcia addition also increases the critical transformation stress, increasing therefore the strength. The drop in strength with 3 mol% calcia might be associated with the increase of transformability of the tetragonal phase due to the higher presence of cubic phase, slightly lowering the critical transformation stress. The increase in transformability is also reflected on the amount of monoclinic phase detected on the fracture surfaces. However, for 12-1 grade, hardly any monoclinic phase was detected, so that the strength might be controlled by natural defects. Since K_{Ic} for 12-1 is only 3.9 MPa$\sqrt{m}$, the size of the equivalent ideal surface semicircular crack for the measured strength would be one with a radius of about 11 μm, which is similar to the reported values for 3Y-TZP [62], [63].

Finally, all grades had a high ageing resistance, with only a small amount (< 10 vol%) of monoclinic phase detected for the 10-3 grade after 30h in steam. This composition was expected to be the more susceptible to LTD, as it was also the more transformable with the highest t-ZrO_2 phase tetragonality among the CaO-doped ceramics (see Fig. 2c, Fig. 7b and Fig. 8), and because of the oxygen vacancies introduced by Ca^{2+} into the pristine oxygen vacancy-free Ce-ZrO_2 material. The detrimental influence of the cubic phase in a 3Y-TZP on the ageing resistance due to the dopant deprivation of the tetragonal grains has been observed previously in literature [64]. However, as the ageing resistance of Ce-ZrO_2 base compositions is much higher than for a 3Y-TZP [5], the influence of the impoverished tetragonal grains is limited in this work.

5. Conclusions

In summary, the addition of 1 or 3 mol% CaO to 10 and 12Ce-ZrO_2 ceramics effectively reduces the grain size, increasing the hardness, fracture strength and cubic ZrO_2 phase content without compromising the hydrothermal ageing resistance. The CaO addition initiates the formation of a larger grained cubic ZrO_2 phase which accumulates a substantial amount of the stabilizing Ca^{2+} and Ce^{4+} cations, concomitantly reducing the stabiliser content of the tetragonal ZrO_2 phase making the ceramic more transformable, as the cubic ZrO_2 content increases with increasing CaO addition.

Acknowledgements

The authors gratefully acknowledge the financial support given by the "Ministerio de Economía y Competitividad" of Spain through research grant MAT2014-60720-R, as well as the fellowship award BES-2012-052393 and the mobility grants EEBB-I-2015-09234 and EEBB-I-16-10603 received by M.T-V. M.T-V. also thanks the JECS Trust (grant 2016115) and "La Caixa" Foundation for the mobility awards received. The authors acknowledge the Flemish Hercules Foundation under Project AKUL/1319 (CombiS(T)EM).

The authors thank Daiichi Kigensu Kagaku Kogyo Co. for supplying the commercial zirconia powders, and Dr. T. Trifonov, Dr. F. Garcia Marro and B. Tunca for their assistance with the FIB/SEM, Raman and TEM equipment, respectively.

References

[1] C. Piconi, W. Burger, H. G. Richter, A. Cittadini, G. Maccauro, V. Covacci, N. Bruzzese, G. A. Ricci, and E. Marmo, "Y-TZP ceramics for artificial joint replacements," *Biomaterials*, vol. 19, pp. 1489–1494, 1998.

[2] C. Piconi and G. Maccauro, "Zirconia as a ceramic biomaterial," *Biomaterials*, vol. 20, pp. 1–25, 1999.

[3] R. C. C. Garvie, R. H. H. Hannink, and R. T. T. Pascoe, "Ceramic steel?," *Nature*, vol. 258, no. 5537, pp. 703–704, 1975.

[4] J. Chevalier, L. Gremillard, and S. Deville, "Low-Temperature Degradation of Zirconia and Implications for Biomedical Implants," *Annu. Rev. Mater. Res.*, vol. 37, no. 1, pp. 1–32, 2007.

[5] J. Chevalier, L. Gremillard, A. V. Virkar, and D. R. Clarke, "The tetragonal-monoclinic transformation in zirconia: Lessons learned and future trends," *J. Am. Ceram. Soc.*, vol. 92, no. 9, pp. 1901–1920, 2009.

[6] J. A. Muñoz-Tabares, E. Jiménez-Piqué, and M. Anglada, "Subsurface evaluation of hydrothermal degradation of zirconia," *Acta Mater.*, vol. 59, no. 2, pp. 473–484, 2011.

[7] G. S. A. M. Theunissen, A. J. A. Winnubst, and A. J. Burggraaf, "Effect of dopants on the sintering behaviour and stability of tetragonal zirconia ceramics," *J. Eur. Ceram. Soc.*, vol. 9, no. 4, pp. 251–263, 1992.

[8] K. Tsukuma and M. Shimada, "Strength, fracture toughness and Vickers hardness of CeO2-stabilized tetragonal ZrO2 polycrystals (Ce-TZP)," *J. Mater. Sci.*, vol. 20, no. 4, pp. 1178–1184, 1985.

[9] G. S. A. M. Theunissen, A. J. A. Winnubst, and A. J. Burggraaf, "Segregation aspects in the ZrO2-Y2O3 ceramic system," *J. Mater. Sci. Lett.*, vol. 8, pp. 55–57, 1989.

[10] M. M. R. Boutz, A. J. A. Winnubst, and A. J. Burggraaf, "Yttria-ceria stabilized tetragonal zirconia polycrystals: Sintering, grain growth and grain boundary segregation," *J. Eur. Ceram. Soc.*, vol. 13, no. 2, pp. 89–102, 1994.

[11] T. Masaki, "Mechanical properties of Y-PSZ after aging at low temperature," *Int. J. High Technol. Ceram.*, vol. 2, no. 2, pp. 85–98, 1986.

[12] J. Chevalier and L. Gremillard, "Ceramics for medical applications: A picture for the next 20 years," *J. Eur. Ceram. Soc.*, vol. 29, no. 7, pp. 1245–1255, 2009.

[13] F. Zhang, K. Vanmeensel, M. Inokoshi, M. Batuk, J. Hadermann, B. Van Meerbeek, I. Naert, and J. Vleugels, "Critical influence of alumina content on the low temperature degradation of 2–3mol% yttria-stabilized TZP for dental restorations," *J. Eur. Ceram. Soc.*, vol. 35, no. 2, pp. 741–750, 2015.

[14] F. Zhang, K. Vanmeensel, M. Batuk, J. Hadermann, M. Inokoshi, B. Van Meerbeek, I. Naert, and J. Vleugels, "Highly-translucent, strong and aging-resistant 3Y-TZP ceramics for dental restoration by grain boundary segregation," *Acta Biomater.*, vol. 16, pp. 215–222, 2015.

[15] K. Matsui, H. Yoshida, and Y. Ikuhara, "Nanocrystalline, Ultra-Degradation- Resistant Zirconia: Its Grain Boundary Nanostructure and Nanochemistry," *Sci. Rep.*, vol. 4, no. 4758, pp. 1–6, 2014.

[16] T. Sato, S. Ohtaki, T. Endo, and M. Shimada, "Improvement of thermal stability of Yttria-doped tetragonal zirconia polycrystals by alloying with various oxides," *Int. J. High Technol. Ceram.*, vol. 2, no. 3, pp. 167–177, 1986.

[17] J.-G. Duh, H.-T. Dai, and W.-Y. Hsu, "Synthesis and sintering behaviour in CeO2-ZrO2 ceramics," *J. Mater. Sci.*, vol. 23, no. 8, pp. 2786–2791, 1988.

[18] J.-G. Duh, H.-T. Dai, and B.-S. Chiou, "Sintering, Microstructure, Hardness, and Fracture Toughness Behavior of Y2O3-CeO2-ZrO2," *J. Am. Ceram. Soc.*, vol. 71, no. 10, pp. 813–819, 1988.

[19] J.-D. Lin and J.-G. Duh, "Correlation of mechanical properties and composition in tetragonal CeO2-Y2O3-ZrO2 ceramic system," *Mater. Chem. Phys.*, vol. 78, pp. 246–252, 2002.

[20] S. G. Huang, J. Vleugels, L. Li, O. Van der Biest, and P. L. Wang, "Composition design and mechanical properties of mixed (Ce,Y)-TZP ceramics obtained from coated starting powders," *J. Eur. Ceram. Soc.*, vol. 25, no. 13, pp. 3109–3115, 2005.

[21] M. Turon-Vinas, J. J. Roa, F. G. Marro, and M. Anglada, "Mechanical properties of 12Ce–ZrO2/3Y–ZrO2 composites," *Ceram. Int.*, vol. 41, no. 10, pp. 14988–14997, 2015.

[22] J. A. Allemann, B. Michel, H.-B. Märki, L. J. Gauckler, and E. M. Moser, "Grain growth of differently doped zirconia," *J. Eur. Ceram. Soc.*, vol. 15, no. 10, pp. 951–958, 1995.

[23] S.-L. Hwang and I.-W. Chen, "Grain size control of tetragonal zirconia polycrystals using the space charge concept," *J. Am. Ceram. Soc.*, vol. 77, no. 198024, 1990.

[24] J. H. Park and S. W. Moon, "Stability and sinterability of tetragonal zirconia polycrystals costabilized by CeO2 and various oxides," *J. Mater. Sci. Lett.*, vol. 11, no. 15, pp. 1046–1048, 1992.

[25] A. Takemura, A. Nakahira, T. Sekino, T. Koyama, and N. Kouichi, "Effects of Oxide Doping on Microstructure and Mechanical Properties of Ce-TZP," *J. Soc. Mater. Sci. Japan*, vol. 43, no. 489, pp. 606–612, 1994.

[26] I. W. Chen, "Mobility control of ceramic grain boundaries and interfaces," *Mater. Sci. Eng. A*, vol. 166, no. 1–2, pp. 51–58, 1993.

[27] F. Zhang, M. Batuk, J. Hadermann, G. Manfredi, A. Mariën, K. Vanmeensel, M. Inokoshi, B. Van Meerbeek, I. Naert, and J. Vleugels, "Effect of cation dopant radius on the hydrothermal stability of tetragonal zirconia: Grain boundary segregation and oxygen vacancy annihilation," *Acta Mater.*, vol. 106, pp. 48–58, Mar. 2016.

[28] R. C. Garvie and P. S. Nicholson, "Phase Analysis in Zirconia Systems," *J. Am. Ceram. Soc.*, vol. 55, no. 6, pp. 303–305, 1972.

[29] H. Toraya, M. Yoshimura, and S. S. Somiya, "Calibration Curve for Quantitative Analysis of the Monoclinic-Tetragonal Zr02 System by X-Ray Diffraction.," *J Am. Ceram. Soc.*, vol. 67, pp. C119–C121, Jun. 1984.

[30] A. Börger, P. Supancic, and R. Danzer, "The ball on three balls test for strength testing of brittle discs: stress distribution in the disc," *J. Eur. Ceram. Soc.*, vol. 22, pp. 1425–1436, 2002.

[31] A. Börger, P. Supancic, and R. Danzer, "The ball on three balls test for strength testing of brittle discs: Part II: Analysis of possible errors in the strength determination," *J. Eur. Ceram. Soc.*, vol. 24, no. 2004, pp. 2917–2928, 2004.

[32] T. Fett, G. Rizzi, M. Esfehanian, and R. Oberacker, "Simple Expressions for the Evaluation of Stresses in Sphere-Loaded Disks Under Biaxial Flexure," *J. Test. Eval.*, vol. 36, no. 3, p. 101402, 2008.

[33] M. Turon-Vinas and M. J. Anglada, "Fracture toughness of zirconia from a shallow notch produced by ultra-short pulsed laser ablation," *J. Eur. Ceram. Soc.*, vol. 34, no. 15, pp. 3865–3870, 2014.

[34] M. Turon-Vinas and M. Anglada, "Assessment in Si3N4 of a new method for determining the fracture toughness from a surface notch micro-machined by ultra-short pulsed laser ablation," *J. Eur. Ceram. Soc.*, vol. 35, no. 6, pp. 1737–1741, 2015.

[35] L. Melk, M. Turon-Vinas, J. J. Roa, M.-L. Antti, and M. Anglada, "The influence of unshielded small cracks in the fracture toughness of yttria and of ceria stabilised zirconia," *J.*

Eur. Ceram. Soc., vol. 36, no. 1, pp. 147–153, 2016.
[36] M. Turon-Vinas, J. Morillas, P. Moreno, and M. Anglada, "Evaluation of damage in front of starting notches induced by ultra-short pulsed laser ablation for the determination of fracture toughness in zirconia," *J. Eur. Ceram. Soc.*, vol. 37, no. 15, pp. 5127–5131, 2017.
[37] G. D. Quinn and R. C. Bradt, "On the Vickers Indentation Fracture Toughness Test," *J. Am. Ceram. Soc.*, vol. 90, no. 3, pp. 673–680, 2007.
[38] K. Niihara, R. Morena, and D. P. . Hasselman, "Evaluation of Klc of brittle solids by the indentation method with low crack-to-indent ratios," *J. Mater. Sci. Lett.*, vol. 1, pp. 13–16, 1982.
[39] M. Nawa, S. Nakamoto, T. Sekino, and K. Niihara, "Tough and strong Ce-TZP/Alumina nanocomposites doped with titania," *Ceram. Int.*, vol. 24, no. 7, pp. 497–506, 1998.
[40] G. Katagiri, H. Ishida, A. Ishitani, and T. Masaki, "Direct determination by a Raman microprobe of the transformation zone size in Y2O3 containing tetragonal ZrO2 polycrystals," *Adv. Ceram.*, vol. 24, pp. 537–544, 1988.
[41] J. A. Muñoz-Tabares and M. J. Anglada, "Quantitative Analysis of Monoclinic Phase in 3Y-TZP by Raman Spectroscopy," *J. Am. Ceram. Soc.*, vol. 93, no. 6, pp. 1790–1795, 2010.
[42] P. Li, I.-W. Chen, and J. E. Penner-Hahn, "Effect of Dopants on Zirconia Stabilization—An X-ray Absorption Study: II, Tetravalent Dopants," *J. Am. Ceram. Soc.*, vol. 77, no. 5, pp. 1281–1288, 1994.
[43] S. Y. Kwon and I. H. Jung, "Critical evaluation and thermodynamic optimization of the CaO-ZrO2 and SiO2-ZrO2 systems," *J. Eur. Ceram. Soc.*, vol. 37, no. 3, pp. 1105–1116, 2017.
[44] J. Chevalier, "What future for zirconia as a biomaterial?," *Biomaterials*, vol. 27, no. 4, pp. 535–543, 2006.
[45] H. El Attaoui, M. Saâdaoui, J. Chevalier, and G. Fantozzi, "Static and cyclic crack propagation in Ce-TZP ceramics with different amounts of transformation toughening," *J. Eur. Ceram. Soc.*, vol. 27, no. 2–3, pp. 483–486, 2007.
[46] T. Sata and M. Yoshimura, "Reduction Process from CeO2 to Ce2O3 in Hydrogen," *Bull. Tokyo Inst. Technol.*, vol. 84, pp. 13–23, 1968.
[47] J. S. Moya, R. Moreno, J. Requena, and J. Soria, "Black Color in Partially Stabilized Zirconia," *J. Am. Ceram. Soc.*, vol. 71, no. 11, pp. 479–480, 1988.
[48] H.-Y. Zhu, T. Hirata, and Y. Muramatsu, "Phase Separation in 12 mol% Ceria-Doped Zirconia Induced by Heat Treatment in H2 and Ar," *J. Am. Ceram. Soc.*, vol. 75, no. 10, pp. 2843–2848, 1992.
[49] H.-Y. Zhu and T. Hirata, "Ce3d and Zr3d X-ray photoelectron spectroscopy spectra of ZrO2-12 mol% CeO2 after heat-treatments and Ar+ etching," *J. Mater. Sci. Lett.*, vol. 12, pp. 749–751, 1993.
[50] V. M. Orera, R. I. Merino, and F. Peña, "Ce3+↔Ce4+ conversion in ceria-doped zirconia single crystals induced by oxido-reduction treatments," *Solid State Ionics*, vol. 72, no. PART 2, pp. 224–231, 1994.
[51] C. Zhao, J. Vleugels, C. Groffils, P. J. Luypaert, and O. Van Der Biest, "Hybrid sintering with a tubular susceptor in a cylindrical single-mode microwave furnace," *Acta Mater.*, vol. 48, no. 14, pp. 3795–3801, 2000.
[52] J. Vleugels and O. Van Der Biest, "Engineering the toughness of CeO2-stabilised ZrO2," *Key Eng. Mater.*, vol. 213, pp. 273–276, 2002.
[53] M. Matsuzawa, M. Abe, S. Horibe, and J. Sakai, "The effect of reduction on the mechanical properties of CeO2 doped tetragonal zirconia ceramics," *Acta Mater.*, vol. 52, no. 6, pp. 1675–1682, 2004.
[54] S. G. Huang, K. Vanmeensel, O. Van Der Biest, and J. Vleugels, "Influence of CeO2 reduction on the microstructure and mechanical properties of pulsed electric current sintered Y2O3-CeO2 co-stabilized ZrO2 ceramics," *J. Am. Ceram. Soc.*, vol. 90, no. 5, pp. 1420–1426, 2007.
[55] C. Zhao, J. Vleugels, B. Basu, and O. Van Der Biest, "High toughness Ce-TZP by sintering in an inert atmosphere," *Scr. Mater.*, vol. 43, no. 11, pp. 1015–1020, 2000.
[56] J. Vleugels, C. Zhao, and O. Van Der Biest, "Toughness enhancement of Ce-TZP by annealing in argon," *Scr. Mater.*, vol. 50, no. 5, pp. 679–683, 2004.
[57] K.-H. Heussner and N. Claussen, "Strengthening of Ceria-Doped Tetragonal Zirconia Polycrystals by Reduction-Induced Phase Transformation," *J. Am. Ceram. Soc.*, vol. 72, no. 6, pp. 1044–1046, 1989.
[58] P. F. Becher and M. V. Swain, "Grain-Size-Dependent Transformation Behavior in Polycrystalline Tetragonal Zirconia," *J. Am. Ceram. Soc.*, vol. 75, no. 3, pp. 493–502, 1992.
[59] K. Niihara, "A fracture mechanics analysis of indentation-induced Palmqvist crack in ceramics," *J. Mater. Sci. Lett.*, vol. 2, pp. 221–223, 1983.
[60] D. Casellas, J. Alcalá, L. Llanes, and M. J. Anglada, "Fracture variability and R-curve behavior in yttria-stabilized zirconia ceramics," *J. Mater. Sci.*, vol. 36, pp. 3011–3025, 2001.
[61] C. S. Yu and D. K. Shetty, "Transformation yielding, plasticity and crack-growth-resistance (R-curve) behaviour of CeO2-TZP," *J. Mater. Sci.*, vol. 25, no. 4, pp. 2025–2035, 1990.
[62] T. Kosmač, Č. Oblak, P. Jevnikar, N. Funduk, and L. Marion, "The effect of surface grinding and sandblasting on flexural strength and reliability of Y-TZP zirconia ceramic.," *Dent. Mater.*, vol. 15, no. 6, pp. 426–33, Nov. 1999.
[63] T. Kosmač, Č. Oblak, P. Jevnikar, N. Funduk, and L. Marion, "Strength and reliability of surface treated Y-TZP dental ceramics.," *J. Biomed. Mater. Res.*, vol. 53, no. 4, pp. 304–13, Jan. 2000.
[64] J. Chevalier, S. Deville, E. Münch, R. Jullian, and F. Lair, "Critical effect of cubic phase on aging in 3 mol% yttria-stabilized zirconia ceramics for hip replacement prosthesis," *Biomaterials*, vol. 25, no. 24, pp. 5539–5545, 2004.

GLOSSARY OF ACRONYMS

3Y-TZP	TZP stabilised with 3% mol of Y_2O_3
AFM	Atomic force microscopy
AS	As-sintered
ASTM	American Society for Testing and Materials
ATZ	Alumina-toughened zirconia
B3B	Ball-on-three-balls strength test
c→t	Cubic-to-tetragonal transformation
Ce-TZP	TZP stabilised with CeO_2
CIP	Cold isostatic pressing
CLSM	Confocal laser scanning microscopy
COD	Crack opening displacement
CSM	Continuous stiffness measurement
CSZ	Cubic-stabilised zirconia
CVN	Chevron-notched beam
E	Elastic or Young's modulus
EBSD	Electron backscatter diffraction
EDS/EDX	Energy-dispersive X-ray spectroscopy
EPMA	Electron-probe micro-analyzer
ESIS	European Structural Integrity Society
FESEM	Field emission scanning electron microscopy
FGM	Functionally-graded material
FIB	Focused ion beam
FSZ	Fully-stabilised zirconia
GB	Grain boundary
HAADF	High angle dark annular field
HIP	Hot isostatic pressing
HRSTEM	High-resolution Scanning transmission electron microscopy
HV	Vickers hardness
ISO	International Organization for Standardization

K	Stress intensity factor
K_{Ic}	Fracture toughness
LEFM	Linear elastic fracture mechanics
LTD	Low-temperature degradation
MAJ	Mehl-Avrami-Johnson
OM	Optical microscopy
PSZ	Partially-stabilised zirconia
RMTP	Reference Material Testing Program
SCF	Surface crack in flexure
SEM	Scanning electron microscopy
SENB	Single-edge-notched beam
SEPB	Single-edge precracked beam
SEVNB	Single-edge V-notched beam
SOFC	Solid oxygen fuel cells
STEM	Scanning transmission electron microscopy
T_0	Transformation temperature
t→m	Tetragonal-to-monoclinic transformation
TBC	Thermal barrier coating
TEM	Transmission electron microscopy
THR	Total hip replacement
TTT	Time-temperature-transformation curve
TZP	Tetragonal polycrystalline zirconia
UPLA	Ultra-short pulsed laser ablation
VAMAS	Versailles Project on Advanced Materials and Standards
VIF	Vickers indentation fracture toughness test
XPS	X-ray photoelectron spectroscopy
XRD	X-ray diffraction
YSZ	Yttria-stabilised zirconia
ZTA	Zirconia-toughened alumina

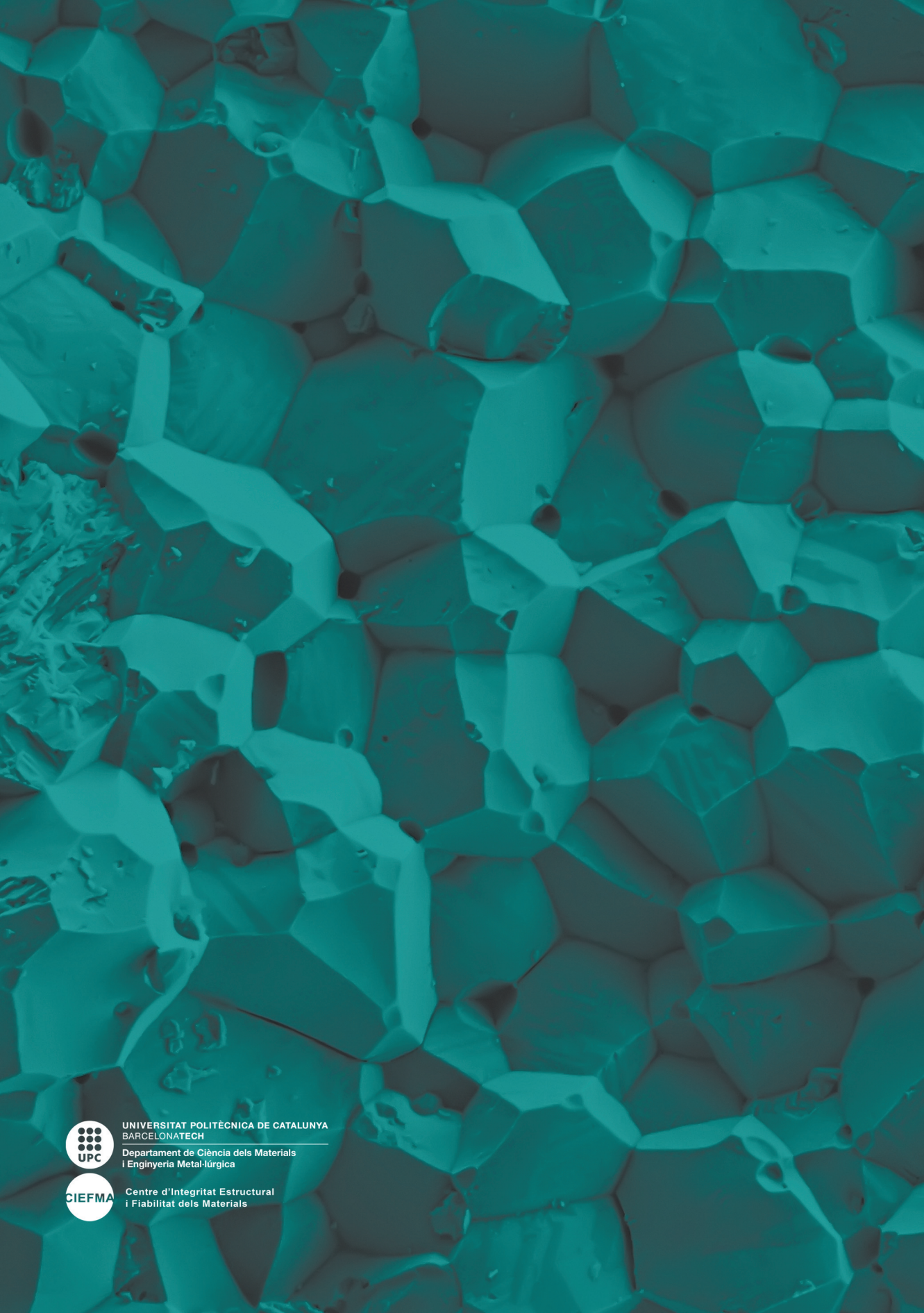

UNIVERSITAT POLITÈCNICA DE CATALUNYA
BARCELONATECH
Departament de Ciència dels Materials
i Enginyeria Metal·lúrgica

Centre d'Integritat Estructural
i Fiabilitat dels Materials